AD-A173 342 PROCESSING SCIENCE TO INCREASE THE RELIABILITY OF CERAMICS(U) ROCKWELL INTERNATIONAL THOUSAND OAKS CA SCIENCE CENTER B J KELLETT ET AL. SEP 86 SC410.FR 1/2

UNCLASSIFIED N00014-84-C-0298 F/G 11/2 NL

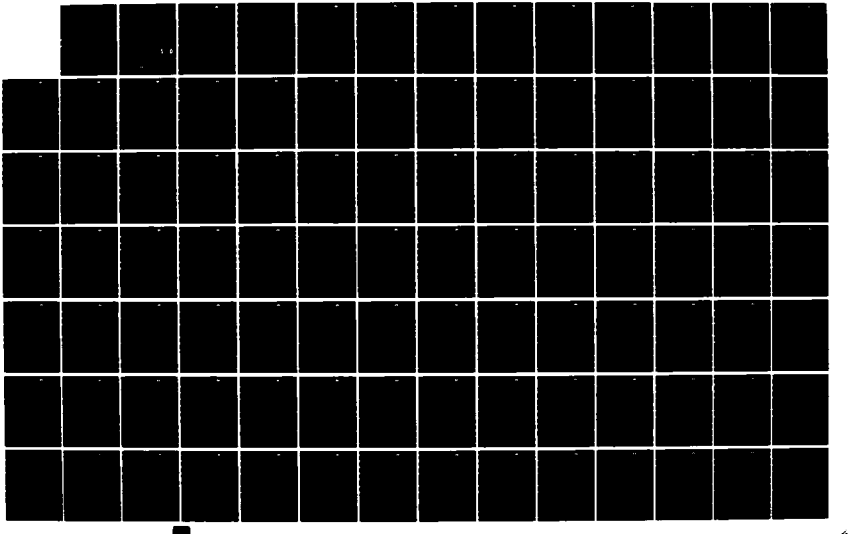

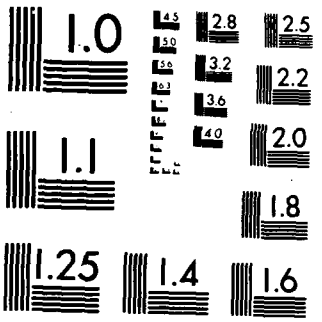

(12)

SC5410.FR

Copy No. 17

PROCESSING SCIENCE TO INCREASE THE RELIABILITY OF CERAMICS

TECHNICAL REPORT NO. 1
THERMODYNAMICS OF DENSIFICATION, PART I: SINTERING OF SIMPLE PARTICLE ARRAYS, EQUILIBRIUM CONFIGURATIONS, PORE STABILITY, AND SHRINKAGE

B.J. Kellett and F.F. Lange

TECHNICAL REPORT NO. 2
THERMODYNAMICS OF DENSIFICATION, PART II: GRAIN GROWTH IN POROUS COMPACTS AND RELATION TO DENSIFICATION

F.F. Lange and B.J. Kellett

TECHNICAL REPORT NO. 3
THERMODYNAMICS OF DENSIFICATION, PART III: EXPERIMENTAL RELATION BETWEEN GRAIN GROWTH AND PORE CLOSURE

B.J. Kellett and F.F. Lange

TECHNICAL REPORT NO. 4
EXPERIMENTS ON PORE CLOSURE DURING HIPing AND FORGING

B.J. Kellett and F.F. Lange

FINAL REPORT FOR THE PERIOD
July 1, 1984 through March 31, 1986

CONTRACT NO. N00014-84-C-0298
PROJECT NO. 431e037

Prepared for

Office of Naval Research
800 North Quincy Street
Arlington, Virginia 22217

F. Lange and B. Kellett
Principal Investigators

SEPTEMBER 1986

Approved for public release; distribution unlimited

Rockwell International
Science Center

TABLE OF CONTENTS

SC5410.FR

THERMODYNAMICS OF DENSIFICATION, PART I: SINTERING OF SIMPLE PARTICLE ARRAYS, EQUILIBRIUM CONFIGURATIONS, PORE STABILITY, AND SHRINKAGE

B. Kellett and F.F. Lange

Department of Materials Science and Engineering
University of California, Los Angeles

and

Structural Ceramics Department
Rockwell International Science Center

THERMODYNAMICS OF DENSIFICATION, PART I: SINTERING OF SIMPLE PARTICLE ARRAYS, EQUILIBRIUM CONFIGURATIONS, PORE STABILITY, AND SHRINKAGE

B. Kellett and F. F. Lange

Department of Materials Science and Engineering
University of California, Los Angeles

and

Structural Ceramics Department
Rockwell International Science Center

ABSTRACT

Equilibrium configurations for linear and closed (rings and regular polyhedra containing a single pore) arrays of identical particles (cylinders or spheres) were determined by minimizing the array's surface and grain boundary energies (related through Young's equation) with the assumption that each particle conserves its mass. As expected, the lowest free energy configuration occurs when the angle that defines the surface-grain boundary intersection is defined by Young's equation. The change in free energy between the initial and equilibrium configuration increases with dihedral angle (i.e., the equilibrium angle). The effective sintering 'stress' (i.e., driving force) increases with the dihedral angle, and decreases to zero as the equilibrium configuration is reached. More significantly, it is shown that pores can shrink to an equilibrium size if the number (n) of coordinating particles is greater than a critical value. The critical pore coordination number (n_c) increases with the dihedral angle. Only pores with $n < n_c$ are thermodynamically unstable during sintering. It is also shown that any mass transport mechanism will lead to pore shrinkage while a connecting path to the pore remains open. Sintering 'stresses' increase with decreasing coordination number. It is also shown that the shrinkage strain and strain rate for closed arrays increase with the pore coordination

number, i.e., arrays containing more particles will shrink more and at a faster rate as they approach their equilibrium configuration. These results are related to a powder compact assumed to be formed by adjoining polyhedra. These relations suggest that the resultant force acting on a particle will depend on the coordination numbers of polyhedra it shares. These forces can cause disruptive rearrangement. The compact's shrinkage strain and strain rate is expected to mimic the average polyhedron, i.e., is expected to be inversely proportional to the compact's initial relative density.

1.0 INTRODUCTION

Most sintering theories have been based on ideas developed by Herring,[1] who reasoned that local surface curvature determines local vacancy concentration and differential surface curvature motivates mass transport. Herring's thermodynamic concept has been rigorously applied to models concerning the different mass transport paths associated with two touching spheres.[2,3] These models have focussed on the kinetics of mass transport, and they have been extended, with some success, to estimate the densification behavior of powder compacts.[4,5] Conclusions drawn from these theories are not always in agreement with experiments. For example, theory suggests that densification kinetics should increase with decreasing particle size. Yet, common experience indicates that powders with a very small crystallite size can be difficult to densify. It is now commonly accepted that agglomerates, common to chemically derived powders, are one cause for poor sinterability, and that particle packing has a great influence on densification. Mounting evidence suggests[6] that the two-particle models, which lack pores, are insufficient. It must be concluded that since the practical aim of densification is to rid the powder compact of its void phase, thus, the void phase produced by particle arrangements must be studied along with the mass transport produced by the particles.

Early studies[7,8] concerned with the kinetics of mass transport driven by differential surface curvature in a powder compact assumed that the void phase could be described during a latter stage of densification as spherical

pores. Pores, however, are only spherical in a polycrystalline material if they reside within a single grain where the surface energy is isotropic. As first pointed out by Coble[9] and further developed by Kingery and Francois,[10] isolated pores intersected by grain boundaries will exhibit a surface curvature that depends on the number of intersecting grain boundaries (or, the number of grains coordinating the pore) and the dihedral angle (defined through Young's equation* by the ratio of the grain boundary to surface energy ratio). Using geometrical arguments, they showed that if the dihedral angle was to be maintained at each grain-boundary/pore surface intersection, then the curvature of the pore surface between these intersections depends on the pore's coordination number. They concluded that if the coordination number is less than a critical value, then the pore's surface will be concave (looking from within), which will promote mass transport into the pore and pore closure. They also concluded that if the pore's coordination number is greater than a critical value, its surface curvature will be convex, promoting mass transport away from the pore, and thus, pore growth. The critical pore coordination number depends on the dihedral angle. A more rigorous energy analysis[11] has shown that the isolated pore will be stable (neither shrink nor grow) when its coordination number is greater than the critical value.

Hoge and Pask[12] were the first to use thermodynamics to analyze the void phase within a powder compact by determining the lowest free energy configuration developed by periodic arrangements of identical spheres. The spheres were allowed to penetrate one another and conserve their mass (grain boundaries formed during penetration remain flat). Invoking thermodynamics by using Young's equation* they showed that the array can reach an equilibrium configuration without complete pore closure if the dihedral angle for the material in question is less than a critical value. Although Hoge and Pask did not develop a general relation for pore closure, they were the first to suggest that under certain conditions, the void phase can form pores with an equilibrium size.

---

*See Eq. (2).

The packing of particles, such as identical spheres or otherwise, rarely results in a periodic arrangement. The random, dense packing of identical spheres has been described[13] as an arrangement of different, irregular polyhedra where touching spheres are centered at vertices. The different polyhedra are joined at corners, edges and/or faces by shared vertices (spheres). The void space within each polyhedron, which may develop into a pore, has three pertinent properties, viz., a surface area, a volume and a coordination number (number of spheres (or vertices) that define the polyhedron). Using this idea, one might approximate any powder compact with an arrangement of polyhedra, each containing a pore. The compact's macroscopic (bulk scale) behavior can be approximated by the behavior of the average polyhedron. The coordination number of the average polyhedron will be inversely proportional to the compact's bulk density. Microscopic (particle scale) behavior can be approximated by the differential behavior of the polyhedra. With this concept in mind, it would be instructive to examine the behavior of polyhedra which might be used to estimate the behavior of a powder compact.

The object here is to determine the behavior of symmetric arrays of identical cylinders or spheres that are allowed to undergo mass transport to minimize their free energy without losing their individuality, i.e., the mass of each particle (cylinder or sphere) will be held constant. The case where intra-particle diffusion is allowed, i.e., some particles grow as others disappear, will be presented elsewhere.[14] Both linear arrays and closed arrays (arrays containing a single 'pore') are examined. Calculations will involve the particle free energy as a function of configurational change, determination of the array's equilibrium configuration, conditions for pore disappearance and stability, sintering 'stresses', and the array's shrinkage strain. The results of these calculations are consistent with some of Cannon's[15] theoretical observations and lead to several interesting conclusions concerning sintering behavior not taught by current theory.

2.0 ENERGY CALCULATIONS

2.1 General Approach

Arrays where identical particles (spheres and cylinders) are identically related to one another, viz., lines, rings and regular polyhedra were considered. The energy per particle determined from the sum of the energies associated with its surface area (A_s) and its grain boundary area (A_b) formed with other adjacent particles is expressed as

$$E = \gamma_s A_s + \gamma_b A_b \quad , \tag{1}$$

where γ_s and γ_b are the energies per unit area associated with the surface and the grain boundary, respectively; both are assumed to be isotropic. All other energies associated with the particle are assumed to be constant as the array changes its configuration during mass transport. It was assumed that γ_s and γ_b are related through Young's equation

$$\gamma_b = 2\gamma_s \cos(\psi_e/2) \quad , \tag{2}$$

where ψ_e is the equilibrium (dihedral) angle formed where the grain boundary intersects the particle's surface. Equation (1) can be rewritten as

$$E = \gamma_s(A_s + 2\cos(\psi_e/2)A_b) \quad . \tag{3}$$

By differentiating Eq. (3), it can be seen that the contact area will only grow ($dA_b > 0$) when the external surface area decreases ($dA_s < 0$), and it will cease to grow when $dA_s/dA_b = -2\cos(\psi_e/2)$, i.e., when $dE = 0$. The configuration of the array when the contact area ceases to grow is defined as the equilibrium configuration. As defined, the development of the equilibrium configuration precludes mass transport between particles, i.e., particles maintain their initial mass during sintering.

To determine the energy of the array as the contact area grows between the touching particles, one needs to define an initial particle shape, how the particle changes its shape, and the relation between the external surface area and the grain boundary area during mass transport. Theory and experiments concerning two touching spheres show that mass is transported to the contact position due to the negative surface curvature at this position relative to other positions on the particle's surface.[16] Since mass transport is a kinetic phenomenon, the surface curvature will depend on the distance from the grain boundary developed between the particles during the attempt to develop an equilibrium configuration. The nonuniform surface curvature would make the definition of the particle shape change analytically intractable. Therefore, to allow analytical calculations, it is assumed that the surface curvature is independent of position as the array develops its equilibrium configuration, e.g., the initial touching spheres remained spherical as they interpenetrate, but increase their radius to conserve mass. Relative to the real system (surface curvature is some function of position), this assumption will result in a different array energy (expected to be lower) during mass transport towards equilibrium. But, since the equilibrium configuration is defined by particle surface and grain boundary configurations that minimize free energy, it will be independent of the configurational changes prior to equilibrium. Thus, although the assumed particle configurational change used to calculate the array's energy will be different from the real system, their configuration and energy will be identical at equilibrium.

By assuming that the curvature of the external surface is independent of position and each particle conserves its mass, the relations between external and grain boundary areas and the determination of the surface curvature becomes a matter of geometry and trigonometry, and only become somewhat complex for the polyhedra where one must keep track of the number of spheres that penetrate one another as the configuration changes toward equilibrium. The condition that curvature is independent of position also imposes one important limitation, i.e., calculations concerning spheres are limited to the cases where the distance between mass centers decreases. This limitation is not imposed upon

cylinders which will be used to investigate the array energetics for mass transport paths where the distance between mass centers is constant (i.e., expected for transport by surface diffusion and/or evaporation/condensation).

Several geometric variables can be used to describe the configurational change of the array as the contact area grows. They include 1) the angle defined by the tangents to the external surface at the grain boundary, termed the contact angle (ψ, see Fig. 1b), 2) the grain boundary length (h), and 3) the radius (R_p, see Fig. 4) of the circle (or sphere) that circumscribes the grain boundary intersections on the internal surfaces and describes the pore size for closed arrays. Although these variables are interrelated, and for the appropriate cases can be used interchangeably, it is most convenient to express the configurational changes in terms of the contact angle, which is equal to zero ($\psi = 0$) when the particles are just touching, and increases as the array develops its equilibrium configuration.*

2.2 Infinite, Linear Arrays

2.2.1 Cylinders; Approaching Centers

Consider an infinite line of identical touching cylinders, with an initial radius r_i, shown in Fig. 1 at different stages of interpenetration. As mass centers approach and the cylinders interpenetrate, their radius (r) increases. Using the geometrical variables shown in Fig. 1b and Eq. (2), it can be shown that the energy per unit length of cylinder can be written as a function of four variables, viz., the contact angle (ψ), the normalized radius ($R = r/r_i$), normalized grain boundary length ($H = h/r_i$), and the dihedral angle (ψ_e):

$$E = 2\pi r_i \gamma_s \left[R(\pi - \psi) + H \cos(\psi_e/2) \right] \frac{1}{\pi} \quad . \tag{4}$$

*As shown in Appendix 1, the equilibrium configuration can also be determined by a Wulff construction.

Since each particle maintains its initial mass, one can define H in terms of R and ψ:

$$H = \frac{\pi/R + R(\psi - \pi + \sin \psi)}{2 \cos \psi/2} \quad . \tag{5}$$

Substituting Eq. (5) into (4), one obtains

$$E = 2\pi r_i \gamma_s \left[R\left(\frac{\pi - \psi}{\pi}\right)\left(1 - \frac{1}{2} \frac{\cos \frac{\psi_e}{2}}{\cos \frac{\psi}{2}}\right) + \frac{R}{\pi} \sin \frac{\psi}{2} \cos \frac{\psi_e}{2} + \frac{1}{2R} \frac{\cos \frac{\psi_e}{2}}{\cos \frac{\psi}{2}} \right] \tag{6}$$

The equilibrium condition is determined by minimizing particle energy with respect to the geometrical variables ψ, and R. It can be shown that when $dE(\psi,R) = 0$, $H = 2r \sin \psi/2$, which allows us to redefine Eq. (6) as

$$E = 2\pi r_i \gamma_s \frac{\pi - \psi + 2 \sin \frac{\psi}{2} \cos \frac{\psi_e}{2}}{\sqrt{\pi(\pi - \psi + \sin \psi)}} \tag{7}$$

and

$$R = \left(\frac{\pi}{\pi - \psi + \sin \psi}\right)^{1/2} \quad . \tag{8}$$

Figure 2 shows that the particle's energy decreases with contact angle and reaches a minimum at $\psi = \psi_e$. Also, lower energies result for larger dihedral angles.

Particle energy can also be related to the distance of particle-particle approach, which can be expressed in units of strain, i.e., $\varepsilon = 1 - R \cos \psi/2$. As shown in Fig. 3 particle energy decreases with particle-particle approach and reaches a minimum energy condition at increasingly larger strains with increased dihedral angle (ψ_e). (Shrinkage strains will be discussed further in Section 4.)

2.2.2 Cylinders; Center-to-Center Distance Constant

When the particle centers of mass are fixed the radius of curvature of the external surface (r) is easily determined from geometry (i.e., $r = r_i/\cos(\psi/2)$). The centers of curvature are neither coincident with one another nor with the center of mass.

It can be shown that the energy per unit length can be written as a function of the contact angle (ψ) and the dihedral angle (ψ_e):

$$E = 2\pi r_i \gamma_s \left[\left(\frac{1}{2} - \frac{\pi - \psi - \sin\psi}{2\pi \cos^2 \frac{\psi}{2}}\right) \cos\frac{\psi_e}{2} + \frac{\pi - \psi}{\pi \cos\frac{\psi}{2}} \right] . \qquad (9)$$

The equilibrium configuration occurs when $dE/d\psi = 0$, which can be shown to occur when $\psi = \psi_e$.

Figure 4 shows particle energy for both approach (solid lines, Eq. (7)) and nonapproach (broken lines, Eq. (9)) of particle centers. As shown, energies are lower for the case of particle-particle approach.

2.2.3 Spheres

For the case of spheres, the restriction that surface curvature is independent of position limits the calculation to conditions were the mass centers approach one another. (The case where the distance between mass centers is fixed results in barrel-shaped particles.) Particle radius of curvature (r) is therefore uniquely defined by the particle's initial radius (r_i) and the contact angle (ψ):

$$r = r_i \left[\frac{1}{2}\cos\frac{\psi}{2}\left(2 + \sin^2\frac{\psi}{2}\right)\right]^{-\frac{1}{3}} . \qquad (10)$$

The energy per particle can be expressed as:

$$E = 4\pi r_i^2 \gamma_s \frac{\cos\frac{\psi}{2} + \frac{1}{2}\sin^2\frac{\psi}{2}\cos\frac{\psi_e}{2}}{\left[\frac{1}{2}\cos\frac{\psi}{2}\left(2 + \sin^2\frac{\psi}{2}\right)\right]^{2/3}} \qquad (11)$$

and is a function of the contact angle (ψ), and dihedral angle (ψ_e).

Similar to the case of the linear array of cylinders, the energy of a particle decreases and reaches equilibrium when $\psi = \psi_e$. The change in energy for different values of ψ_e is similar to that shown in Fig. 2 for the cylinders.

2.3 Closed Arrays

Forming a ring array from a linear array, or a polyhedron from a planar array, introduces several new geometrical variables needed for array calculations. These new variables include the radius (R_p) of the pore enclosed by the particles, and the finite number (n) of particles that coordinate the pore. The pore radius can be defined by a circle (or sphere) that circumscribes the positions where the grain boundaries intersect the pore's surface as shown in Fig. 5. The radius of the pore is dependent on other array variables. The pore's coordination number is an independent variable and can be described by the angle that subtends a single particle. For ring arrays the coordination angle is simply related to the coordination number, $\theta = 2\pi/n$.

One other important difference is that the center of mass for particles in closed arrays moves during mass transport (e.g., particle cross sections become 'pie' shaped), and the center of curvature is no longer coincident with the center of mass. This observation is more important in a latter section concerning shrinkage strains.

2.3.1 Ring of Cylinders; Approaching Centers

It can be shown that when $\psi + 2\pi/n \leq \pi$, the energy per particle in the ring array is identical to that for the linear array, viz., as expressed by Eq. (7). For the condition $\psi + 2\pi/n > \pi$ the particle energy can be shown to be a function of contact angle (ψ), dihedral angle (ψ_e), and pore coordination (n):

$$E = 2\pi r_i \gamma_s \frac{\pi + \frac{2\pi}{n} - \psi + \left(\sin\frac{\psi}{2} + \cos\frac{\psi}{2}/\tan\frac{\pi}{n}\right) 2\cos\frac{\psi_e}{2}}{2\sqrt{\pi}\left(\cos^2\frac{\psi}{2}/\tan\frac{\pi}{n} + \frac{1}{2}\sin\psi + \frac{\pi - \psi}{2} + \frac{\pi}{n}\right)^{1/2}} \qquad (12)$$

The pore size is given by

$$R_p = \frac{\cos\left(\frac{\psi}{2} + \frac{\pi}{n}\right)}{\sin\left(\frac{\pi}{n}\right)} \sqrt{\frac{\pi}{\pi - \psi + \sin\psi}}\, r_i \qquad (13)$$

To determine conditions of pore stability/disappearance, the energy per particle (or array energy) can be related to the pore size. As shown in Fig. 6 (for the condition $\psi_e = 150°$) a minimum energy can occur before the pore disappears, i.e., further pore closure will increase the free energy of the array.

The conditions required for pore closure can best be determined by substituting $\psi = \psi_e$ in Eq. (13) to obtain the relation for the equilibrium pore size. Examination of Eq. (13) shows that the pore will have a finite size when $\psi_e + 2\pi/n < \pi$ and will disappear when $\psi_e + 2\pi/n > \pi$. The condition where $\psi_e + 2\pi/n = \pi$ defines the critical coordination number, viz., $n_c = 2\pi/(\pi - \psi_e)$. Pores will disappear when $n \leq n_c$ and shrink to an equilibrium size when $n > n_c$.

2.3.2 Ring of Cylinders; No Mass Transport Between Pore and External Surface

With mass transport prevented between the inside pore surface and the exterior surface of the array, material which is outside the polygon formed by connecting the centers of adjoining particles (Fig. 5a) cannot be transported to the pore surface. This requires that the inside and outside regions separately conserve mass. The equilibrium configuration given these mass transport constraints will be determined, via Eq. (3), by calculating A_s and A_b with the assumption that the interior and the exterior surfaces of the array have uniform curvatures.

It can be shown that the radius of curvature of the interior-pore (R_i) and exterior-surface (R_o) are a function of the pore coordination (n) contact angle (ψ) and initial particle radius (r_i) and generally are not equal:

$$R_i = r_i K_i$$

$$K_i = \pm \left(\frac{\pi - \frac{2\pi}{n} - 2\cot\frac{\pi}{n}}{\pi - \frac{2\pi}{n} - \psi + \sin\psi - 2\cos^2\frac{\psi}{2}\cot\frac{\pi}{n}} \right)^{1/2} \qquad (14a)$$

where K_i is (+) for $\psi + \frac{2\pi}{n} < \pi$,

$$R_o = r_i K_o$$

$$K_o = \left(\frac{\pi + \frac{2\pi}{n} + 2 \cot \frac{\pi}{n}}{\pi + \frac{2\pi}{n} - \psi + \sin \psi + 2 \cos^2 \frac{\psi}{2} \cot \frac{\pi}{n}} \right)^{1/2} . \quad (14b)$$

Particle energy can also be decoupled into interior and exterior parts, and these parts have been arbitrarily separated by the polygon formed by connecting particle centers. The energy of the interior pore region (E_i) was taken to consist of both the pore surface energy, and the grain boundary energy lying within the polygon formed by connecting particle centers, while the energy of the exterior region (E_o) was taken to consist of both the external surface energy and the grain boundary energy lying outside the polygon. The energy of the interior (E_i) and exterior (E_o) region, per unit length, is a function of the pore coordination number (n), contact angle (ψ), and dihedral angle (ψ_e):

$$E_i = \gamma_s \left[r_i K_i \left(\pi - \psi - \frac{2\pi}{n} - 2 \cos \left(\frac{\psi}{2} + \frac{\pi}{n} \right) \frac{\cos \frac{\psi_e}{2}}{\sin \frac{\pi}{n}} \right) + 2 r_i \frac{\cos \frac{\psi_e}{2}}{\tan \frac{\pi}{n}} \right] \quad (15a)$$

$$E_o = \gamma_s \left[r_i K_o \left(\pi - \psi + \frac{2\pi}{n} + 2 \cos \left(\frac{\psi}{2} - \frac{\pi}{n} \right) \frac{\cos \frac{\psi_e}{2}}{\tan \frac{\pi}{n}} \right) - 2 r_i \frac{\cos \frac{\psi_e}{2}}{\tan \frac{\pi}{n}} \right] \quad (15b)$$

The equilibrium configuration, determined with $d(E_i + E_o)/d\psi = 0$, occurs when $\psi = \psi_e$. The curvatures of the interior pore surface and exterior surface for the equilibrium configuration can be determined by substituting ψ_e for ψ in Eqs. (14a) and (14b). The two curvatures are only equal when their centers of curvature are coincident. For $\psi_e + 2\pi/n < \pi$ the radius of curvature

of the interior pore surface is positive (convex as viewed from the pore). For $\psi_e + 2\pi/n > \pi$, R_i is negative (concave). The radius of curvature of the external surface (R_o) is always positive (convex as viewed from outside the ring). In all cases, the radius of curvature of the internal surface is always such, that if mass could be transported between the two surfaces, the pore would either shrink or disappear as described in the previous section (mass centers approach).

2.3.3 Ring of Spheres

Rings of spheres exhibit similiar behavior as rings of cylinders. The requirement of uniform surface curvature, however, restricts the calculations to particle approach. For conditions where $\psi_e + 2\pi/n < \pi$, it can be shown that the particle energy is identical to that determined for the linear array (Eq. 11); particle energy for these conditions is not a function of pore coordination number. For conditions where the pore disappears ($\psi_e + 2\pi/n > \pi$), all particles penetrate one another and the determination of the particle energy is somewhat complex and given in Appendix 2.

The conclusions concerning the ring of spheres are similar to the ring of cylinders with approaching centers, i.e., when $\psi_e + 2\pi/n < \pi$, the equilibrium configuration contains a stable pore, and when $\psi_e + 2\pi/n > \pi$, the pore disappears.

2.3.4 Regular Polyhedra (See Appendix 2 for Details)

Only polyhedra consisting of identical spheres symmetrically arranged can form equilibrium structures consisting of surfaces of uniform curvature. This limits our analysis to the five regular polyhedron, as described in Table 2 of Appendix II. The energy calculations, more complex due to the varying geometry, are detailed in Appendix II.

It can be shown that conclusions concerning equilibrium configurations and pore stability/disappearance are similar to that of the ring configurations where centers approach.

3.0 SINTERING 'STRESSES'

It is often stated that the change in surface energy is the driving force for sintering. More specifically, the differential of surface energy with respect to either displacement or volume dimensionally corresponds to either force or stress, respectively. Although these 'forces' and 'stresses' have no mechanical origin, they can manifest themselves in mechanical action. For example, when a powder compact densifies around an inclusion, the sintering stresses are manifested as mechanical stresses which arise within the inclusion and the surrounding powder compact that can cause crack extension within the powder compact.[17] From a densification standpoint, the magnitude of the sintering 'stress' should defined the system's potential for densification.

In the above section, the energy of different arrays was determined as a function of their geometric changes produced by intraparticle mass transport. Using these results it is a simple matter to redefine the energy in terms of the distance between mass centers and then differentiate to obtain the sintering 'force' acting between the mass centers. The sintering 'stress' can then be determined by dividing the force by the grain boundary area over which the normal force is acting. For closed particle arrays one can determine the apparent hydrostatic pressure which produces an equivalent sintering force.

3.1 Linear Arrays

3.1.1 Cylinders

As previously determined in Section 2.2.1, particle energy of a linear array of cylinders is expressed as Eq. (7). The distance between mass centers is given by

$$x = 2r_i \cos(\phi/2) \left(\frac{\pi}{\pi - \phi + \sin\phi}\right)^{1/2} . \qquad (16)$$

The sintering 'force,' calculated as

$$F = (dE/d\psi)/(dx/d\psi) \quad , \tag{17}$$

is given in the following expression for the linear array of cylinders

$$F = 2\gamma_s(\cos \psi/2 - \cos \psi_e/2)\left[\frac{2}{\pi - \psi} + \cot \psi/2\right] \quad . \tag{18}$$

The sintering 'stress', per unit length of cylinder, determined by dividing Eq. (18) by the grain boundary area per unit length of cylinder [$2r \sin(\psi/2)$], is given by

$$\sigma_c = \frac{\gamma_s}{r_i}(\cos \frac{\psi}{2} - \cos \frac{\psi_e}{2})(\frac{2}{\pi - \psi} + \cot \frac{\psi}{2}) \frac{1}{\sin \frac{\psi}{2}} \sqrt{\frac{\pi - \psi + \sin \psi}{\pi}} \quad . \tag{19}$$

As shown by Eq. (19), the sintering 'stress' is inversely proportional to the initial particle size (r_i). As shown in Fig. 7, it decreases to zero as $\psi \to \psi_e$, and increases with increasing dihedral angle.

3.1.2 Spheres

In a similar manner, it can be shown that the sintering 'stresses' for the linear array of spheres, can be expressed as

$$\sigma_s = \frac{\gamma_s}{R}(\cos \frac{\psi}{2} - \cos \frac{\psi_e}{2}) \frac{1 + \cos^2 \frac{\psi}{2}}{\sin^2 \frac{\psi}{2} \cos \frac{\psi}{2}} \quad , \tag{20}$$

and exhibits the same behavior previously described for a linear array of cylinders.

3.2 Closed Arrays

The apparent hydrostatic sintering 'pressure' was only determined for the ring array of cylinders. With knowledge of the 'force' acting normal to the

grain boundaries (Eq. (18)), one can determine an apparent hydrostatic pressure acting on the array in the same way as one determines the stress in a thin wall cylinder. That is, the apparent hydrostatic pressure is determined by equating the component of the force (F), in the radial direction, to the hydrostatic pressure, multiplied by the component of surface area perpendicular to the radial direction. The apparent hydrostatic pressure (per unit length of cylinder) is

$$P = \frac{2\,\gamma_s}{r_i}\left(\cos\frac{\psi}{2} - \cos\frac{\psi_e}{2}\right)\frac{\sin\frac{\pi}{n}}{\cos\left(\frac{\psi}{2} - \frac{\pi}{n}\right)}\left(\frac{2}{\pi - \psi} + \cot\frac{\psi}{2}\right)\sqrt{\frac{\pi - \psi + \sin\psi}{\pi}} \quad . \tag{21}$$

Equation (21) shows that P is inversely related to the initial particle size (r_i) and decreases to zero at the equilibrium condition ($\psi = \psi_e$). Also, as shown in Fig. 8, P increases with decreasing coordination number.

Although sintering 'pressures' were not detailed for the polyhedra, an examination of their energy relations shows that similar results would be obtained as shown in Fig. 8.

4.0 SHRINKAGE STRAINS

Engineering strains are usually used to define the shrinkage behavior of a powder compact, thus shrinkage strains determined here are related to the initial array dimension.

Array shrinkage must be related to the particle's center of mass, which for a linear array, is identical to the center of curvature. For closed arrays the center of mass changes its position with respect to the center of curvature as the array changes its configuration (see Fig. 5).

4.1 Linear Array

The shrinkage strain for linear arrays of cylinders and spheres is only a function of contact angle (ψ) as shown by

$$\varepsilon_{cyl} = 1 - \cos\left(\frac{\psi}{2}\right)\left(\frac{\pi}{\pi - \psi + \sin\psi}\right)^{1/2} \tag{22a}$$

$$\varepsilon_{sph} = 1 - \left(\frac{2\cos^2\frac{\psi}{2}}{2 + \sin^2\frac{\psi}{2}}\right)^{1/3} \tag{22b}$$

The maximum shrinkage occurs when the array reaches its equilibrium configuration ($\psi = \psi_e$). The equilibrium shrinkage strain increases with dihedral angle (ψ_e).

4.2 Closed Arrays

Center of mass calculations of particle arrays containing spheres are more tedious than for cylindrical arrays, and do not lead to additional physical insight. For this reason, only rings of cylinders were treated in detail.

It can be shown that prior to pore closure ($\psi + 2\pi/n < \pi$) the shrinkage strain for the ring of cylinders is given by

$$\varepsilon = 1 - \left(\cos\frac{\psi}{2} + \frac{4}{3}\frac{\sin^3\frac{\psi}{2}\sin^2\frac{\pi}{n}}{\pi - \psi + \sin\psi}\right)\sqrt{\frac{\pi}{\pi - \psi + \sin\psi}}\ , \tag{23a}$$

and after pore closure ($\psi + 2\pi/n > \pi$) by

$$\varepsilon = 1 - R^3\frac{1}{\pi}\left[\frac{2}{3}\frac{\cos^3\left(\frac{\psi}{2} - \frac{\pi}{n}\right)}{\sin\frac{\pi}{n}} + \left(\frac{\pi}{2} - \frac{\psi}{2} + \frac{\pi}{n} - \frac{1}{2}\sin\left(\psi - \frac{2\pi}{n}\right)\right)\cos\frac{\psi}{2}\right]$$

where,

$$R = \frac{r}{r_i} = \left(\frac{2\pi}{\pi - \psi + \frac{2\pi}{n} + \sin\psi + 2\frac{\cos^2\frac{2\psi}{2}}{\tan\frac{\pi}{n}}} \right)^{1/2} \quad . \qquad (23b)$$

As shown in Fig. 9, shrinkage strain increases with the pore coordination number. Strains incorrectly calculated from the center of curvature, on the other hand, do not show any variation with pore coordination number. Negligible but finite array shrinkage occurs after pore closure, due to the further cylinderization of the ring array.

5.0 DISCUSSION

The thermodynamic approach to the sintering of simple particle arrays has both quantified some expected behavior and produced some unexpected results.

It was shown that the energy change and the driving force for densification increased with the dihedral angle. This result is expected, and suggests that sintering aids that decrease the grain boundary energy, and thus increase the dihedral angle, will increase the driving force for sintering.

More important, the analysis for closed arrays showed that pore closure is not merely a matter of kinetics as usually postulated. Sound thermodynamic reasoning shows that pores can shrink to an equilibrium size. Identical results are obtained for isolated pores in large, but finite polycrystalline bodies.[11] Both analyses show that pore closure depends on the pore's coordination number and the dihedral angle. Pores shrink to an equilibrium size when the sum of the dihedral angle and the coordination angle is $< \pi$ ($n > n_c$) and disappear when this sum is $> \pi$ ($n < n_c$). Similar results were obtained for a planar array by Cannon[15] who used a different approach to define equilibrium configurations.

Since the critical coordination number n_c increases with the dihedral angle, sintering aids that increase the dihedral angle will allow more pores within a given powder compact to be thermodynamically unstable and disappear. The concept that some pores can be thermodyamically stable leads one to hypothesis ways of reducing their coordination number. As detailed elsewhere,[6] grain

growth will reduce the pore's coordination number and cause stable pores to become unstable and disappear. Thus, grain growth, once thought to be the scourge of sintering phenomena, can be helpful. The thermodynamics of pore closure also describes the role of particle packing. Namely, compacts with higher bulk densities are expected to contain fewer highly coordinated pores, and thus, for a given sintering schedule, a higher end-point density.

It should be noted that one did not need to define the mass transport path for calculations concerning closed arrays with approaching centers. As long as there remains an open path between the external surface of the array and the pore surface, surface diffusion and evaporation/condensation will lead to the same configurational changes that are usually only associated with transport mechanisms that cause mass centers to approach for linear arrays. That is, transport mechanisms that cannot lead to the shrinkage of linear arrays can result in the shrinkage of closed arrays. It must be concluded that although surface diffusion and/or evaporation/condensation will not produce bulk shrinkage in a powder compact, some pores (those with a lower than average coordination number) will shrink and possibly disappear, while others (those with a greater than average coordination number) will grow, i.e., these transport mechanisms can lead to local densification.

It was shown that the shrinkage strain for the closed arrays increases with coordination number. This result is not unexpected since it is common experience that the shrinkage of powder compacts is inversely proportional to their initial bulk density. The following argument will show that the shrinkage strain rate, which cannot be explicitly calculated without a kinetic model, will also increase with the pore coordination number. This argument is based on the fact that as the configuration changes to the point where the pore disappears, the mass transport path is independent of the coordination number, i.e., the transport path is identical from particle to particle and array to array. That is, within the same period, the amount of shrinkage will depend on the array's coordination number, but the amount of mass transport per particle will be the same for all arrays. Since within the same period, the amount of shrinkage is proportional to the arrays' coordination number, both the shrinkage strain and strain rate of an array will be proportional to its coordination number. Thus,

an array with a larger coordination number will shrink more and at a greater rate than an array with a smaller coordination number.

Using the shrinkage behavior of closed arrays, we can now estimate the behavior of powder compacts. As suggested above, the coordination number of the average polyhedron that describes the bulk behavior will be inversely proportional to the compact's bulk density. One might expect that as pores shrink to their equilibrium size, the compact's shrinkage strain and strain rate will be inversely proportional to its initial bulk density. This behavior has been observed in sintering studies where the same powder was compacted to different initial bulk density.[18]

As indicated above the shrinkage strain and strain rate will depend on the pore's coordination number. Since different polyhedra will shrink differently, one could expect the differential behavior of connected polyhedra will give rise to stresses during sintering.

Rearrangement is the term commonly used to describe the nonuniform movement of particles during the initial stages of sintering. Exner's sintering studies[16] of random, planar arrays of identical spheres graphically illustrate this phenomenon. Some groups of particles shrink upon themselves, forming large, irregular voids between the shrinking groups. Mercury infiltration experiments on powder compacts[6,19] also reveal this phenomena. Small equivalent capillaries close during the early stages of sintering, and concurrently, larger capillaries grow even larger. As detailed above, the magnitude of the radial component of the sintering 'force' acting on a particle within a close array is inversely proportional to the coordination number. Particles that share two or more polyhedra within a powder compact therefore can have a resultant force that pulls it into the polyhedron with the smallest coordination number, whereas a neighboring particle could be pulled in the opposite direction. On the particle scale, it can be seen that forces acting on one particle will be different from particle to particle and will certainly give rise to rearrangement. On the polyhedra scale, polyhedra with coordination numbers greater than the average will try to shrink more and at a greater rate than the average. Constraint by the average shrinkage behavior will give rise to disruptive, tensile stress. On

the agglomerate scale, it has been experimentally shown[17] that agglomerates with a lower bulk density than the average will produce circumferential, crack-like voids. Thus, disruptive processes due to differential shrinkage behavior are expected to occur at all scales, Voids produced by disruptive processes will have higher coordination numbers than those present before disruption. Thus, rearrangement processes due to nonuniform packing can be the most detrimental phenomenon that occurs during sintering.

Periodic packing, which requires identical particles, might be suggested as a packing arrangement that would eliminate resultant particle forces, and thus disruptive, rearrangement phenomena. Unfortunately, disruptive, resultant forces would still exist for particles located at boundaries between order domains, which could produce crack-like voids as large as the domain size. Thus, unless periodic packing could be obtained without domain boundaries, one might conclude that packing arrangements such as those based on modifications of dense random packing might minimize the size of the disruptive unit.

ACKNOWLEDGEMENTS

This work was supported by the Office of Naval Research under Contracts No. N00014-84-K-0286 at UCLA, and No. N00014-84-C-0298 at Rockwell International Science Center.

6. REFERENCES

1. C. Herring, "Surface Tension as a Motivation for Sintering," The Physics of Powder Metallurgy, ed. T.E. Kingston, Chapt. 8, McGraw-Hill, NY (1951).

2. W.D. Kingery and M. Berg, "Study of the Initial Stages of Sintering Solids by Viscous Flow, Evaporation-Condensation, and Self-Diffusion," J.A.P. 26, 1205 (1955).

3. F.A. Nichols, "Coalescence of Two Spheres by Surface Diffusion," J.A.P. 37, 2805 (1966).

4. J.G.R. Rockland, "The Determination of the Mechanism of Sintering," Acta. Metall. 15, 277, (1967).

5. D. Lynn Johnson and Ivan B. Cutler, "Diffusion Sintering: I. Initial Stage Sintering Models and Their Application to Shrinkage of Powder Compacts," J. Am. Ceram. Soc. 46, 541 (1963).

6. F.F. Lange, "Sinterability of Agglomerated Powders," J. Am. Ceram. Soc. 67, 83, (1984).

7. R.L. Coble, "Sintering Crystalline Solids. I. Intermediate and Final State Diffusion Models," J.A.P. 32, 787, (1961).

8. G.C. Kuczynski, "The Mechanism of Densification During Sintering of Metallic Particles," Acta. Metall. 4, 58, (1956).

9. R.L. Coble, "Diffusion Sintering in the Solid State," in Kinetics of High Temperature Processes, ed. W.D. Kingery, 147-163, Joint Publication of the Technology Press of M.I.T. and John Wiley & Sons, Inc., New York, (1959).

10. W.D. Kingery and B. Francois, "Sintering of Crystalline Oxides, I: Interaction Between Grain Boundaries and Pores," in Sintering and Related Phenomena, ed. G.C. Kuczynski, N.A. Hooten and G.F. Gilbon, 471-98, Gordon Breach, (1967).

11. B.J. Kellett and F.F. Lange, "Thermodynamics of Densificiation, Part III: Experimental Relation Between Grain Growth and Pore Closure," submitted to J. Am. Ceram. Soc.

12. C.E. Hoge and J.A. Pask, Ceramurgia International 3 [3], 95-9, (1977).

13. H.J. Frost, "Overview 17: Cavities in Dense Random Packing," Acta. Metall. 30 [5], 889-904, (1982).

14. F.F. Lange and BJ. Kellett, "Thermodynamics of Densification, Part II: Grain Growth in Porous Compacts and Relation to Densification," submitted to J. Am. Ceram. Soc.

15. R.M. Cannon, "On the Effects of Dihedral Angle and Pressure on the Driving Force for Pore Growth or Shrinkage," unpublished work, (1981).

16. H.E. Exner, "Principles of Single Phase Sintering," Rev. Powder Metall. Phys. Ceramics 1, 1-251, (1979).

17. F.F. Lange and M. Metcalf, "Processing-Related Fracture Origins: II. Agglomerate Motion and Cracklike Internal Surfaces Caused by Differential Sintering," J. Am. Ceram. Soc. 66 [6], 398-406, (1983).

18. B. Kellett and F.F. Lange, "Stresses Induced by Differential Sintering in Powder Compacts," J. Am. Ceram. Soc. 67, 369, (1984).

19. O.J. Whitermore, Jr., and J.J. Sipe, "Pore Growth During the Initial Stages of Sintering Ceramics," Powder Technol. 9, 159, (1974).

20. G. Wulff, Z. Kristallogr. 34, 449, (1901).

21. W.L. Winterbottom, "Equilibrium Shape of a Small Particle in Contact With a Foreign Substrate," Acta. Metall. 15, 303, (1966).

22. C.A. Sholl and N.H. Fletcher, "Decoration Criteria for Surface Steps," Acta. Metall. 18, 1083, (1970).

SC85-30277

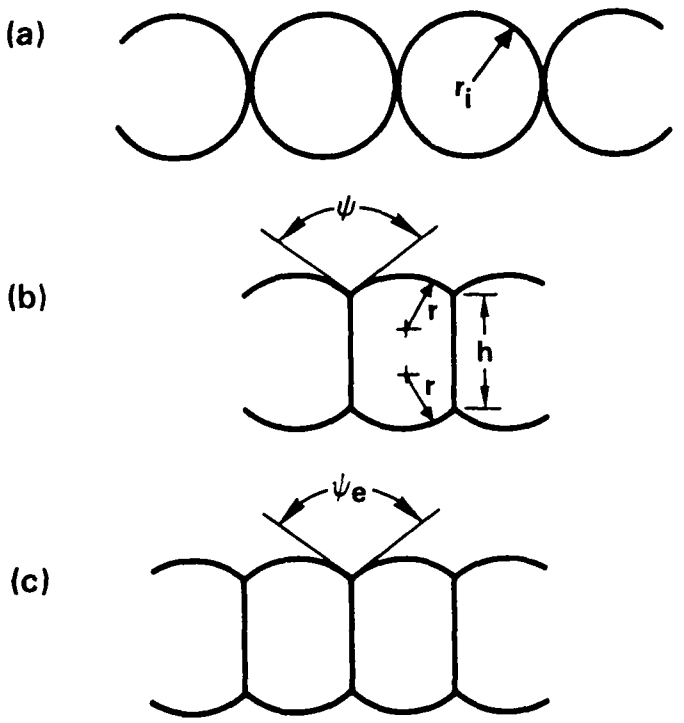

Fig. 1 a) Initial, b) generalized, and c) equilibrium configuration of a linear array of cylinders. r_i is the initial particle radius, r particle radius, ψ is the contact angle defined by the tangents of surface at the grain boundary, h is the grain boundary length and ψ_e is the dihedral angle defined by Young's equation (Eq. (2)).

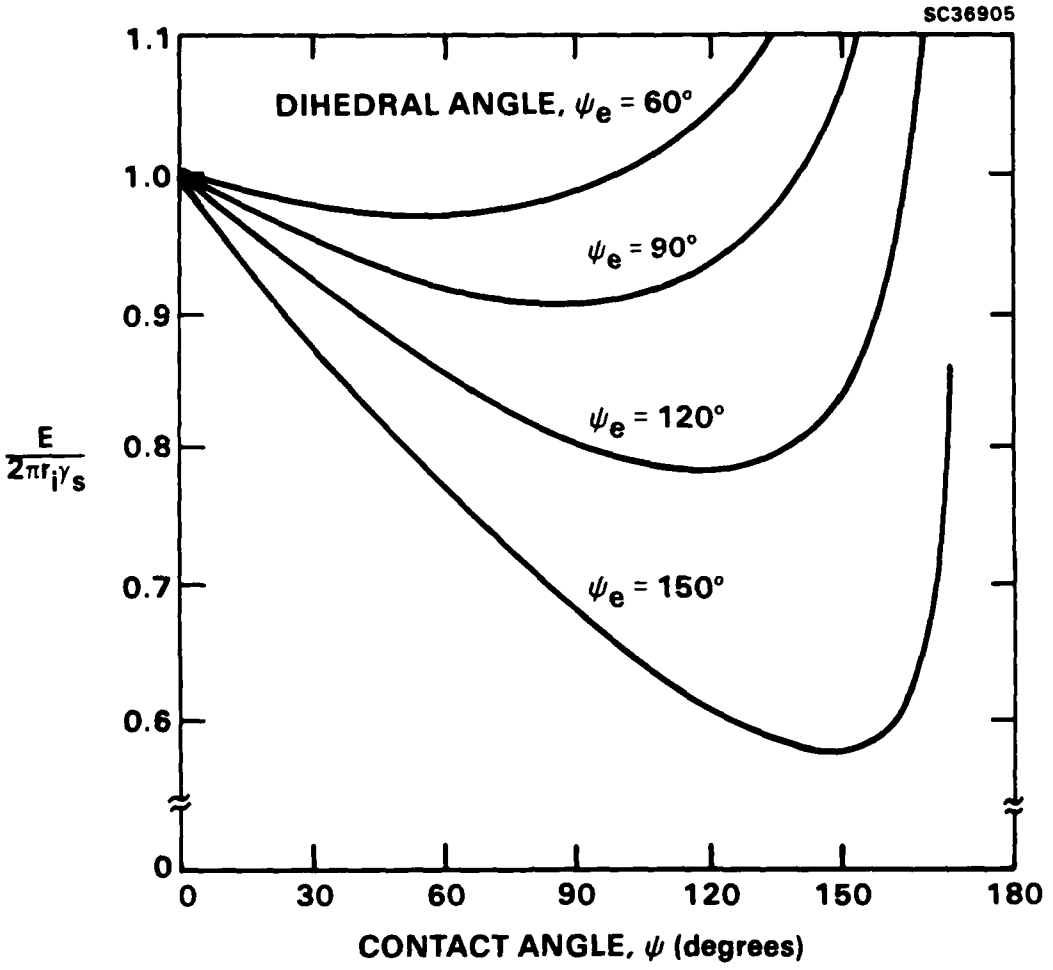

Fig. 2 Particle energy per unit cylinder length, normalized by the initial particle energy, for the linear array of cylinders, as a function of the contact angle (ψ), for different dihedral angles (ψ_e).

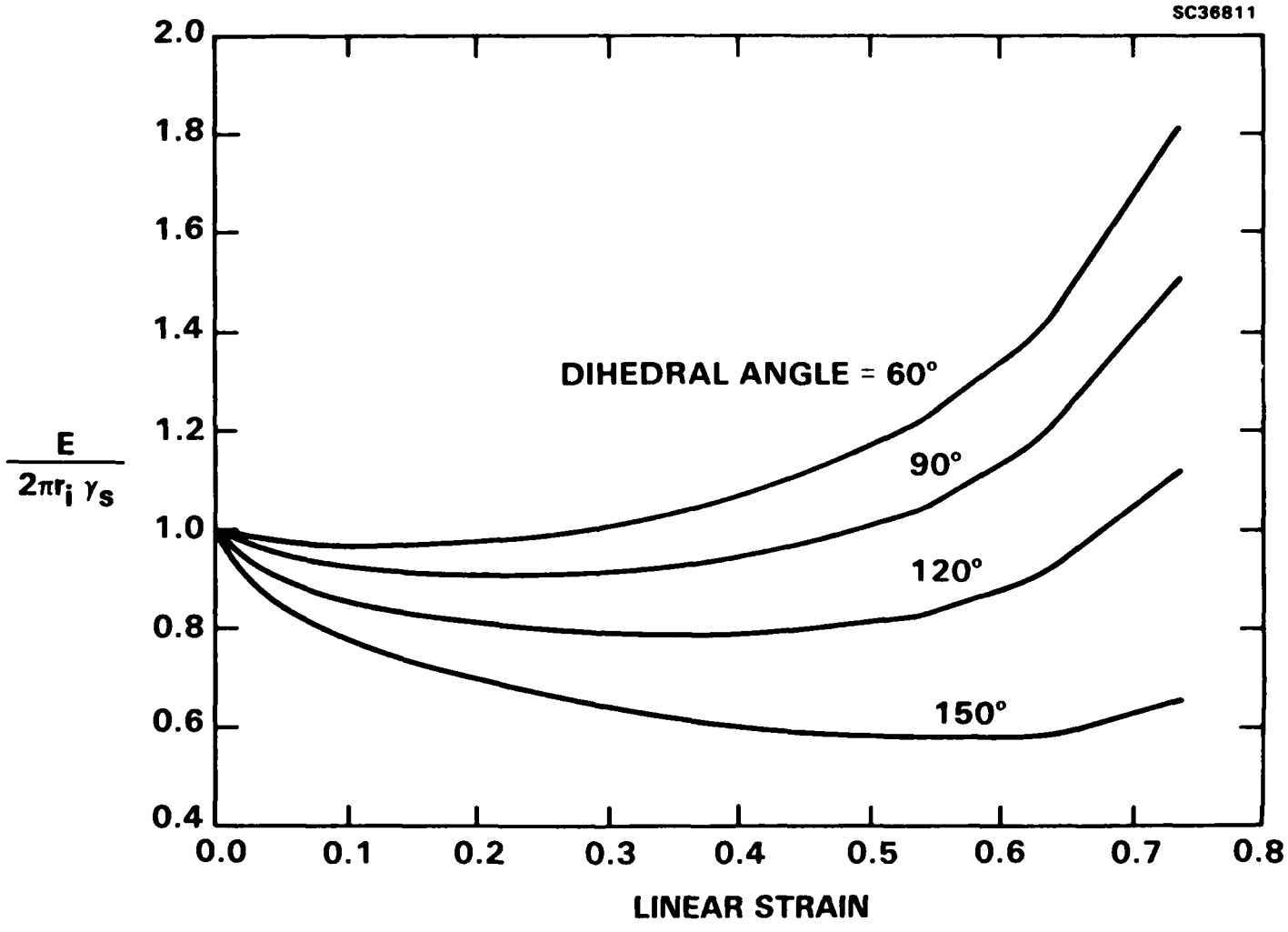

Fig. 3 Particle energy, normalized by the initial particle energy per unit cylinder length, as a function of particle-particle approach (expressed in engineering strain).

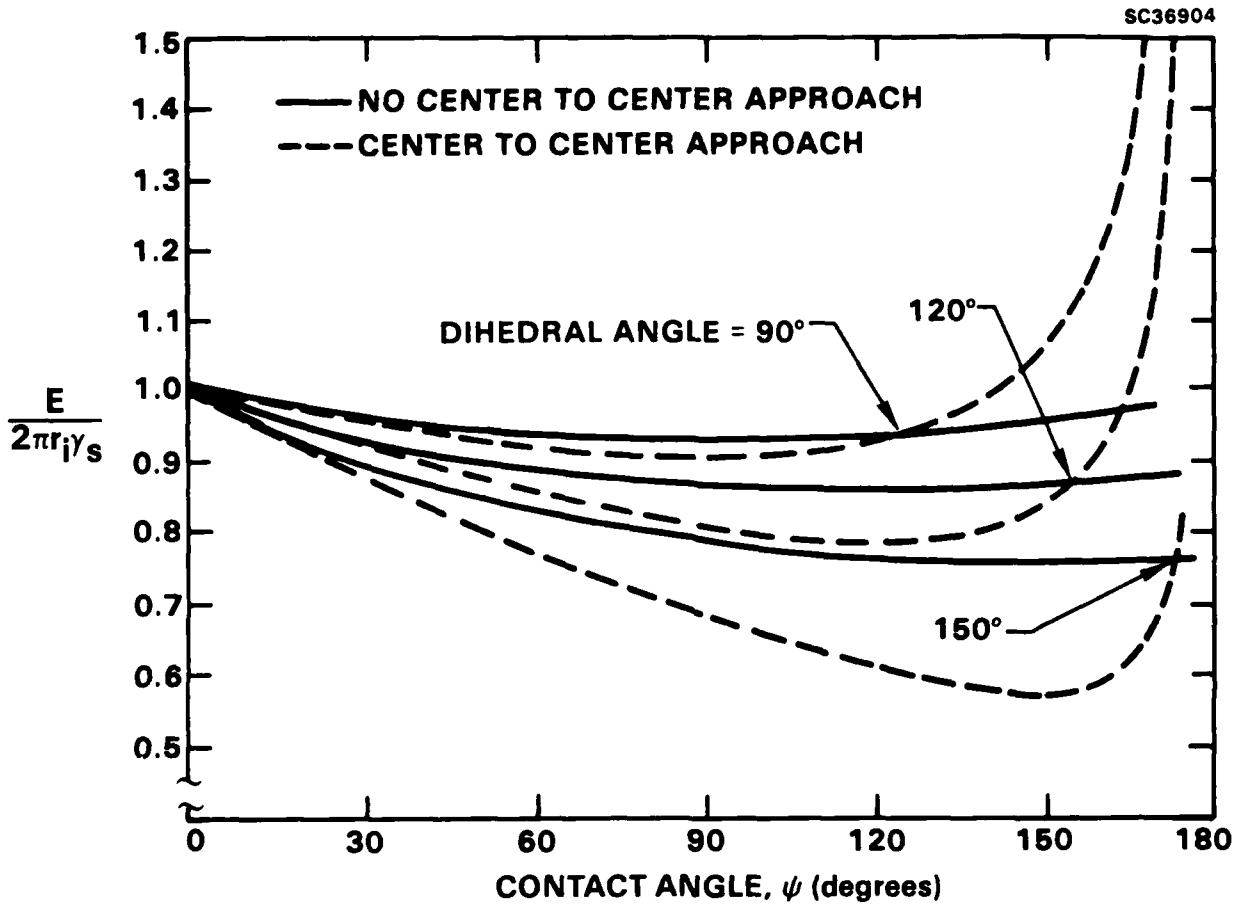

Fig. 4 Particle energy per unit cylinder length, normalized by the cylinder's initial energy, for a linear array of cylinders for the condition of particle-particle approach (dashed line) and no particle-particle approach (solid line), as a function of the contact angle (ψ), for different dihedral angles (ψ_e).

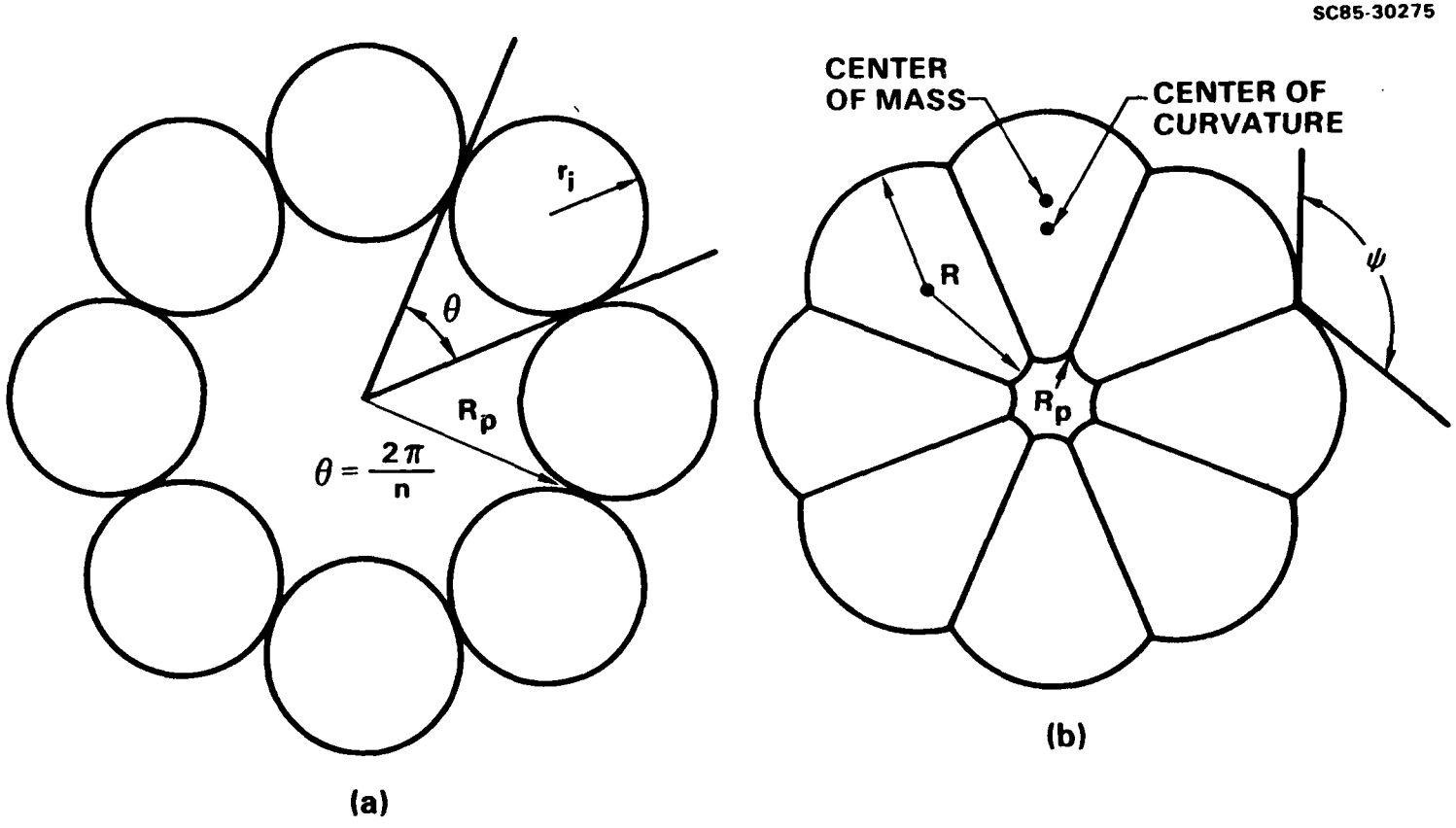

Fig. 5 Schematic of a ring of cylinders or spheres of coordination number n, a) initial, and b) at a condition defined by nonzero contact angle (ψ); where r_i is the initial particle radius, R_p is the circumscribed pore radius, and θ is the coordination angle.

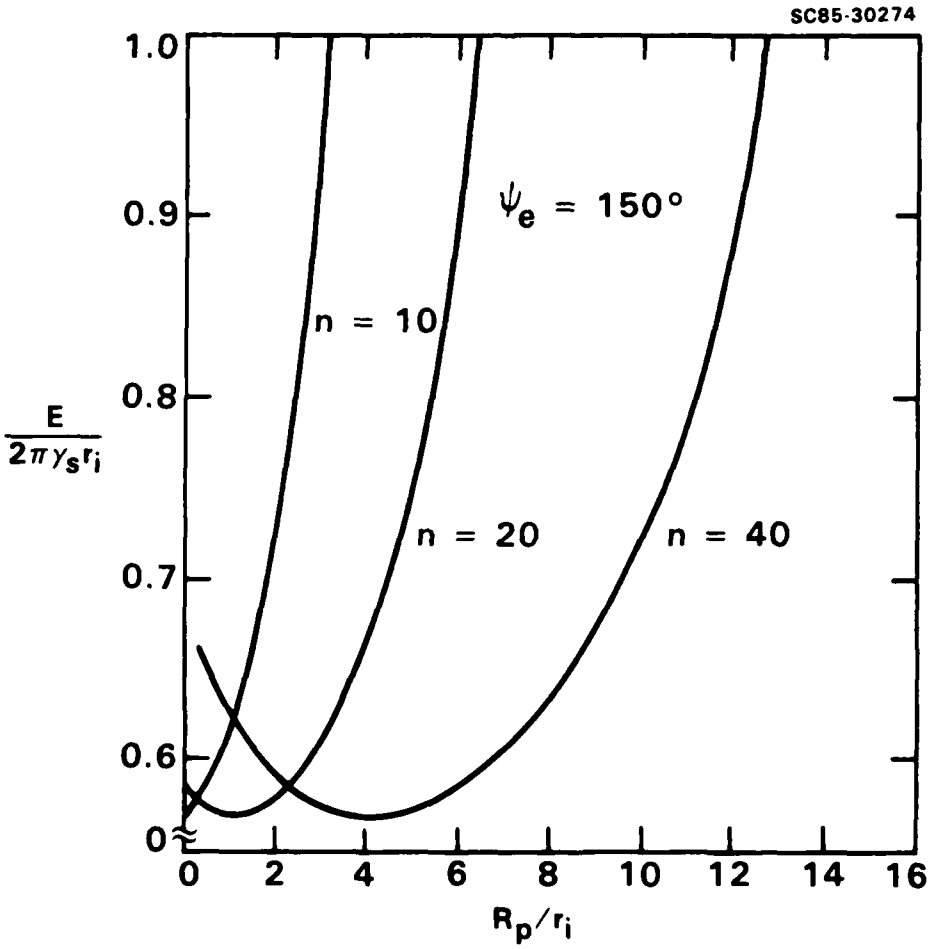

Fig. 6 Particle energy per unit length of cylinder, normalized by the initial energy of a cylinder, as a function of circumscribed pore radius (R_p), for different pore coordination numbers (n). Results are illustrated for a dihedral angle, $\psi_e = 150°$.

Fig. 7 Sintering stress, (σ_c), normalized by the surface energy per unit area (γ_s) and initial cylinder radius (r_j) as a function of the contact angle (ψ) for different dihedral angles (ψ_e).

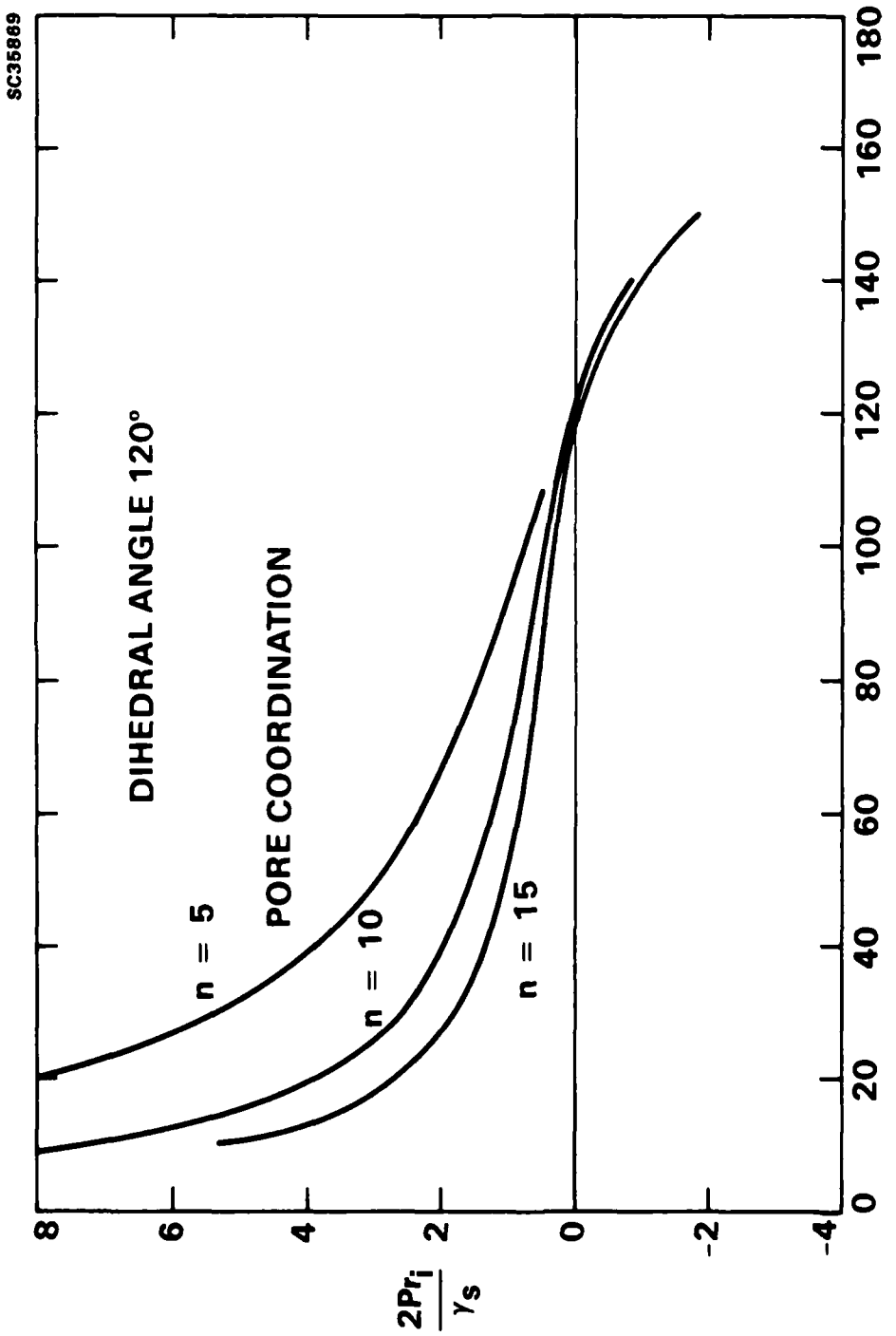

Fig. 8 Effective pressure on cylindrical array, (P), normalized by the surface energy per unit area (γ_s) and initial cylinder radius (r_i), to produce a stress equivalent to the "sintering stress," as a function of the contact angle (ψ), for different pore coordination numbers (n), and a dihedral angle $\psi_e = 120°$.

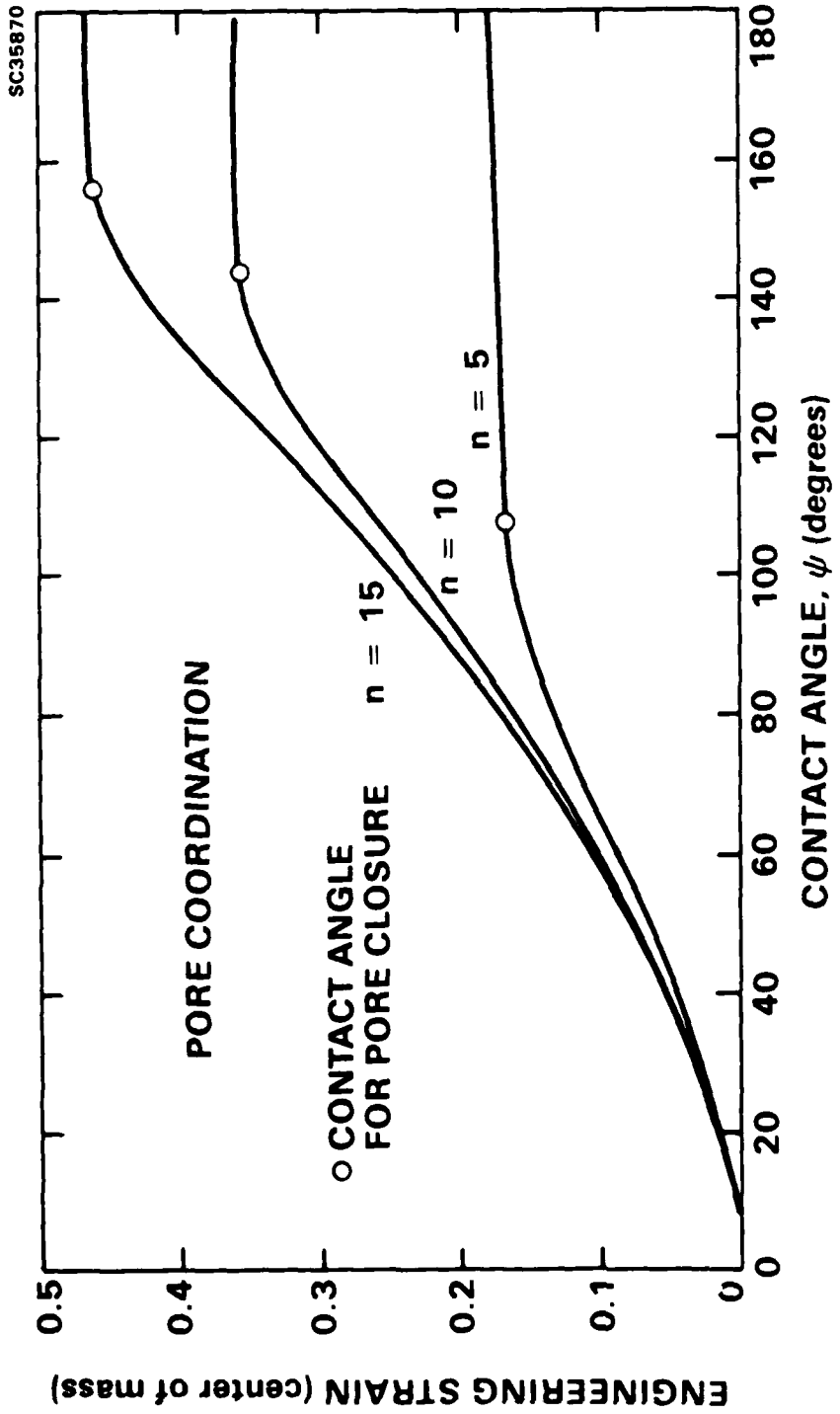

Fig. 9 Engineering strain of a ring of cylinders, calculated from a particles center-of-mass, as a function of the contact angle (ψ), for pore coordination n = 5, 10, 15.

APPENDIX 1

As was shown by Wulff,[20] the equilibrium configuration of an isolated particle can be determined from knowledge of its surface energies. Basically, the Wulff construction determines a particle's equilibrium shape as the interior envelope produced by perpendicular planes placed at the ends of the particle's surface energy vectors. These vectors emanate from a single point (Wulff point), and have an orientation perpendicular to the crystallographic planes they represent. The Wulff construction of a particle of isotropic surface energy is a sphere.

The Wulff construction of an array of identical particles (or any array which forms flat grain boundaries) can be equivalently determined,[21] with the condition that in the direction of the external surface the surface energy vector has magnitude $(\gamma_{s1} - \gamma_{s2} + \gamma_b/2)$, where γ_{s1} = surface energy of the particle, γ_{s2} = surface energy of the adjoining particle, and γ_b = common grain boundary energy.

APPENDIX 2

PARTICLE ENERGY FOR RING AND POLYHEDRON ARRAYS OF IDENTICAL SPHERES

The energy of particles in arrays formed by placing spheres in a ring and at the vertices of regular polyhedra have been calculated using the approach outlined in Section 2.1, and the four functions shown in Table 1. As outlined in Section 2.1 the energy per particle is given by $E = \gamma_s[A_s + 2A_b \cos(\psi_e/2)]$, where the surface area of a particle (A_s), area of the grain boundary (A_b), and particle radius (r), have been listed in Table 3 and 4 for the pertinent arrays.

The function $f_1(z)$ is used in defining the volume of a spherical segment, illustrated in Fig. A1(a), with a base radius of $r \sin(z/2)$. The function $f_2(x,y,z)$ helps define the volume, while function $f_3(x,y,z)$ is used to define the surface area, of the shaded segment shown in Fig. A1(a).[22] The angles x,y and z, shown in Fig. A1(a), will be related to specific arrays in the following paragraphs.

Function $f_4(\psi, n_p, \phi, \theta)$ has been used to define the volume of the pyramid with either a pentagon, square or triangular base (depending on polyhedra), as shown in Fig. A1(b). For polyhedra, it is necessary to determine this volume for array configurations in which the pore does not exist. The angles θ and ψ used in this function are schematically shown in Fig. A2 for a cubic polyhedron; values are listed by polyhedra in Table 2. Also listed in Table 2 is n_p, the number of touching particles surrounding each particle in the polyhedron.

Ring Array of Spheres

When a pore exists within the ring array of spheres ($\psi + 2\pi/n < \pi$), the particle radius (r), surface area (A_s) and grain boundary area (A_b) are simply stated as a function of the contact angle (ψ), as written in Table 3.

For conditions where the pore does not exist ($\psi + 2\pi/n \geq \pi$) the geometry becomes more complicated because all particles penetrate one another.

The particle's radius (r) is calculated using functions $f_1(z)$ and $f_2(x,y,z)$, and the particle's surface area (A_s) is determined using the function $f_3(x,y,z)$. For ring arrays the three angles are given by:

$$x = \gamma = 2 \arccos\left(\frac{1}{\tan\frac{\pi}{n}\tan\frac{\psi}{2}}\right) \quad ,$$

$$y = 2\pi/n \quad , \tag{A1}$$

and

$$z = \psi \quad .$$

The grain boundary area (A_b) is calculated using the contact angle (ψ), the angle γ (given by Eq. (A1)), and the particle's radius (r).

Polyhedron Arrays

For polyhedra the calculations of A_s, A_b, and r are best divided into different ranges of the contact angle (ψ), which describes different configurations of the polyhedron. When $\psi < \pi - 2\pi/n_f$ the pore within the polyhedron is connected to the external surface by a number of channels equal to the number of faces on the polyhedra. The number of particles coordinating a channel n_f, listed in Table 2, is equal to the number of particles on a polyhedron face. Channels close when $\psi = \pi - 2\pi/n_f$ creating an isolated pore, and the pore disappears when $\psi = \pi - 2\theta$ (θ are listed in Table 2) resulting in a fully dense configuration.

For the open pore configuration ($\psi < \pi - 2\pi/n_f$) the particle radius (r), listed in Table 4, is calculated using $f_1(z = \psi)$, and n_p. Particle surface area (A_s) and grain boundary area (A_b), listed in Table 4, are simply stated as a function of r, n_p, and ψ.

The closed pore configuration occurs for contact angles within the range $\pi - 2\pi/n_f < \psi < \pi - 2\theta$. Particle radius (r), given in Table 4, is calculated using function f_1 ($z = \psi$) and f_2 ($x = \gamma$, $y = 2\pi/n_f$, $z = \psi$), where

$$\gamma = 2 \arccos \left(\frac{\sin \phi}{\tan \theta \tan \frac{\psi}{2}}\right) \quad . \tag{A2}$$

Particle surface area (A_s) has been calculated using function f_s ($x = \gamma$, $y = 2\pi/n_f$, $z = \psi$) and n_p. The grain boundary area (A_b) is a simple function of previously described variables.

Geometrical calculations become more tedious with pore closure ($\psi > \pi - 2\theta$), but generally the equations for the particle radius (r) and surface area (A_s) fall within three regimes dependent upon the contact angle. A single equation describes the grain boundary area per particle (A_b) for the three regimes (see Table 4).

For the three different regimes r, A_s, and A_b is calculated using functions $f_1(z = \psi')$, $f_1(z = \psi)$, $f_2(x = \beta, y = \eta, z = \psi)$, $f_2(x = 2\pi/n_p, y = \eta', z = \psi')$, $f_3(x = \beta, y = \eta, z = \psi)$, $f_3(x = 2\pi/n_p, y = \eta', z = \psi')$ and $f_4(\theta, \psi, n_p, \phi)$. The functional variables are listed below:

$$\psi' = \pm 2 \arccos \left[\pm \left(\cos \frac{\psi}{2} \frac{\sin^2 \zeta}{\sin \theta} - \cos \zeta \sqrt{\sin^2 \frac{\psi}{2} - \frac{\sin^2 \phi \cos^2 \frac{\psi}{2}}{\tan^2 \theta}} \right) \right] \tag{A3}$$

(Angles ψ, θ, ζ are listed by polyhedron in Table 2, with the terms negative for the condition $\cos(\psi/2) < \sin\theta/\tan\zeta$.)

$$\eta' = 2 \arctan \left(\frac{1}{\tan \frac{\psi'}{2} \cos \frac{\pi}{n_p}} \right) \tag{A4}$$

$$\eta = \pi + \eta' - 2\theta \tag{A5}$$

(except for the tetrahedron when $\psi < \frac{\pi}{2}$, then $\eta = \pi - \eta' + 2\theta$)

$$\beta = 2 \arccos \left(\frac{1}{\tan \frac{\eta}{2} \tan \frac{\psi}{2}} \right) \tag{A6}$$

Table 1

$$f_1(z) = \frac{2}{3} - \cos\frac{z}{2} + \frac{1}{3}\cos^3\frac{z}{2}$$

$$f_2(x,y,z) = \cos\frac{z}{2}\left[\sin^2\frac{z}{2}\sin x - x\left(3 - \cos^2\frac{z}{2}\right)\right] + 4\arcsin\left(\sin\frac{x}{2}\sin\frac{y}{2}\right)$$

$$f_3(x,y,z) = 4\arcsin\left(\sin\frac{x}{2}\sin\frac{y}{2}\right) - 2x\cos\frac{z}{2}$$

$$f_4(\psi,n_p,\phi,\theta) = \frac{n_p}{3\tan\theta\tan\left(\frac{\pi}{2} - \frac{\pi}{n_p}\right)}\left(\cos\frac{\psi}{2}\cos\theta + \cos\phi\sqrt{\sin^2\frac{\psi}{2}\sin^2\theta - \cos^2\frac{\psi}{2}\sin^2\phi\cos^2\theta} - \sin^2\phi\cos\frac{\psi}{2}\cos\theta\right)^3$$

Table 2

Polyhedron	Pore Coordination (n)	Channel Coordination (n_f)	Particle Coordination (n_p)	ϕ	θ	ζ
Tetrahedron	4	3	3	54.73	54.73	70.527
Octahedron	6	3	4	35.264	45	54.736
Cube	8	4	3	45	35.264	54.736
Icosahedron	12	3	5	20.908	31.721	37.38
Dodecahedron	20	5	3	31.717	20.905	37.38

Table 3

Sphere Ring Array

$\psi + \frac{2\pi}{n} < \pi$	$\psi + \frac{2\pi}{n} > \pi$
$r = r_i\left[\frac{\cos\frac{\psi}{2}}{2}\left(3 - \cos^2\frac{\psi}{2}\right)\right]^{-\frac{1}{3}}$	$= r_i\left(1 - \frac{3}{2}f_1(\psi) + \frac{1}{4\pi}f_2\left(\gamma, \frac{2\pi}{n}, \psi\right)\right)^{-\frac{1}{3}}$
$A_s = 4\pi\cos\frac{\psi}{2}\, r^2$	$= 4\pi\left[\cos\frac{\psi}{2} + 2f_3\left(\gamma, \frac{2\pi}{n}, \psi\right)\right] r^2$
$A_b = \pi\sin^2\frac{\psi}{2}\, r^2$	$= \sin^2\frac{\psi}{2}\left(\pi - \gamma + \sin\gamma\right) r^2$

Table 4

Polyhedra

Open Pore	Closed Pore
$\psi < \pi - \frac{2\pi}{n_f}$	$\pi - \frac{2\pi}{n_f} \leq \psi < \pi - 2\theta$
$r = r_i\left[1 - n_p \frac{3}{4} f_1(\psi)\right]^{-\frac{1}{3}}$	$= r_i\left[1 - n_p\frac{3}{4} f_1(\psi) + \frac{n_p}{4\pi} f_2(\gamma, \frac{2\pi}{n_f}, \psi)\right]^{-\frac{1}{3}}$
$A_s = 2\pi r^2\left[2 - n_p(1 - \cos\frac{\psi}{2})\right]$	$= 2\pi r^2\left[2 - n_p\left(1 - \cos\frac{\psi}{2} - \frac{1}{2\pi} f_3\ (\gamma, \frac{2\pi}{n_f}, \psi)\right)\right]$
$A_b = \frac{n_p}{2}\pi r^2 \sin^2\frac{\psi}{2}$	$= \frac{n_p}{2} r^2 \sin^2\frac{\psi}{2}(\pi - \gamma + \sin\gamma)$

Tetrahedron

$\pi - 2\theta \leq \psi \leq 90$

$$R = r_i\left(\frac{4\pi}{3}\right)^{\frac{1}{3}}\left[\frac{4\pi}{3} - \pi f_1(\psi') - 3\pi f_1(\psi) + \frac{1}{2}\left(f_2(\beta, \eta, \psi) + f_2(\frac{2\pi}{n_p}, \eta', \psi')\right) + f_4(\theta, \psi, n_p, \phi)\right]^{-\frac{1}{3}}$$

$$A_s = 2\pi R^2\left[1 + \cos\frac{\psi'}{2} - n_p(1 - \cos\frac{\psi}{2}) + \frac{n_p}{4\pi}\left(f_3(\beta, \eta, \psi) + f_3(\frac{2\pi}{n_p}, \eta', \psi')\right)\right]$$

$$A_b = \frac{n_p}{2} R^2\left[\sin^2\frac{\psi}{2}(\pi + 2\phi - \gamma + \sin\gamma) + \cos^2\frac{\psi}{2}\frac{\sin(2\phi)}{\tan^2\theta}\right]$$

Table 4
(Continued)

Polyhedra

$$\frac{\pi}{2} - \theta < \frac{\psi}{2} < \arccos\left(\frac{\sin\theta}{\tan\zeta}\right)$$

$$R = r_i\left(\frac{4\pi}{3}\right)^{\frac{1}{3}}\left[f_4(\theta, \psi, n_p, \phi) + \frac{4\pi}{3} - \pi f_1(\psi') - \frac{n_p}{6}\left(f_2(\beta, \eta, \psi) - f_2\left(\frac{2\pi}{n_p}, \eta', \psi'\right)\right)\right]^{-\frac{1}{3}}$$

$$A_s = R^2\left[2\pi\left(1 + \cos\frac{\psi'}{2}\right) - \frac{n_p}{2}\left(f_3(\beta, \eta, \psi) - f_3\left(\frac{2\pi}{n_p}, \eta', \psi'\right)\right)\right]$$

$$A_b = \frac{n_p}{2}R^2\left[\sin^2\frac{\psi}{2}(\pi + 2\phi - \gamma + \sin\gamma) + \cos^2\frac{\psi}{2}\frac{\sin(2\phi)}{\tan^2\theta}\right]$$

Polyhedra

$$\frac{\psi}{2} > \arccos\left(\frac{\sin\theta}{\tan\zeta}\right)$$

$$R = \left(\frac{4\pi}{3}\right)^{\frac{1}{3}}\left[f_4(\theta, \psi, n_p, \phi) + \pi f_1\left(\frac{\psi'}{2}\right) - \frac{n_p}{6}\left(f_2(\beta, \eta, \psi) + f_2\left(\frac{2\pi}{n_p}, \text{abs}(\eta'), \psi'\right)\right)\right]^{-\frac{1}{3}}$$

$$A_s = R^2\left[2\pi\left(1 - \cos\frac{\psi'}{2}\right) - \frac{n_p}{2}\left(f_3(\beta, \eta, \psi) + f_3\left(\frac{2\pi}{n_p}, \text{abs}(\eta'), \psi'\right)\right)\right]$$

$$Ab = \frac{n_p}{2}R^2\left[\sin^2\frac{\psi}{2}(\pi + 2\phi - \gamma + \sin\gamma) + \cos^2\frac{\psi}{2}\frac{\sin(2\phi)}{\tan^2\theta}\right]$$

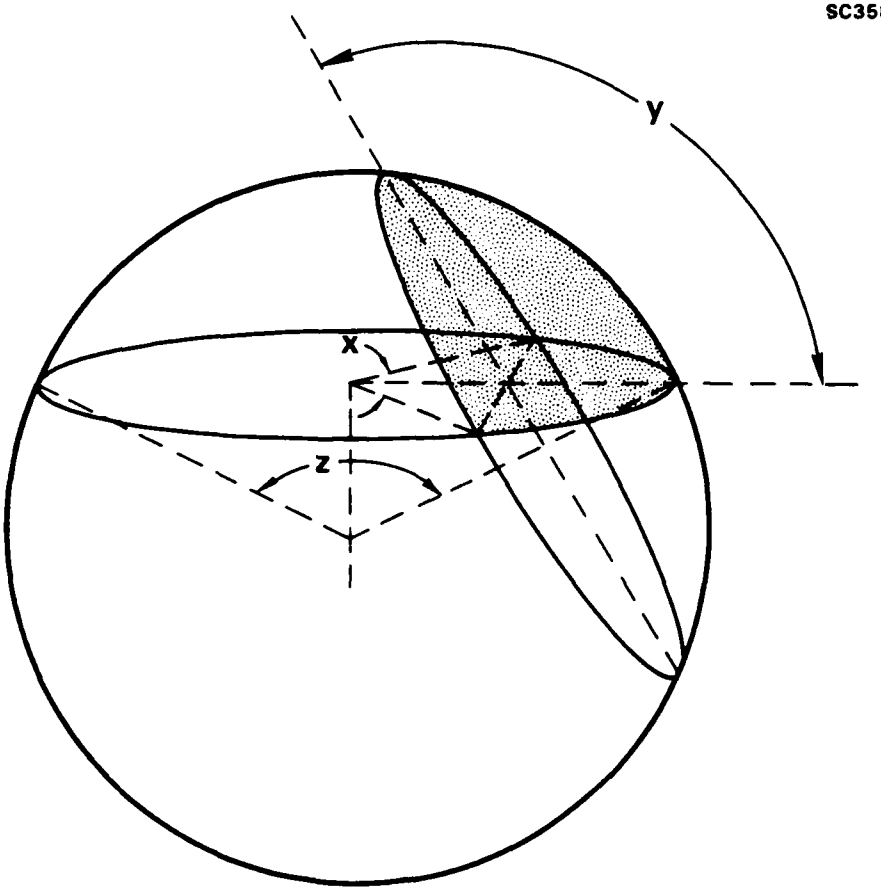

(a)

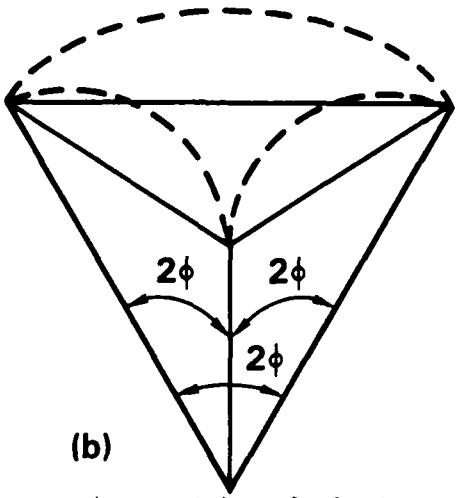

(b)

Fig. A.1 a) Angles x, y and z used in calculating the surface area and volume of the shaded spherical segment, and b) a schematic of the triangular pyramid that needs to be calculated for a dodecahedron array after pore closure.

SC35892

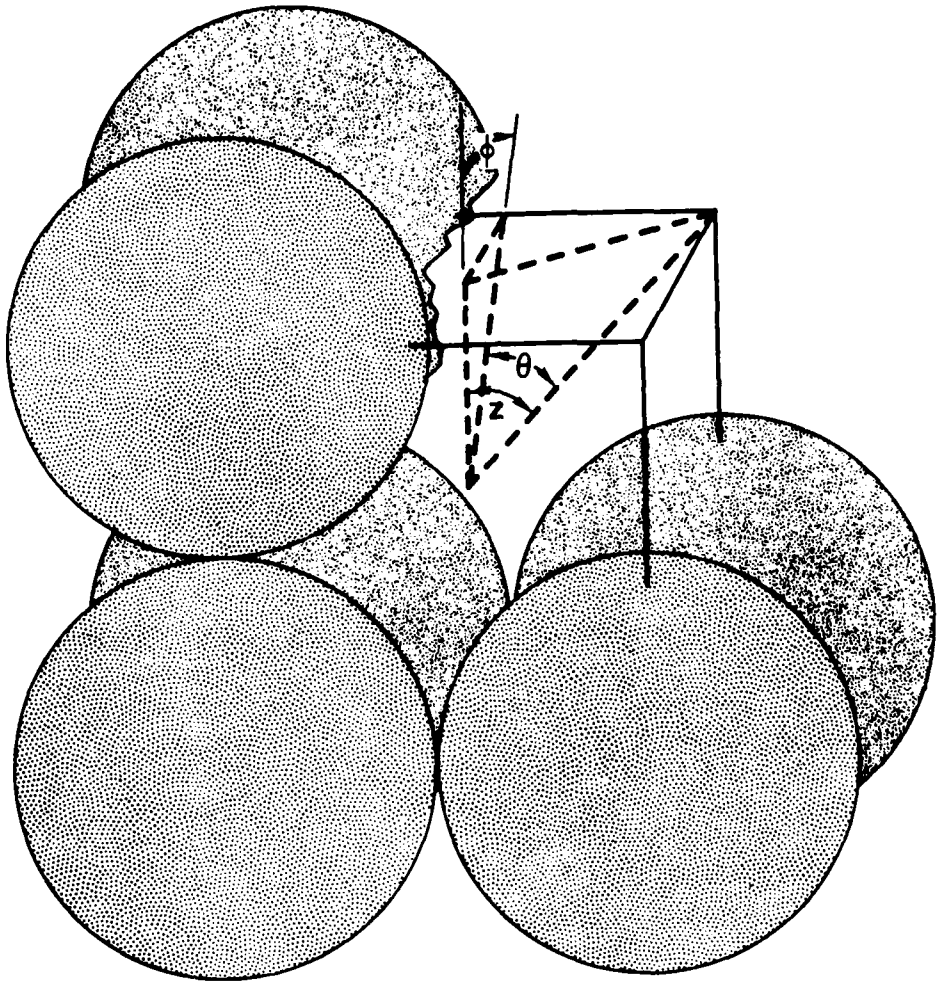

Fig. A.2 Schematic representation of angles ϕ, θ and ξ for a cubic polyhedron.

SC5410.FR

THERMODYNAMICS OF DENSIFICATION, PART II: GRAIN GROWTH IN POROUS COMPACTS AND RELATION TO DENSIFICATION

F.F. Lange and B. Kellett

Rockwell International Science Center
1049 Camino Dos Rios
Thousand Oaks, CA 91360

THERMODYNAMICS OF DENSIFICATION , PART II: GRAIN GROWTH IN POROUS COMPACTS AND RELATION TO DENSIFICATION

F.F. Lange and B. Kellett*

Rockwell International Science Center
1049 Camino Dos Rios
Thousand Oaks, CA 91360

Abstract

It is shown that grain boundary motion in a sintering array of particles can be limited by geometry. Despite its curvature, the grain boundary can encounter an energy barrier if it were to move through the smaller grain. This energy barrier decreases to zero when the radius ratio (R) between adjacent grains approaches a critical value, $R \rightarrow R_c = -(\cos(\psi_e))^{-1}$, where ψ_e is the dihedral angle relating surface and grain boundary energies. The change in radius ratio ($R \rightarrow R_c$) occurs by interparticle mass transport, driven by the differential surface curvature of the adjacent grains. This result suggests that grain growth within a sintering array primarily occurs by interparticle mass transport making it distinctly different from grain growth in the fully dense material.

More significantly, it is shown that when a grain disappears from between other grains, the driving force for mass transport to the newly formed region between the remaining grains is reinitiated, i.e., the angle formed

*Department of Materials Sciences
University of California at Los Angeles

where the grain boundary meets the surfaces is smaller than the equilibrium (dihedral) angle. That is, grain growth via interparticle mass transport and boundary motion can continually drive sintering and array shrinkage. It is shown that the interparticle mass transport phenomenon causing grains to disappear and their neighbors to grow does not lead to array shrinkage when $\psi_e \geq 130°$, but can lead to significant shrinkage via the sintering of remaining neighbors. Thus, array shrinkage and densification is predictably related to grain growth. It is shown that the relative density of a ring of spheres that undergoes cyclic sintering and grain growth is nearly linearly related to grain size. Conceptual relations between density and grain growth for real powder compacts are discussed and related to the function that describes the compact's distribution of pore coordination numbers. Finally, since interparticle mass transport producing grain growth can be the rate-limiting step for densification, the theory and related experiments associated with densification kinetics should be reevaluated.

1.0 INTRODUCTION

Grain growth in dense materials is associated with grain boundary curvature. Due to curvature, the chemical potential is greater on one side, causing atoms or ions to hop across. Because hopping (diffusion) distances are very small, boundary motion can be rapid. Grain growth also occurs during the densification of a powder compact. Greskovich and Lay[1] have observed the growth

of grains in Al_2O_3 powder compacts with initial bulk densities as low as 30% of theoretical, e.g., upon densification from 30 to 40% of theoretical, grains grow from 0.3 μm to 0.5 μm. Their observations indicated that boundaries will only move after necks have fully formed between the sintering particles. Gupta's[2] analysis of literature data for Cu, Al_2O_3, BeO, and ZnO showed that grain size increased very slowly during most of the densification process, but increased very rapidly once the compact's density was ≥ 90 % of theoretical. He also stated that within the regime of slow grain growth, the grain size is linearly proportional to density and independent of the sintering temperature. Bruch[3] also showed that the grain size was only dependent on density and independent on temperature. These combined observations strongly suggest that (a) grain growth occurs after a substantial amount of mass transport has occurred to form necks, (b) grain growth within the partially sintered body appears not to be thermally activated, but depends only on density, and (c) grain growth and densification are, in some way, intimately related.

In a previous paper, Kellett and Lange[4] calculated the free energy and shrinkage of symmetric rings and/or regular polyhedra of identical particles (cylinders and spheres) that were allowed to develop an equilibrium configuration by sintering. Each array contains a single pore. Configurational changes occurred when mass was transported to the contact region increased the contact area (grain boundary) between the initially touching particles. To allow tractable analytical calculations, it was assumed that the curvature of the particle's surface was independent of surface position. That is, the surfaces of spheres remained spherical, but increased their radius to conserve mass

as the particle penetrated one another. It was also assumed that each particle would undergo identical shape changes. This assumption implicitly requires no net transport of mass between particles and that grain boundaries remain planar. The free energy per particle was determined as a function of array's configurational change by summing the energies associated with its surface and grain boundaries. Young's equation was used to equate the grain boundary energy per unit area to the particle's external surface energy per unit area. The angle, ψ, defined by the tangents to the free surface where the grain boundary meets the free surface, was used to define the configurational change (ψ = 0 when the particles are just touching and increases as the spheres penetrate one another).

The results pertinent to this paper are: the free energy of the arrays depends on configuration (defined by ψ) and exhibits a minimum when the contact angle equals the dihedral angle ($\psi = \psi_e$); the dihedral angle is defined by the surface to grain boundary energy ratio through Young's equation. When the array's coordination number exceeds a critical value ($n > n_c$) the equilibrium configurations still contain a pore, i.e. the pore shrinks to an equilibrium size. When $n \leq n_c$, the pore disappears as the array shrinks to its equilibrium configuration; n_c increases with the dihedral angle. The same result concerning pore stability/disappearance is reached when an isolated pore in a finite polycrystalline body is analyzed by a similar method, e.g., the isolated pore will be stable when the surface curvature of the grains surrounding the pore is identical to the surface curvature of grains on the external surface.[5]

In another paper,[5] it was hypothesized that grain growth would decrease the coordination number of stable pores to the condition where they would be

thermodynamically unstable and disappear (i.e., where $n \leq n_c$). This hypothesis was tested by studying the grain growth required to eliminate mono-sized spherical voids in an otherwise dense body. The spherical voids were produced by incorporating plastic spheres into the powder compact prior to sintering. It was observed that the number density of spherical voids decreased with grain growth, whereas the voids that remained after a given period of grain growth did not change in size. These observations are consistent with the initial hypothesis, suggesting that grain growth was helpful in eliminating thermodynamically stable voids.

The object of this paper is to examine the conditions for grain growth in a powder compact and to relate this grain growth phenomena to the compact's sintering behavior. Arrays of spheres will be used to examine the conditions for grain growth, and densification produced by grain growth in a similar manner used previously.[5] It will be shown that (1) grain growth in a powder compact is not a simple matter of boundary motion, (2) grain growth reinitiates sintering and therefore densification, and (3) the amount of grain growth required to produce a dense body is related to the pore coordination number distribution within the initial powder compact.

2.0 CONFIGURATIONAL CHANGES FOR GRAIN BOUNDARY MOTION

In the current work, the initial mass of adjoining particles will be different, producing differential free energies and the development of nonplanar

grain boundaries. The object of this section is to examine the configurational change required to produce an incremental decrease in free energy for an incremental displacement of the grain boundary, i.e., the configuration where grain boundary motion will continually decrease the free energy of the system.

In temperature regimes for mass transport, the net negative curvature that develops at the contact position between touching particles results in a large chemical potential difference, relative to other surface regions, and thus a large driving force for material transport to the region where the particles touch and a grain boundary develops. Mass transported to the contact (or neck) region can primarily come from one of the adjoining particles if their initial free energies (i.e., surface curvatures) are very different, or from both particles. When the size of the adjoining particles are different, their differential surface curvature can also result in interparticle mass transport. But, because the driving force causing mass transport to the neck region is much greater, it might be assumed little net transport between the particles will occur until the driving force to the neck region is dissipated through configurational change. For this reason, although intraparticle transport producing neck growth (sintering) and interparticle transport producing grain growth may be concurrent within a powder compact, one might expect that when the driving force exists, mass transport to the neck region will dominate relative to mass transport between particles.

For all arrays considered, it is assumed that the curvature of each particle's surface is independent of surface position, e.g., spherical surfaces remain spherical. With this assumption, touching spheres within the array change their configuration by penetrating one another. As they penetrate, their

radii change either to conserve their mass (condition of intraparticle mass transport) or change their mass as one particle grows at the expense of a neighboring particle (interparticle mass transport). Although this type of configurational change is not theoretically expected or experimentally observed during the initial stages of neck growth (changes are much more rapid closer to the neck region), it does approximate the real situation and allows tractable analytical calculations.

2.1 Two Particles

Figure 1 illustrates the expected configurational change for two touching spheres with the assumptions that mass is only transported to the neck region. As detailed elsewhere,[4] the contact angle, ψ, is a convenient parameter to describe the configurational change. When the spheres are just touching, $\psi = 0$. A previous analysis has shown that the particles will interpenetrate until the contact angle equals the dihedral angle, i.e., $\psi = \psi_e$. Because each particle conserves its mass, each increases its radius of curvature. Using the geometric parameters shown in Fig. 2a, the radius of each particle ($r_{1,2}$), normalized by its initial radius ($r_{i1,2}$) can be determined using the following equations:

$$R_1 = r_1/r_{i1} = [1-0.25(1 - \cos\theta_1)^2(2 + \cos\theta_1) + 2(\frac{R}{R-1})^3\cos^3(\psi/2)(1 - \cos\phi)^2(2 + \cos\phi)]^{-1/3} \qquad (1)$$

$$R_2 = r_2/r_{i2} = [1 - 0.25\,(1 - \cos\theta_2)^2(2 + \cos\theta_2)$$

$$- \frac{2}{(R-1)^3}\cos^3(\psi/2)(1 - \cos\phi)^2(2 + \cos\phi)]^{-1/3} \qquad (2)$$

where $\theta_1 = \arctan\left(\frac{R\sin\psi}{R\cos\psi + 1}\right)$

$$\theta_2 = \psi - \theta_1$$

$$\phi = \theta_1 - \psi/2.$$

R defines the radius ratio of the two particles ($R = r_2/r_1$) during their configurational change. The initial radius ratio ($R_i = r_{i2}/r_{i1}$) can be calculated using

$$R_i = R\,(R_1/R_2). \qquad (3)$$

The radius of curvature for the grain boundary is given by

$$r_b = 2r_1r_2/(r_2 - r_1)\cos(\psi/2) = [2r_2/(R - 1)]\cos(\psi/2). \qquad (4)$$

Before we examine the configurational changes produced by mass transport between the particles, let us examine the conditions for grain boundary motion that can produce a continuous decrease in the system's free energy.

Figure 1 shows that one of two configurations can be reached when $\psi = \psi_e$. The upper configuration (c) occurs when $R < -(\cos(\psi_e))^{-1}$. For this configuration, the two particles could lower their free energy by allowing the grain boundary to become planar, but if the boundary were to move through the smaller grain, it would have to increase its area and thus the free energy of the system. That is, an energy barrier exists for grain boundary motion when particles develop configuration (c) during sintering. Configuration (d), occurs when $R \geq -(\cos(\psi_e))^{-1}$. Here it is obvious that the grain boundary can move through the smaller particle and decrease its surface area (and the free energy of the system) either with or without changing its curvature. From this configuration, grain boundary motion will cause a continuous decrease in free energy. This configuration occurs when the size ratio of the particles, developed during the configurational change, satisfies the relation

$$R = R_c = -(\cos(\psi))^{-1}, \tag{5}$$

where R_c is the critical radius ratio which allows the grain boundary to move through the smaller grain and continually decrease its surface area.

Figure 2b details the geometry for the condition which just allows the grain boundary to move through the smaller grain without encountering an energy barrier. Note that for this special configuration, the center of curvature of the smaller grain lies on the imaginary plane (broken line in Fig. 2b) separating the two grains. Also, for this configuration the radius of curvature of the grain boundary is given by

$$r_g' = -r_2(\cos\psi/\cos(\psi/2)). \quad (6)$$

Thus, it can concluded that when the size ratio of the two particles becomes greater than the critical ratio, i.e., $R \geq R_c = -(\cos(\psi_e))^{-1}$, the grain boundary can move through the small grain and continuously decrease the free energy of the system without mass transport between the two particles. Figure 3 illustrates the critical size ratio (expressed as the initial size ratio, R_i) as a function of the dihedral angle (ψ_e). For dihedral angles ranging from 100-150°, the initial particle size ratio, which can cause the grain boundary to spontaneously move through the small grain, decreases from 6.6 to 1.1.

Figure 1(c) shows that the differential free energy produced by the different particle curvatures can cause mass to be transported from the smaller to the larger particle. During interparticle mass transport, the radius of the larger particle increases as that of the smaller decreases. Since material has already been transported to the neck region, the dihedral angle remains constant. The increase in the radius ratio will cause $R \rightarrow R_c$ shown by step (d), Fig. 1, and the condition when the grain boundary can move through the smaller grain while decreasing the free energy of the system. Once the grain boundary has disappeared leaving the unusually shaped single grain (step (e), Fig. 1) it can further decrease its free energy by spheridizing.

2.2 Three Particles

Three touching spheres can be arranged such that their centers are either colinear or noncoliner. Configurational changes will be considered for both cases since they produce simply visualized results pertinant to arrays that enclose void space.

2.2.1 Three Colinear Particles

Two of the three particles are assumed to be identical. The case where the third particle is larger and sandwiched between the two smaller particles is nearly identical to the case for the two particles considered above. The radius of the sandwiched particle increases more rapidly with changing ψ because of the two interpenetrating smaller particles. The radius ratio where the boundaries can move through the small grains will still be defined by Eq. (5), but this will be developed by a somewhat smaller initial radius ratio than for the case of the two spheres.

The most interesting case is where a smaller particle is sandwiched by two larger particles schematically shown in Fig. 4. We will only detail the case where $R \leq R_c = -(\cos(\psi_e))^{-1}$. Configurational changes from where the particles are touching ($\psi = 0$) to where $\psi \rightarrow \psi_e$ are shown in steps (a) to (b) in Fig. 4. This configurational change, developed by mass transport to the neck region is similar to that for the two particles except that since the smaller particle is penetrated by two particles its radius ratio increases more rapidly with ψ (while conserving its mass). The radius of the grain boundaries is given by Eq. (4). Step (b) represents the configuration where the driving force for mass transport to the neck region has diminished to

zero, i.e., the equilibrium contact angle (ψ_e) has been achieved. In this configuration, an energy barrier exists for grain boundary motion.

Interparticle diffusion, driven by the differential surface curvature between the smaller and larger grains, will increase the radius ratio and result in the configuration shown by step (c), Fig. 4. This configuration develops when the radius ratio increases to $R = R_c = -(\cos(\psi_e))^{-1}$, i.e., the condition found for two particles where the grain boundary could move without encountering an energy barrier. It should be noted that when $R = R_c$, the two larger particles just touch one another but are still separated by the smaller grain (shown by broken lines). It can be shown (see Fig. 6, $\beta = \pi$) that the contact angle between the two larger particles is given by

$$\psi = 2\psi_e - \pi. \tag{7}$$

Both grain boundaries can move without encountering an energy barrier to produce a single boundary that separates the two larger grains, as shown by step (c), Fig. 4. Since the contact angle developed between the larger grains by interparticle mass transport is less than the dihedral angle, viz., $\psi = 2\psi_e - \pi < \psi_e$, a new driving force exists for mass transport to the neck region between the larger particles. Further mass transport to the neck region will cause $\psi \rightarrow \psi_e$ and the development of the stable configuration shown by step (d), Fig. 4.

This simplistic analysis illustrates that the disappearance of the smaller grain from between the larger grains produces a condition for mass transport to the neck region between the larger grains. That is, grain growth

produced by interparticle mass transport can reestablish the stronger driving force for sintering.

2.2.2 Three Noncolinear Particles

Figure 5 illustrates the configurational change for the case where the three particles are noncolinear and the smaller particle separates the two, larger identical particles; β defines the angle between the centers. Configuration (b) is produced as the contact angle increases and the distance between the larger and smaller particles decreases due to mass transport to the neck regions. As the contact angle continues to increase, a special configuration can be produced where the two larger spheres just touch one another at one position (configuration c). It can be shown that this configuration will develop whenever $\beta \leq 2 \arctan(R \sin\psi_e/(R \cos\psi_e + 1))$, or for the case where $R = 1$, when $\beta \leq \psi_e$. If this configuration is not produced by mass transport to the neck region (i.e; $\beta > \psi_e$) it will be produced eventually by interparticle mass transport. When the particles just touch, it can be shown (see geometric of Fig. 6) that the contact angle formed between them can be expressed as

$$\psi' = 2\psi - \pi = \beta - \pi + 2 \arcsin\left(\frac{\sin\frac{\beta}{2}}{R}\right) \qquad (8)$$

Since $\psi' < \psi$, a greater driving force for mass transport will exist at the neck region where the two larger particles touch relative to where the larger particles are in contact with the smaller particle. It should be pointed out that the same situation is developed when all particles are identical, $R_i = 1$ and $\beta \leq \psi_e$.

Interpenetration of the two larger particles, which initiates at configuration (c) and ends with configuration (e), causes β to decrease, i.e., the two larger particles rotate toward each other about the smaller particle.* (In addition, if the particles are cylinders, a portion of the boundaries between the larger and smaller cylinders can move to form a planar boundary between a portion of the larger cylinders without encountering an energy barrier; a configuration similar to that shown by (d) is formed. This cannot occur for spherical particles, and thus the details will not be presented.)

Configuration (e) develops when $\psi \rightarrow \psi_e$ at all contact positions. If the condition expressed by Eq. (5) was not met before $\psi \rightarrow \psi_e$, then interparticle mass transport will take place, driven by the different particle curvatures, to produce configuration (e) where the two curved boundaries can

* As shown previously,[4] an infinite linear array of identical particles will form an equilibrium configuration where the surface curvature of every grain is identical to one another. If, on the other hand, the same linear array is kinked such that the angle β between the three particles that form the kink satifies the relation $\beta \leq \psi_e$, then it can be shown that the three particles will develop surface curvature different than the rest. This condition arises because the three penetrate one another, whereas, all others only penetrate their neighbors. Thus, even when the particles are initially identical and conserve their mass during neck growth, differential surface curvature can develop leading to interparticle mass transport and grain growth.

move together without encountering an energy barrier. Final mass transport can result in the same configuration shown as (d) in Fig. 4, i.e., two identical, penetrating spheres separated by a planar boundary.

3.0 GRAIN GROWTH AND ARRAY SHRINKAGE

The above analysis showed that it is energetically favorable for grain boundaries to move across sintering particles only (1) after substantial neck growth and (2) when the radius ratio of adjacent grains exceeds a critical value (see Eq. (5)). The first of these two conditions was implied by Greskovich and Lay.[1] It was also shown that when the initial particles are somewhat similar in size (see Fig. 3), interparticle mass transport is first required to develop the critical radius ratio for boundary motion. More significantly, it was shown that when smaller grains disappear between larger grains, a new (or increased) driving force is established for neck growth between the larger grains. That is, the disappearance of smaller grains produced by a combination of interparticle mass transport and boundary motion can either reestablish or enhance the driving force for mass transport to the neck region, viz., grain growth can enhance the sinterability of a powder compact. The object of this section will be to establish a relationship between grain growth and shrinkage of simple particle arrays.

3.1 Linear Arrays

Assume that the configurations in Fig. 4 are repeated to form a linear array with two separating sets of spheres, with initial radii r_{i1} and r_{i2}. Configuration (b), developed by mass transport to the neck regions, is assumed to produce a dihedral angle where the grain boundaries intersect the surface, i.e., $R < R_c$. This requires that the initial radius ratio ($R_i = r_{i1}/r_{i2}$) is less than a given size (similar to that illustrated in Fig. 3; for the linear array, each particle penetrates two others which changes the relation between the initial and final radius under conditions of mass conservation from that for the two penetrating spheres detailed above). Configuration (c) develops by interparticle mass transport causing the larger particles (defined by subscript 2) to increase their mass at the expense of diminishing the mass of the smaller particles. Interparticle mass transport causes $R \rightarrow R_c$ where the two boundaries move together to form a single boundary between the two touching, larger particles as discussed above for the case of three colinear particles. The contact angle, $\psi = 2\psi_e - \pi$, developed between the two larger particles in configuration (c) is given by Eq. (7). Since $\psi < \psi_e$, mass transport to the neck regions is reinitiated to develop the dihedral angle between the larger particles as shown in configuration (d).

The shrinkage of the linear array can be determined for each of the configurational steps. Since engineering strains are used to characterize the shrinkage of powder compacts during densification, the shrinkage strain of the linear array will be determined by

$$\varepsilon = 1 - l_{b,c,d}/l_a, \qquad (9)$$

where the initial center to center distance between the touching larger spheres (configuration a) is given by $l_a = r_{i1} + r_{i2} = r_{i1}(R_i + 1)$ and l_b, l_c, and l_d are the distances between the larger grains for configurations (b) through (d) and are given by the following equations:

$$l_b = r_{i1} R_1 [\cos\theta_1 + R\cos\theta_2] \tag{10a}$$

$$l_c = r_{i1}(1 + R_i^3)^{1/3} F(2\psi_e - \pi) \sin\psi_e \tag{10b}$$

$$l_d = r_{i1}(1 + R_i^3)^{1/3} F(\psi_e) \cos(\psi_e/2) \tag{10c}$$

where

$$F(z) = [0.5 \cos(\tfrac{z}{2})(3 - \cos^2(\tfrac{z}{2}))]^{-1/3} ,$$

$$R_1 = [1 - 0.5(1 - \cos\theta_1)^2(2 + \cos\theta_1)$$

$$+ 4(\frac{R}{R-1})^3 \cos^3(\tfrac{\psi_e}{2})(1 - \cos\phi)^2(2 + \cos\phi)]^{-1/3}$$

$$R_2 = [1 - 0.5(1 - \cos\theta_2)^2(2 + \cos\theta_2)$$

$$- \frac{4}{(R-1)^3} \cos^3(\tfrac{\psi_e}{2})(1 - \cos\phi)^2(2 + \cos\phi)]^{-1/3}$$

$$\theta_1 = \arctan[\frac{R \sin\psi_e}{R\cos\psi_e + 1}]$$

$$\theta_2 = \psi_e - \theta_1$$

$$\phi = \theta_1 - \psi_e/2 \ ,$$

and $$R = R_i(R_2/R_1).$$

Figure 7 illustrates the shrinkage strains ($R_i \simeq 1$) for the three configurations, related to the initial configuration, as a function of the dihedral angle, ψ_e. As shown, the major contributions to shrinkage occur when mass is transported to the neck regions, i.e., between configurations (a) and (b), and (c) and (d). Interparticle mass transport, which causes the smaller particles to disappear, also causes the larger particles to grow and thus does not produce significant shrinkage of the linear array. Although interparticle mass transport does not directly contribute to shrinkage, it does lead to the reinitiation of neck growth which produces significant shrinkage once the smaller particles disappear. Thus, it might be concluded that grain growth within the linear array, which occurs by a combination of interparticle mass transport and boundary motion, reinitiates the driving force for sintering and thus, shrinkage.

One can show that if the initial radius ratio is large enough such that $R \geq R_c$, configuration (c) is reached directly from (a) without interparticle mass transport. The same conclusions concerning shrinkage are obtained without interparticle mass transport. It can also be shown that if $R_i > 1$, but $R < R_c$, the same conclusions are obtained as shown in Fig. 8

except that the shrinkage strain for each configurational change decreases with increasing R_i.

The grain growth phenomena and its associated shrinkage between configurations (b) and (d) can be repetitive. To illustrate this, let us consider a finite linear array of n_o nearly identical spheres of radius r_i, i.e., $R_i = 1$. The initial length of the array is $L_o = 2r_i n_o$. Mass transport to the contact regions will result in configuration (b) and a shrinkage of the array to a new length defined as $L_1 = 2r_i\, F(\psi_e) \cos(\psi_e/2)\, n_o$, where the function $F(\psi_e)$ defines the new radius of the penetrating spheres in terms of the initial radius, i.e., $r = r_i\, F(\psi_e) = r_i[\cos(\psi_e/2)(3 - \cos^2(\psi_e/2))]^{-1/3}$. Now assume that interparticle mass transport occurs such that every other grain disappears and the array develops configuration (d). During this process, the number of grains is reduced by a factor of 2 or, conversely, the new grains increase their radius by a factor of $2^{1/3}$ (configuration (c)). Upon further mass transport to the contact regions (configuration (c) to (d)), the array shrinks to a new length given by $L_2 = 2r_i(2^{1/3})\, F(\psi_e) \cos(\psi_e/2)\, (n_o/2)$. Configuration (d) now reinitiates a new cycle of grain growth via interparticle mass transport and boundary motion as configuration (b). During each cycle, the number of grains is reduced by a factor of 2, and the array shrinks by the difference between the mass centers of configurations (b) and (d). At the end of each cycle (defined by m) it can be shown that the grain size is given by

$$D_m = 2r_i(2^{m/3}), \tag{11}$$

and the array length by

$$L_{m+1} = 2^{-m}(D_m/2r_i)\, F(\psi_e)\, \cos(\psi_e/2) L_o. \qquad (12)$$

Equation (12) can be expressed as the shrinkage strain of the array, relating shrinkage strain after m cycles of grain growth to grain size:

$$\varepsilon_{m+1} = L_{m+1}/L_o - 1 = 2^{-m}(D_m/2r_i)\, F(\psi_e)\, \cos(\psi_e/2) - 1. \qquad (13)$$

3.2 Closed Arrays

Unlike linear arrays, closed arrays, viz, rings of cylinder or spheres and polyhedra, contain a void space that develops into a pore upon sintering. The number of particles coordinating the void (or pore) is defined as the pore coordination number, n. As discussed above, it was shown[4] that during sintering, the pore formed with identical particles can either disappear ($n \leq n_c$) or shrink to an equilibrium size ($n > n_c$), where n_c is a critical coordination number which depends on the dihedral angle (n_c decreases as ψ_e increases). It has been suggested[5,6] that grain growth will lower the coordination number of stable pores ($n > n_c$), such that it will disappear (when $n \leq n_c$). Using the iterative grain growth phenomena described above, the relation between grain growth, shrinkage (or densification), and pore disappearance will be detailed below for the ring of spheres.

Consider a symmetric ring containing two different sets of spheres with nearly the same radius, r_i ($R_i \rightarrow 1$); the total number of spheres is n_o. The total mass of material in the ring is $n_o(4/3)\,\pi\, r_i^3\, \rho_t$, where ρ_t is the

material density. The ring's volume can be described by a disc with a radius that circumscribes the ring and a height equal to the sphere diameter; its initial volume is given by $2\pi\ r_i^3(1 + (\sin(\theta_o/2))^{-1})^2$, where θ_o is the angle which initially subtends one particle, i.e., $\theta_o = 2\pi/n_o$. Upon sintering, the radius of the circle that circumscribes the array decreases to $r_i\ F(\psi_e/2)\ (1 + \cos(\psi_e/2)(\sin(\theta_o/2))^{-1})$ and its volume becomes $2\pi\ r_i^3\ F(\psi_e/2)^3\ (1 + \cos(\psi_e/2)(\sin(\theta_o/2))^{-1})^2$. Since $n_o > n_c$, the pore within the array does not disappear during this initial step of sintering.

Interparticle mass transport can now dominate which is assumed to cause every other grain to disappear, as described for the case of the noncolinear particles above. (If the initial ring was not symmetrical, the analysis for the case of the noncolinear particles shows that torques would develop during grain growth causing the ring to distort from its initial configuration.) During the first cycle of grain growth, the pore's coordination number is reduced by a factor of two ($n_1 = n_o/2$), the angle subtending each grain is increased by the same factor (i.e., $\theta = 2\theta_o = 4\pi/n_o$), and the radius of the circumscribed circle decreases by a factor of $2^{1/3}$ (i.e., $= 2^{1/3}\ r_i\ F(\psi_e/2)\ (1 + \cos(\psi_e/2)(\sin(\theta_1/2))^{-1})$. As for the arrays discussed above, it is not the disappearance of the grains, but the reinitiation of sintering that causes the array to shrink upon grain growth. If $n_1 > n_c$, the pore will still remain after the first cycle of grain growth; subsequent cycles of grain growth will cause $n \leq n_c$ and pore disappearance.

Subsequent cycles (m) of grain growth will cause the volume of the ring array to decrease in a manner similar to that described for the first cycle. Since its mass remains constant, its density increases with grain

growth. It can be shown that the density of the ring array can be expressed as

$$\rho_{m+1} = (2/3)(D_m/2r_i)^{-3}\, F(\psi_e/2)^{-3}\, (1 + \cos(\psi_e/2)(\sin(\theta_m/2))^{-1})^{-2} n_o \rho_t, \tag{14}$$

where $D_m/2r_i$ is the grain size normalized to the initial sphere diameter (see Eq. (11)), $\theta_m = (2^m)\,\theta_o = 2\pi/n_m$, and $n_m = (2^{-m})n_o$. The pore will just close when $n_m = n_c$ (i.e, when $\theta_m = \pi - \psi_e$). The density of the array when the pore just closes (chosen as the theoretical density of the array*) can be expressed as

$$\rho_t(\text{array}) = (2/3)\, F(\psi_e/2)^{-3}(1 + \cos(\psi_e/2)(\sin((\pi - \psi_e)/2))^{-1})^{-2} n_c \rho_t. \tag{15}$$

Figure 9 illustrates the relative density of the ring array ($\rho_{m+1}/\rho_{t(\text{array})}$) as a function of grain size normalized by the diameter of the initial spherical particles. As illustrated, the near linear relationship between relative density and grain size over much of the densification range is remarkably similar to the experimental relations reported by Gupta.[2] Also,

* Further grain growth will result in the interpenetration of all grains and the production of one spherical grain. The one spherical grain only occupies 2/3 of the disc volume used in the array calculations and would appear to cause the density of the array to decrease when $n_m < n_c$. This artifact of the calculation can be avoided by either redefining the array volume by the sphere that circumscribes the array or by choosing the array's theoretical density as that expressed by Eq. (15).

the amount of grain growth that takes place during densification is also remarkably similar to the experimental data. Figure 9 also shows that more grain growth is required for densification with decreasing dihedral angle.

DISCUSSION

It has been shown that a special geometrical relation must exist ($R \geq R_c$) between two adjoining grains before their grain boundary can move, without encountering an energy barrier. This result strongly suggests that the motion of grain boundaries will be governed by geometrical considerations within a densifying powder compact, i.e., its relative density. Because a given relative density can be achieved by different temperature/time schedules, grain growth will appear to be unrelated to these different schedules.

As shown, grain growth in a densifying powder compact is primarily a result of interparticle mass transport. Since the diffusion distance for interparticle mass transport is some fraction of the grain size, whereas that for boundary motion is related to atomic distances, one would expect grain growth kinetics in densifying bodies to be much slower than when the same body is fully dense.

The most significant observation of the current work is that when grains disappear from between adjoining grains by a combination of interparticle mass transport and boundary motion, the driving force for mass transport to the neck regions is reinitiated. That is, once the initial particles

sinter together, further densification is driven by grain growth. This observation leads to the near linear relation between density and grain size for the ring array of particles. The following will discuss other implications concerning densification and grain growth in powder compacts and densification kinetics can be implied from this observation.

In a previous paper,[6] it was suggested that the thermodynamics of densification are controlled by the function that describes the distribution of pore coordination numbers within a powder compact. This function, V(n), describes the volume fraction of pores associated with each and every coordination number. The total volume fraction of void phase within the compact is the sum of the coordination number distribution function over all coordination numbers. For example, if identical particles are packed with a simple cubic arrangement, all pores are coordinated by 8 particles. The function V(n) is only nonzero when n = 8, viz., $V(8) = 1 - \pi/6 = 0.48$ (the volume fraction of voids within this arrangement). If this particle arrangement was sintered for the case where $\psi_e \geq 109.5°$ (or $n_c \leq 8$), all pores would be thermodynamically unstable and disappear, kinetics permitting. For this case, pores do not need to be recoordinated through grain growth, i.e., grain growth is not required for densification of this special array.

In general, because particles are not packed in a symmetrical arrangement, the coordination number for pores can be widely distributed. This is particularly true for real powders that are packed as agglomerates.[6] In addition, because of their nonsymmetric arrangement, particles rearrange during the initial stages of neck growth causing some pores to increase their coordination number.[4] It is suspected that a large fraction of pores in a

real powder compact have coordination numbers greater than critical. Thus, during initial sintering, only a fraction of the pores are thermodynamically unstable and disappear without grain growth. Stable pores (i.e., those with $n \geq n_c$) will shrink until grain growth can lower their coordination number to make them unstable and disappear. With grain growth, the stable pores will shrink in proportion to the increased grain size with the same relation as observed for the ring of spheres. If the void volume is equally distributed between pores with coordination numbers $\leq 8n_c$, then a grain size increase of $(2^{1/3})^3$ will lead to complete densification and a near linear grain size vs densification relation similar to that shown in Fig. 9 for the ring array. If, on the other hand, the void volume was weighted toward smaller coordination numbers, then most of the densification will only require a modest increase in grain size, while the last and smallest increase in density will require the greatest increase in grain size. Thus, the extent of grain growth required for densification will depend on the pore coordination number distribution function. Assuming that pores remain coordinated by grains (i.e., pores are not swallowed up by abnormally growing grains), the grain size required to achieve theoretical density will depend on the pore with the largest coordination number.

With the recognition that grain growth leads to densification, it should also be recognized that densification kinetics will depend on both sintering kinetics (intraparticle mass transport to the neck region) and grain growth kinetics (interparticle mass transport). If the path length for interparticle mass transport is larger and/or the driving force for interparticle mass transport smaller than those for sintering, grain growth kinetics will be

the rate-limiting process and dominate the densification kinetics. In addition, grain growth will increase the path lengths for both intra- and interparticle mass transport. This increase in path length is prescribed by the amount of grain growth required to reduce the coordination numbers of all pores to their critical number and is thus related to the coordination number distribution function. Theoretical and experimental kinetic studies of densification should be reevaluated with these thoughts in mind.

ACKNOWLEDGEMENTS

Without the useful discussion with colleagues P.E.D. Morgan, D.B. Marshall, and J.R. Porter, the concept relating grain growth and densification would not be as succinctly stated. This work was supported by the Office of Naval Research under Contracts N00014-84-C-0298 at Rockwell International Science Center, and N00014-84-K-0286 at UCLA.

REFERENCES

1. C. Greskovich and K.W. Lay, "Grain Growth in Very Porous Al_2O_3 Compacts," J. Am. Ceram. Soc. 55[3], 142-6 (1972).

2 T.K. Gupta, "Possible Correlations Between Density and Grain Size During Sintering," J. Am. Ceram. Soc. 55[5], 176 (1972).

3. C.A. Bruch, "Sintering Kinetics for the High Density Alumina Process," Am. Ceram. Soc. Bull. 41[12], 799-806 (1962).

4. B. Kellett and F.F. Lange, "Thermodynamics of Densification, Part I: Sintering of Simple Particle Arrays Equilibrium Configurations, Pore Stability, and Shrinkage," submitted to Am. Ceram. Soc.

5. B. Kellett and F.F. Lange, "Experimental Thermodynamics of Densification, Part III: Relation Between Grain Growth and Pore Closure," submitted to Am. Ceram. Soc.

6. F.F. Lange, "Sinterability of Agglomerated Powders," J. Am. Ceram. Soc. 67[2], 83 (1984).

SC35814

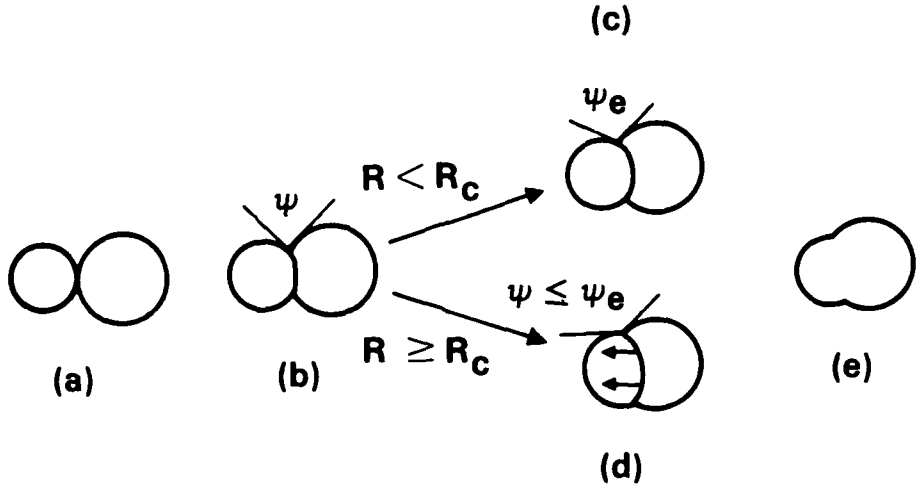

Fig. 1 Configurational changes during sintering and interparticle mass transport leading to special configuration (d) where grain boundary can move through small grain and decrease the free energy of the system.

SC35813

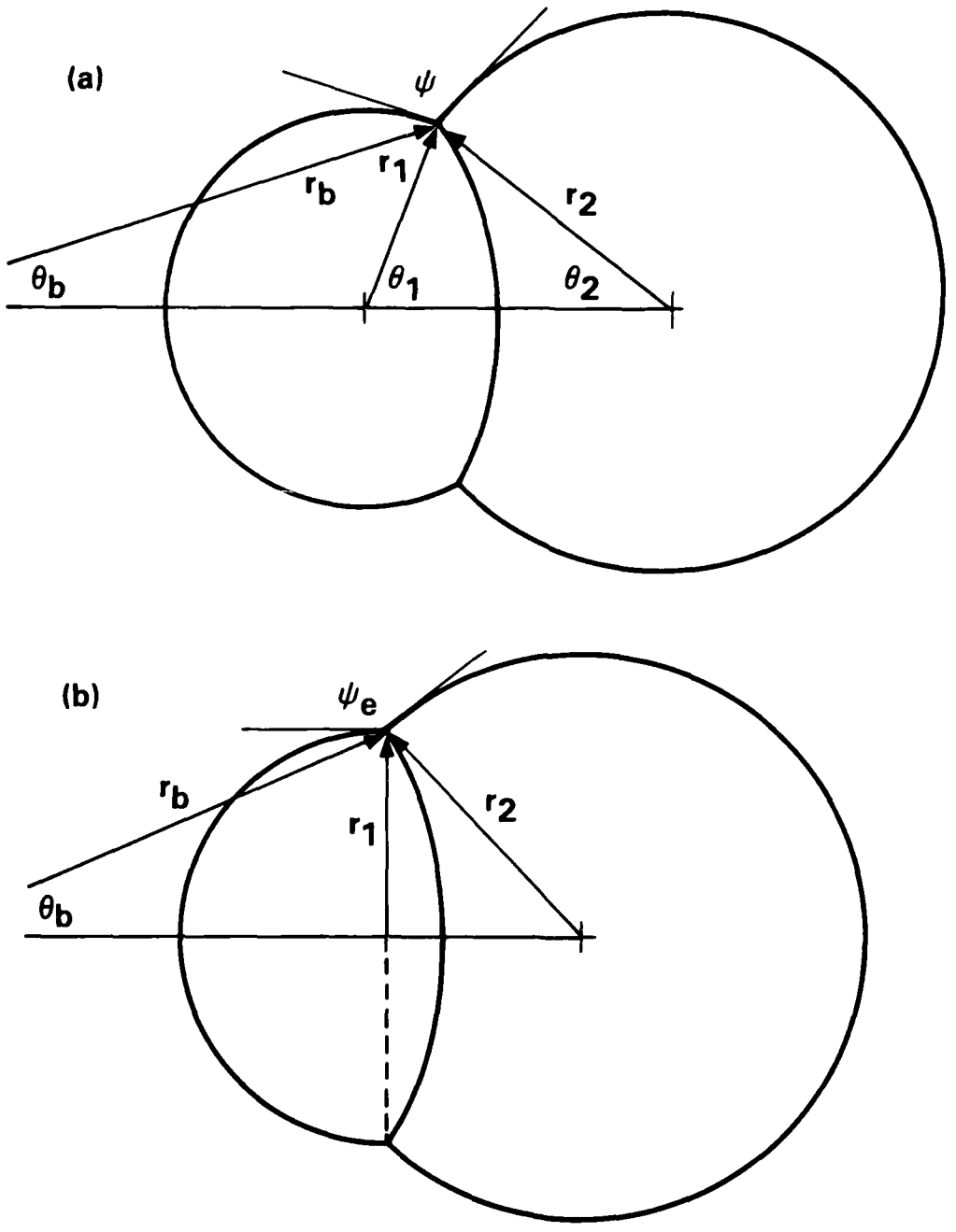

Fig. 2 (a) Geometrical parameters needed to define the radii of the grains and grain boundary. (b) Geometrical parameters that define the special configuration for boundary motion through the smaller grain.

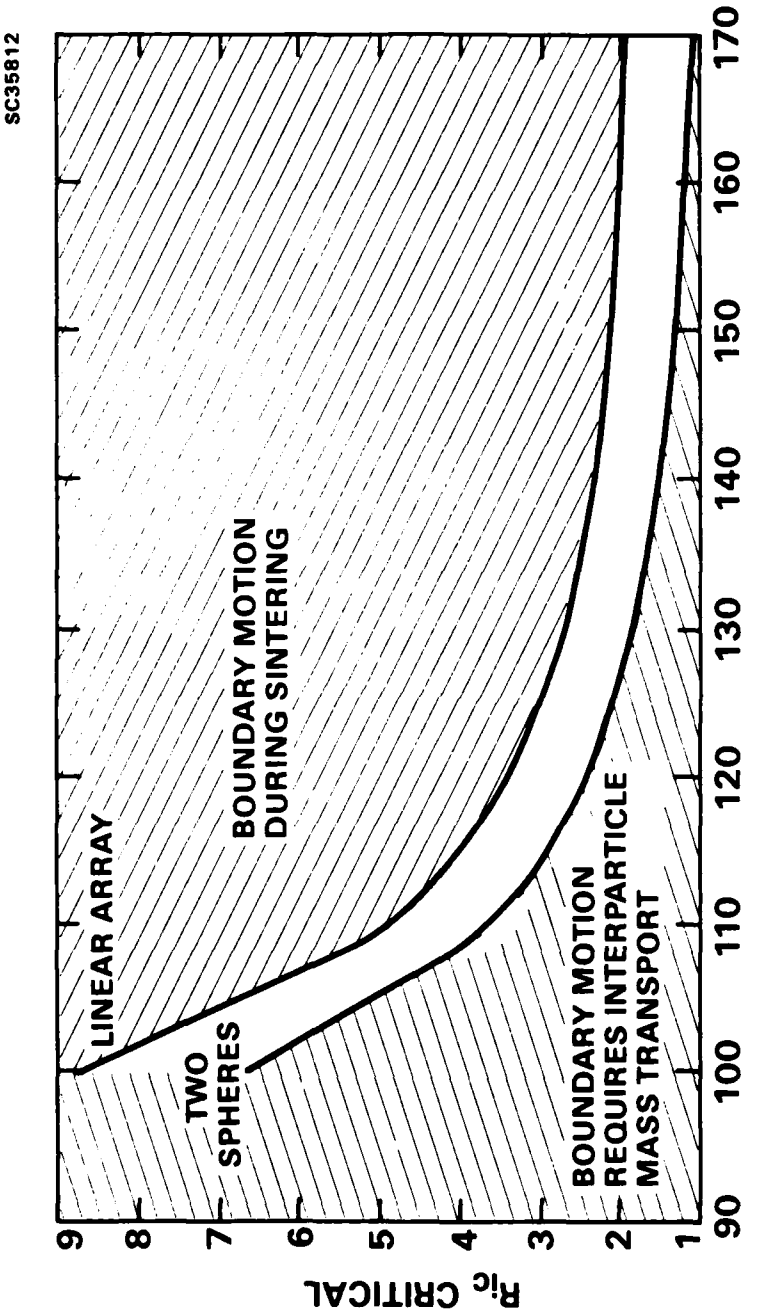

Fig. 3 Critical radius ratio of initial particles required to produce special geometry for boundary motion without interparticle mass transport as a function of the material's dihedral angle.

SC35810

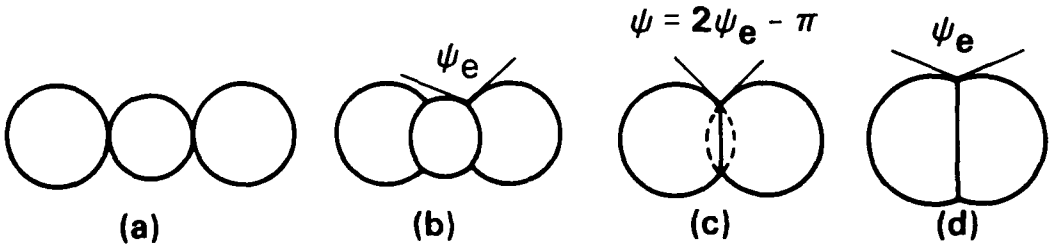

Fig. 4 Configurational changes produced during sintering and interparticle mass transport for three colinear particles. Note that disappearance of smaller grain (configuration c) reinitiates sintering.

SC35811

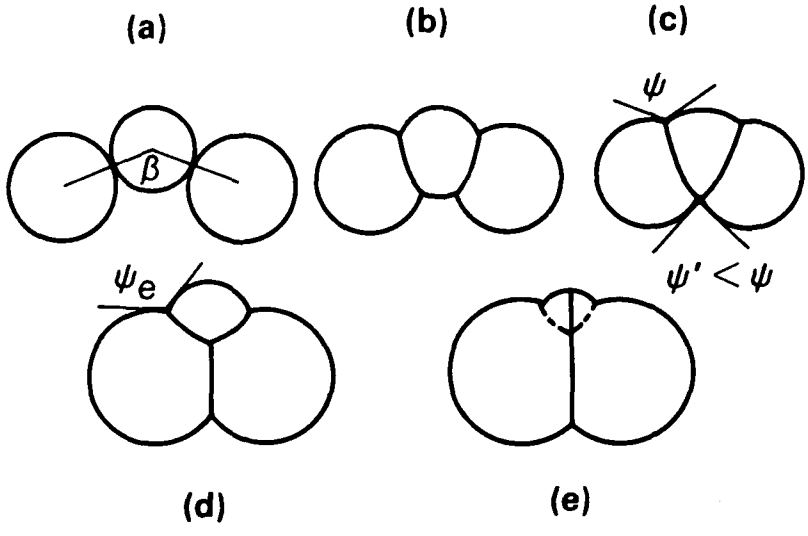

Fig. 5 Configurational changes produced during sintering and interparticle mass transport for three noncolinear particles. Note that sintering is reinitiated first at one point (configuration c).

SC35809

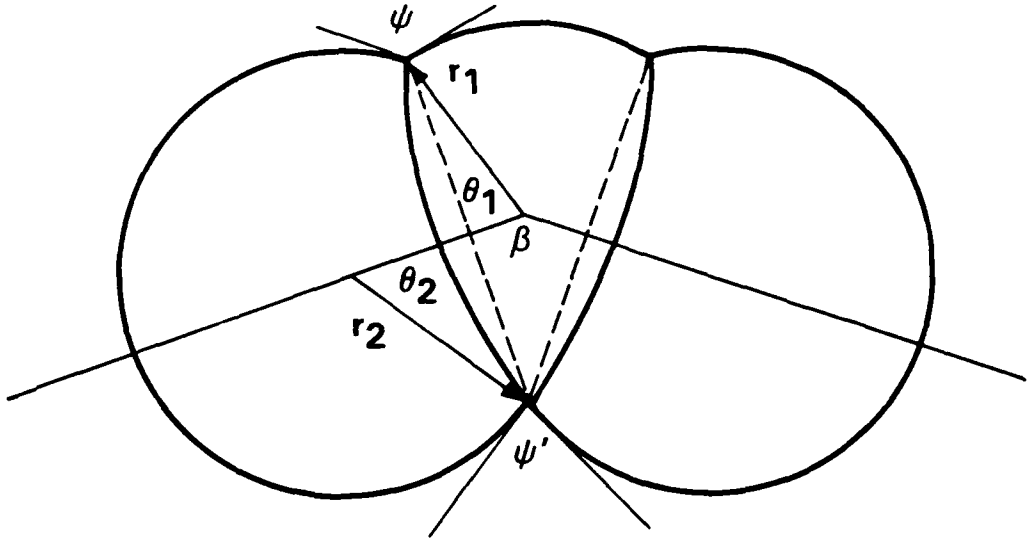

Fig. 6 Geometrical parameters needed to define contact angle where two larger grains touch during sintering of noncolinear particles.

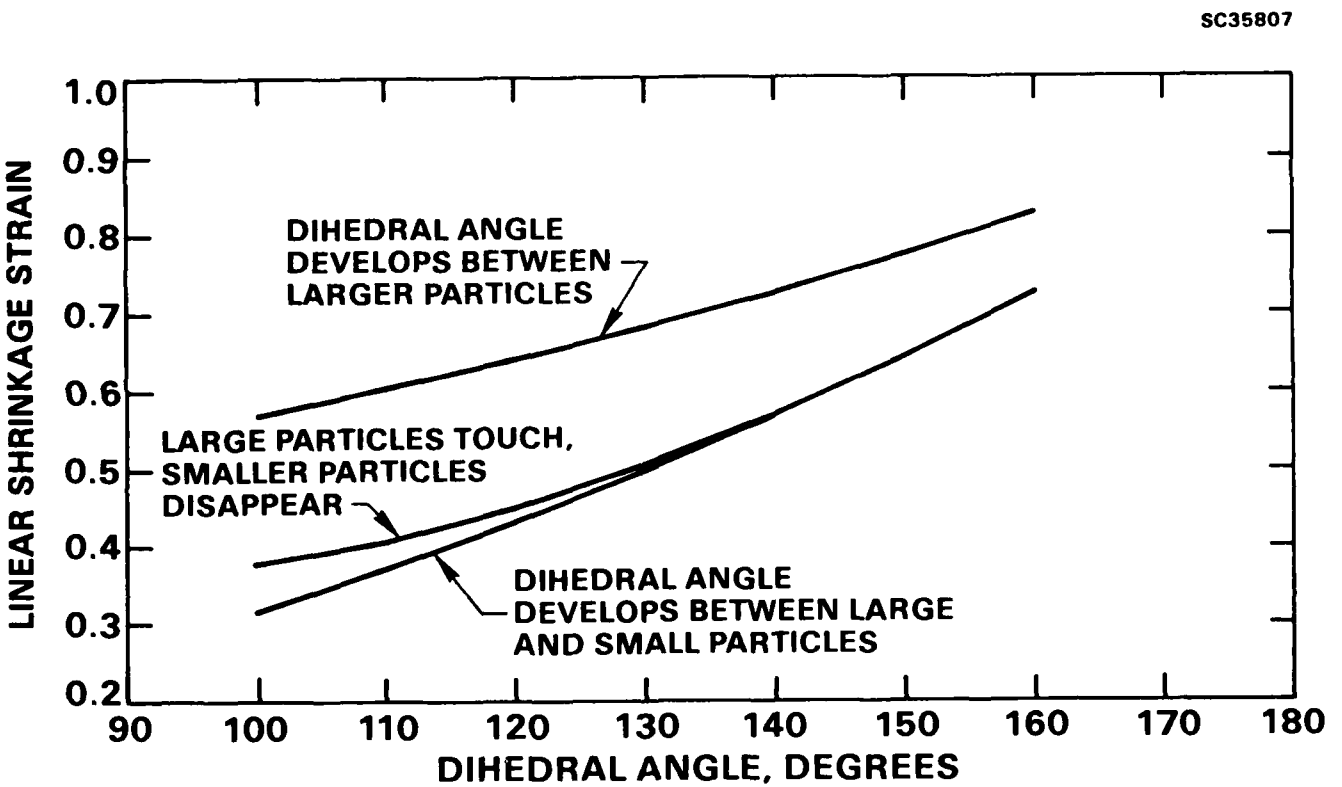

Fig. 7 Shrinkage strain for linear array of two different sets of particles as a function of dihedral angle. Lower curve represents shrinkage when particles sinter. Middle curve represents shrinkage when every other particle disappears by interparticle mass transport and boundary motion. Upper curve is shrinkage-produced when remaining grains sinter.

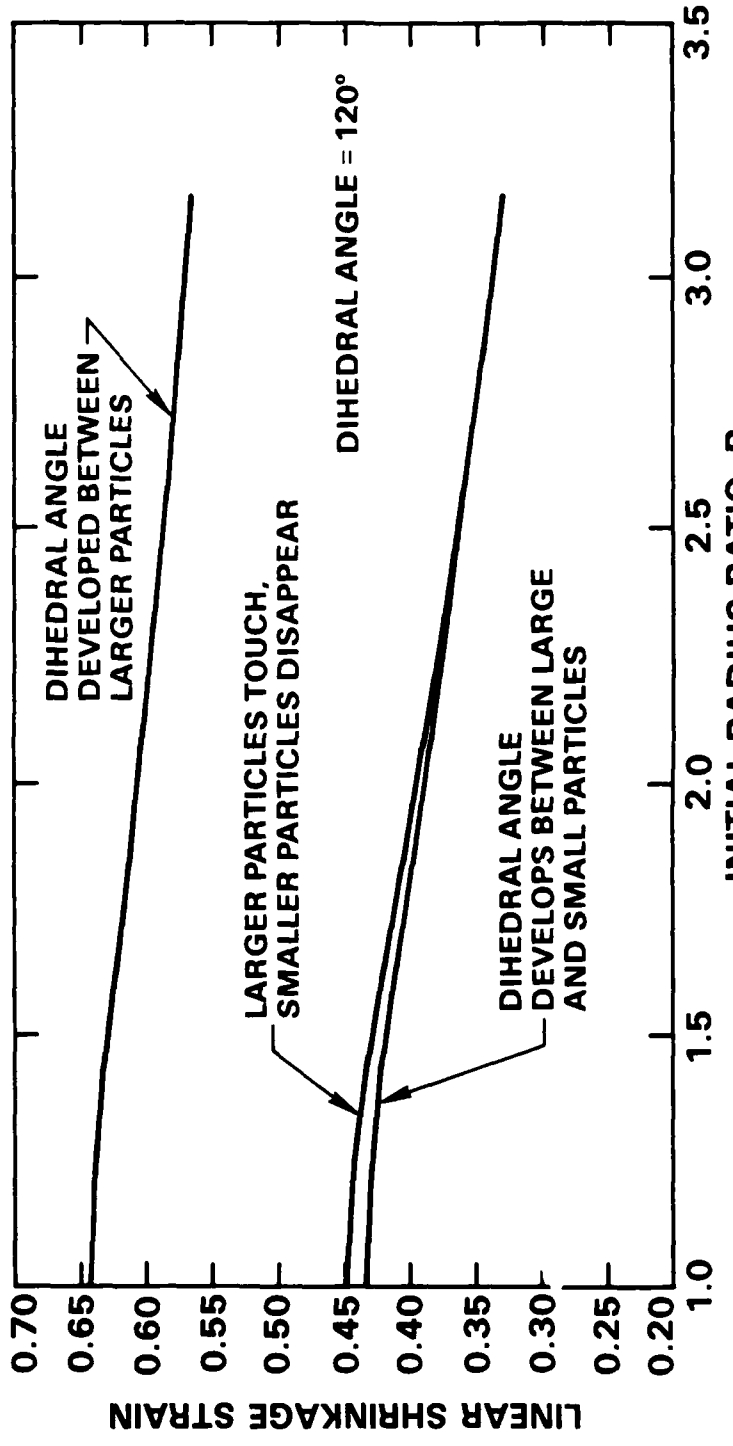

Fig. 8 Effect of initial radius ratio on shrinkage strain for linear arrays of two different sets of spherical particles.

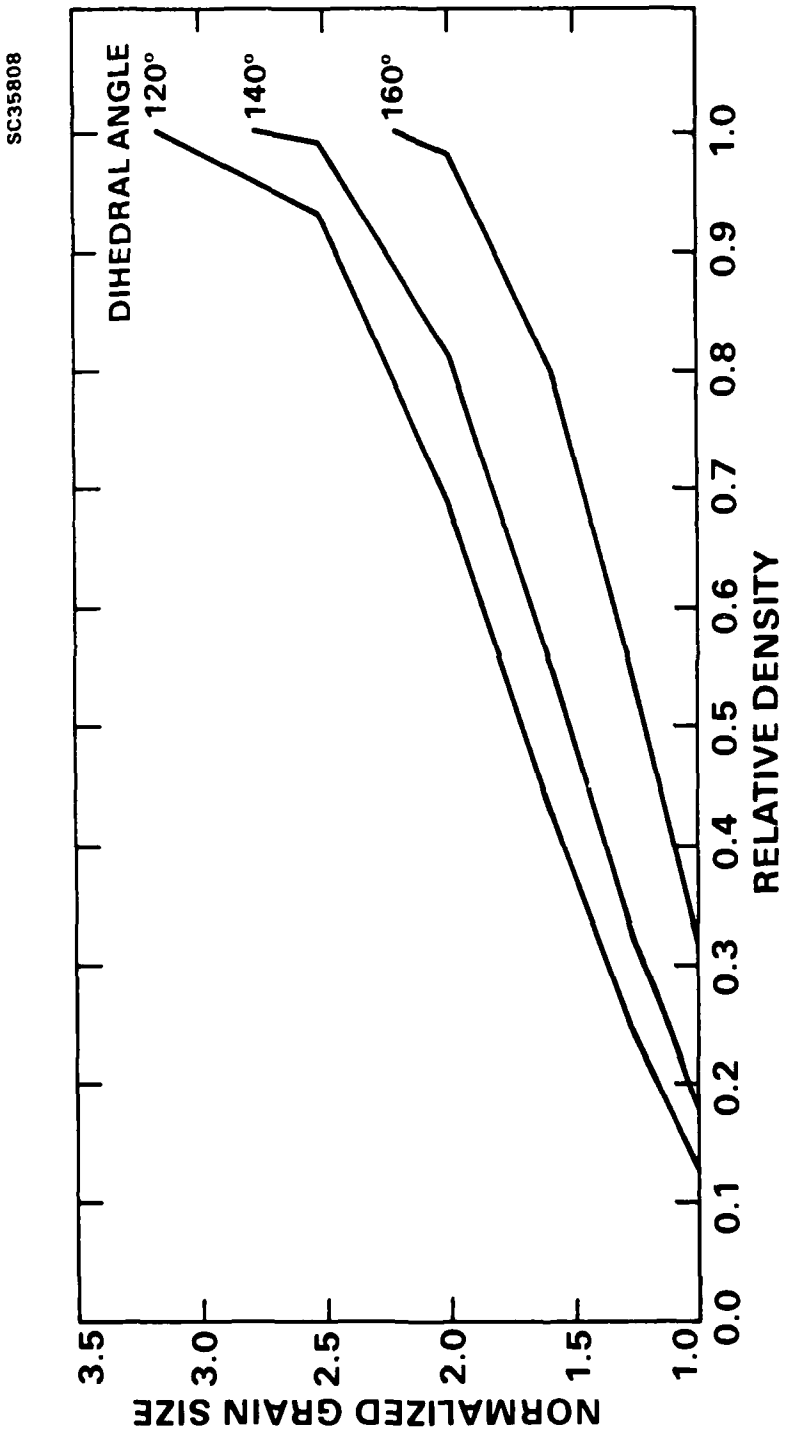

Fig. 9 Relation between grain growth and relative density for symmetric ring of spheres. Note relation is nearly linear over much of the densification range.

SC5410.FR

THERMODYNAMICS OF DENSIFICATION, PART III: EXPERIMENTAL RELATION BETWEEN GRAIN GROWTH AND PORE CLOSURE

Bruce Kellett
Department of Materials Science and Engineering
University of California - Los Angeles
Los Angeles, California 90024

F.F. Lange
Structural Ceramics
Rockwell International Science Center
1049 Camino Dos Rios
Thousand Oaks, California 91360

THERMODYNAMICS OF DENSIFICATION, PART III: EXPERIMENTAL RELATION BETWEEN GRAIN GROWTH AND PORE CLOSURE

Bruce Kellett
Department of Materials Science and Engineering
University of California - Los Angeles
Los Angeles, California 90024

F.F. Lange
Structural Ceramics
Rockwell International Science Center
1049 Camino Dos Rios
Thousand Oaks, California 91360

ABSTRACT

The effect of grain growth on conditions for pore disappearance was studied, using an Al_2O_3/ZrO_2 composite containing monosize pores introduced by incorporating plastic spheres (1 μm, 2 μm and 4 μm) into the powder prior to sintering at 1600°C. Pores uncovered within several microns of the surface by careful polishing were characterized with respect to their size and number density after different periods of heat treatment at 1600°C. Grain growth, which occurred during heat treatment, was also characterized. Results show that the pores maintain their size while decreasing their number density during grain growth. Pores that remained after heat treatment were coordinated by more than six grains in the plane of polish. These results are consistent with theoretical work, which suggests that pores are stable when coordinated by more than a critical number of grains. The current experimental work suggests that pores quickly disappear once grain growth reduces their coordination number to a critical value.

INTRODUCTION

Most sintering theories have been based on ideas formulated by Herring,[1] who pointed out that mass will be transferred to surfaces of lower curvature. Kuczynki's[2] analysis of spherical pores, based on these ideas, concluded that pores continuously decrease in size at a rate dependent on the mode of mass transport. In a polycrystal, pores are only spherical if they reside within a single grain that exhibits isotropic surface energy. Pores intersected by grain boundaries exhibit surface curvatures that depend on the number of intersecting grain boundaries and the dihedral angle (ψ_e, the dihedral angle depends on the ratio of surface and grain boundary energies). Previous sintering theories based on mass transport to the contact region (region of negative surface curvature) between two spherical particles do not examine the conditions for pore closure because two touching particles cannot define a pore.

Kingery and Francois[3] were the first to consider the geometry of pore closure in polycrystalline materials. They suggested that the flow of mass either into or away from a pore will depend on its surface curvature and that the surface curvature of the pore would depend on both the number of grains coordinating the pore and the dihedral angle. Using geometrical arguments, they showed that if the dihedral angle was to be maintained at each grain-boundary/pore-surface intersection, the curvature of the pore surface between these intersections would depend on the number of intersecting grain boundaries. They concluded that if the number of intersecting boundaries (number of grains coordinating the pore) is less than a critical value, then the

pore's surface will be concave (looking from within the pore), which would promote mass transport to the pore's surface and pore closure. They also concluded that if the pore's coordination number is greater than a critical value, its surface will be convex, promoting mass transport away from the pore and thus, pore growth. The critical pore coordination number separating pore closure from pore growth is dependent on the dihedral angle. It must be concluded that they compared the pore's surface with an external, flat surface.

In a companion paper,[4] we determined the lowest free energy configuration for closed arrays of identical particles which contained a single pore (rings and polyhedra). They showed that all pores within closed arrays will shrink during sintering, but only those with a coordination number less than a critical value disappear. Pores with a coordination number greater than a critical number will shrink to an equilibrium size. As shown in the next section, the same conclusion is obtained for the case of an isolated pore within a bulk specimen.

As shown in Fig. 1, grain growth can significantly lower a pore's coordination number and change its surface curvature from convex to concave. It is well known that grain growth occurs throughout all stages of sintering.[5] It is thus hypothesized that grain growth can be a desirable phenomenon in helping to eliminate pores by changing their mean surface curvature. Experiments were designed to test this hypothesis. Materials were fabricated containing spherical voids, which were the only detectable, remnant porosity after sintering. These materials were heat treated to induce grain growth. Observations were made to determine the conditions where the large, spherical pores disappeared. As will be seen, these conditions are consistent with the initial hypothesis.

THERMODYNAMIC ASPECTS OF ISOLATED PORES RELATIVE TO THE EXTERNAL SURFACE

Our calculations on pore growth and shrinkage are based on a two-dimensional model in which all pores, surrounded by identical grains, are within a bulk specimen of radius (R), as shown in Fig. 2. The dihedral angle, determined through Young's equation ($\cos(\psi_e/2) = \gamma_b/2\gamma_s$), is identical at all grain boundary-surface junctions.

As described by Kingery and Francois,[3] pores with a coordination number greater than a critical value, i.e., $n > n_c$, where

$$n_c = 2\pi/(\pi-\psi_e) \tag{1}$$

have a convex curvature, pores with a coordination number equal to the critical value have flat surfaces, and pores with $n < n_c$ have a concave curvature. The external surface always has concave curvature.

Pore energy was equated to its surface energy minus the grain boundary energy it removes from the dense body, expressed as

$$E = \gamma_s A_s - \gamma_b A_b \quad . \tag{2}$$

The surface area per unit thickness (A_s) and the grain boundary area per unit thickness (A_b) removed by the pore are a function of the pore coordination (n), pore radius of curvature (r_p) and pore size (R_p), as shown in Fig. 2:

$$A_s = n(2\pi/n+\psi_e-\pi)r_p \quad , \tag{3}$$

$$A_b = n\, R_p \quad . \tag{4}$$

It can also be shown that pore volume per unit thickness (V_p) is given by

$$V_p = n/2([2\pi/n+\psi_e-\pi+\sin(\psi_e+2\pi/n)]r_p^2 + \sin(2\pi/n)R_p^2) \quad . \tag{5}$$

Using the relationship between r_p and R_p:

$$r_p = R_p \sin(\pi/n)/\cos(\psi_e/2+\pi/n) \quad , \tag{6}$$

the derivative of pore enegy with respect to pore volume simplifies to*

$$dE_p/dV_p = -\gamma_s/r_p \quad . \tag{7}$$

Equation (7) implies that when considered alone, isolated pores with convex surfaces decrease their energy by growing, and pores with concave surfaces decrease their energy by disappearing.** The energy of pores with flat sides ($r_p = \infty$) is independent of pore size. These conclusions were expressed by Kinergy and Francois,[3] and taken to define the condition for pore growth or

*Pore radius of curvature is positive for convex pore curvature and negative for concave pore curvature.

**Equation (7) is equivalent to the Kelvin Equation: $\mu = \Omega\gamma_s\,(1/R_1 + 1/R_2)$; μ chemical potential, Ω atomic volume, R_1 and R_2 are the orthogonal radii of surface curvature.

disappearance. However, this cannot be correct because changes in pore volume also cause changes in the energy of the external surface.

To calculate the change in energy of the exterior surface with respect to pore volume, consider the external region shown in Fig. 2. The change in the energy of the exterior surface can then be calculated as the sum of the change in its surface and grain boundary energies,

$$dE_e = \gamma_s \, dA_s' + \gamma_b \, dA_b' \quad , \tag{8}$$

where dA_s' is the derivative of the surface area per unit thickness, and dA_b' is the derivative of the grain boundary area per unit thickness. It can be shown that

$$dA_s' = n_e(\pi+2\pi/n_e-\psi_e)dr_e \quad , \tag{9}$$

$$dA_b' = n_e dR \quad , \tag{10}$$

where n_e is the number of grains surrounding the specimen, and dr_e is the derivative of the exterior surface curvature.

Using the relationship between r_e and R,

$$r_e = R \sin(\pi/n_e)/\cos(\psi_e/2-\pi/n_e) \quad , \tag{11}$$

and Young's equation, the derivative of the exterior energy with respect to the volume of the specimen (V_s) simplifies to:

$$dE_e/dV_s = \gamma_s/r_e \quad . \tag{12}$$

Since the exterior surface curvature is positive, the exterior surface energy always increases with increasing volume.

If we assume that the change in pore volume is equal to the change in specimen volume ($dV_p = dV_s$), then the total change in the system's energy with respect to pore volume is the sum of Eqs. (7) and (12), and is a function of the radius of curvature of the pore's surface (r_p), and the radius of curvature of grains on the external surface (r_e):

$$dE_t/dV_p = \gamma_s(1/r_e - 1/r_p) \quad . \tag{13}$$

For concave pores ($r_p < 0$), the energy of the system decreases with pore volume, implying that these pores will continuously shrink and disappear, kinetics permitting. Convex pores ($r_p > 0$) will either shrink or grow depending on the relative values of the curvatures, i.e., when $r_e > r_p$ pore growth decreases system energy, and for $r_e < r_p$, pore shrinkage decreases system energy. Similar conclusions were obtained by Cannon[6] through a different approach.

Equilibrium ($dE_t/dV_p = 0$) occurs when:

$$r_e = r_p \quad , \tag{14}$$

suggesting that pores with convex surfaces will be stable when their curvature equilibrates with that of the exterior surface.

The exterior radius of curvature can be equated to the grain size (D) (see Fig. 2):

$$R_e = D/[2\cos(\psi_e/2)] \quad . \tag{15}$$

Using Eqs. (6), (14) and (15), it can be shown that at equilibrium, the pore size is dependent on the grain size (D) and the pore coordination number (n):

$$R_p = D \frac{\cos\left(\frac{\psi_e}{2} + \frac{\pi}{n}\right)}{2\cos\left(\frac{\psi_e}{2}\right)\sin\left(\frac{\pi}{n}\right)} \quad . \tag{16}$$

Equation (16) shows that when $n \leq n_c = 2\pi/(\pi-\psi_e)$, $R_p = 0$ (the pore disappears), and when $n \geq n_c$, the pore is stable with a finite size ($R_p > 0$). Equation (16) also shows that if grain growth occurs without changing the pore's coordination number, the pore will grow. On the other hand, if grain growth lowers the coordination of the stable pore, a condition will be reached such that the pore will become unstable and will disappear.

These results differ from those of Kingery and Francois[3] who stated that pores of $n > n_c$ experience a driving force for growth.

EXPERIMENTAL

Pores of uniform size were introduced into a sintered body by mixing a small fraction (≤ 1 vol%) of polystrerene microspheres of narrow size distribution (~ 1%) into a flocced, two-phase (Al_2O_3/ZrO_2) powder slurry. The colloidal method of treating the powders to decrease agglomerate size and the method of mixing has been reported elsewhere.[7] The slurry was consolidated by slip casting and was sintered after drying at 1600°C. The plastic microspheres burned out prior to the initiation of bulk shrinkage. The resulting microstructure contained spherical pores, diminished in size due to bulk shrinkage, highly coordinated by smaller grains. Different specimens were fabricated containing pores produced with 1 μm, 2 μm and 4 μm plastic spheres. Grain growth was induced by reheating to the sintering temperature for different periods. Grain size and pore size distributions and pore number densities were determined as a function of heat treatment period.

Preliminary work with single phase Al_2O_3 powder produced abnormal grain growth at the heat treatment temperature causing many of the pores to relocate within the larger abnormal grains, preventing observations on the influence of grain growth on pore closure. For this reason, 10 vol% ZrO_2 (+6.6 mole% Y_2O_3) was incorporated with the Al_2O_3 to prevent abnormal grain growth, as described elsewhere.[6]

After each heat treatment, pores located several microns beneath the surface were uncovered, without producing significant pull-outs, by careful diamond polishing with sequential grit sizes of 4, 1 and 1/4 μm. After the specimens were polished, they were thermally etched at 1450°C to reveal grain

boundaries. Scanning electron micrographs were taken at a magnification suitable to obtain statistical information concerning grain size, pore size and to determine the number of pores per unit area (pore number density). The appropriate microstructural features were traced separately onto a transparent overlay to allow the use of an image analyzer* without the ambiguous definition of grain and pore boundaries. The software associated with the image analyzer converted the areas of the microstructural features to an equivalent circle; grain size and pore size are reported as equivalent circle diameters.

RESULTS

Figure 3 illustrates that the median grain size of both the Al_2O_3 and ZrO_2 grains in the Al_2O_3/ZrO_2 composite was observed to increase linearly with respect to log time for heat treatment at 1600°C. The smaller ZrO_2 inclusions, primarily located at four-grain junctions, grew by coalescence;[6] the ratio of the median sizes of the two phases was constant (~ 0.6) throughout the heat treatment. The three grain size histograms shown in Fig. 4 illustrate that the increased median grain size is due principally to the broadening of the grain size distribution with increasing heat treatment periods.

Figure 5 illustrates two pore size histograms (heat treatment periods of 1 and 13 h) for material fabricated with the 2 μm plastic spheres. The smaller median size of the pores relative to the size of the starting plastic spheres reflects the linear shrinkage of the powder compact (i.e. all pores

*Cambridge Model 900

shrink during sintering) and the statistical mean diameter intersected by the polished plane. As shown, the pore size distribution does not significantly change during heat treatment.

The median pore size and the pore number density plotted as a function of grain size are illustrated in Fig. 6a and 6b for the materials fabricated with the three different sized plastic spheres. As shown, the median pore size remains constant, whereas the pore number density decreases with increasing grain size. The decrease in pore number density for the larger pores produced with 4 μm plastic spheres was less dramatic than the smaller pores. The slight increase in pore size at the largest grain size observed for the smaller pores (produced with the 1 μm and 2 μm spheres) is not considered significant since as the pore coordination number decreased, fewer pores were observed and their shape became more irregular, making them more difficult to distinguish from the occasional pull-out of ZrO_2 inclusions during polishing.

DISCUSSION

Pores, remnants of plastic microspheres, were observed to remain at a uniform size while their number density decreased with increasing grain size. This observation implies that pores do not continuously shrink, but are quickly removed in a discontinuous manner. The thermodynamics of pore stability suggests that pores coordinated by a greater than critical number of grains are stable and can only disappear when their coordination number becomes equal to the critical number. Since the mass transport distance between

the observed pore surface and the external surface was no greater than several pore diameters in the experiments described above, once the critical coordination condition was achieved by grain growth, pore disappearance could be rapid. Because real polycrystalline materials exhibit a grain size distribution, the coordination of some pores will decrease to the critical number before others; thus, pore number density would be expected to decrease gradually. Remaining pores would have a coordination number greater than the critical value.

Figure 7 illustrates the coordination number of the pores remaining after heat treatment, determined on the polished plane, as a function of grain size for materials fabricated from three different sphere sizes. The coordination number of the pores produced with the 2 μm and 4 μm spheres initially decreases with increasing grain size, whereas the coordination number of the smaller pores produced with the 1 μm spheres remains nearly constant throughout grain growth. For the case of the pores produced from the 1 μm and 2 μm spheres, the smallest, average coordination number achieved at larger grain sizes was 6, whereas that for the larger pores produced with the 4 μm spheres was slightly larger.

In an approximate way, one could relate this in-plane coordination to the coordination of a dissected polyhedron; i.e., an in-plane coordination of 5 or 6 would result from the bisection of a dodecahedron (pore coordination 12), and from this polyhedron predict the equilibrium dihedral angle (for a dodecahedron shaped pore the dihedral angle is 138°). However, grains are not symmetrically arranged around real pores. Also, the dihedral angle would be expected, for an anisotropic material, to depend on the relative orientations

of adjoining grains. Thus, it would be difficult to determine the critical coordination number with the current data.

A reasonable conclusion is that if pores within the initial powder compact have a coordination number greater than the critical value, then grain growth would be a desirable phenomenon, since it causes stable pores to disappear by decreasing their coordination number. Thus, the initial distribution of pore coordination numbers within a crystalline powder compact will determine the amount of grain growth required to achieve a dense material. Pores that can not be eliminated through grain growth must be removed by deformation, e.g. hot-pressing or HIPing.

ACKNOWLEDGEMENT

This work was supported by the Office of Naval Research, Contract No. N00014-83-C-0469.

AD-A173 342 PROCESSING SCIENCE TO INCREASE THE RELIABILITY OF CERAMICS(U) ROCKWELL INTERNATIONAL THOUSAND OAKS CA SCIENCE CENTER B J KELLETT ET AL. SEP 86 SC410.FR 2/2

UNCLASSIFIED N00014-84-C-0298 F/G 11/2 NL

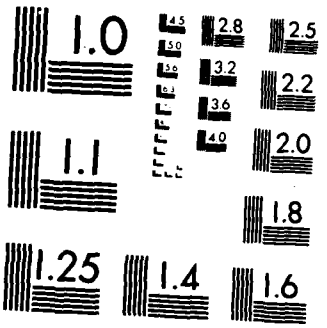

REFERENCES

1. C. Herring, "Surface Tension as a Motivation for Sintering," The Physics of Powder Metallurgy, ed. W.E. Kingston, Chapt. 8, McGraw-Hill, New York (1951).

2. G.C. Kuczynski, "The Mechanism of Densification During Sintering of Metallic Particles," Acta Met. 4, 58, (1956).

3. W.D. Kingery and B. Francois, "Sintering of Crystalline Oxides, I: Interaction Between Grain Boundaries and Pores," in Sintering and Related Phenomena, eds., G.C. Kuczynski, N.A. Hooten and G.F. Gibbon, pp. 471-98, Gordon Breach, (1967).

4. B. Kellett and F.F. Lange, "Thermodynamics of Densification, Part I: Sintering of Simple Particle Arrays, Equilibrium Configurations, Pore Stability and Shrinkage,", submitted to J. Amer. Ceram. Soc.

5. T.K. Gupta, "Possible Correlation Between Density and Grain Size During Sintering," J. Amer. Ceram. Soc. 55, 276, (1972).

6. R.M. Cannon, "On the Effects of Dihedral Angle and Pressure on the Driving Force for Pore Growth or Shrinkage," unpublished work, 1981.

7. F.F. Lange and M.M. Hirlinger, "Hindrance of Grain Growth in Al_2O_3 by ZrO_2 Inclusions," J. Am. Ceram. Soc. 67, [3], 164 (1984).

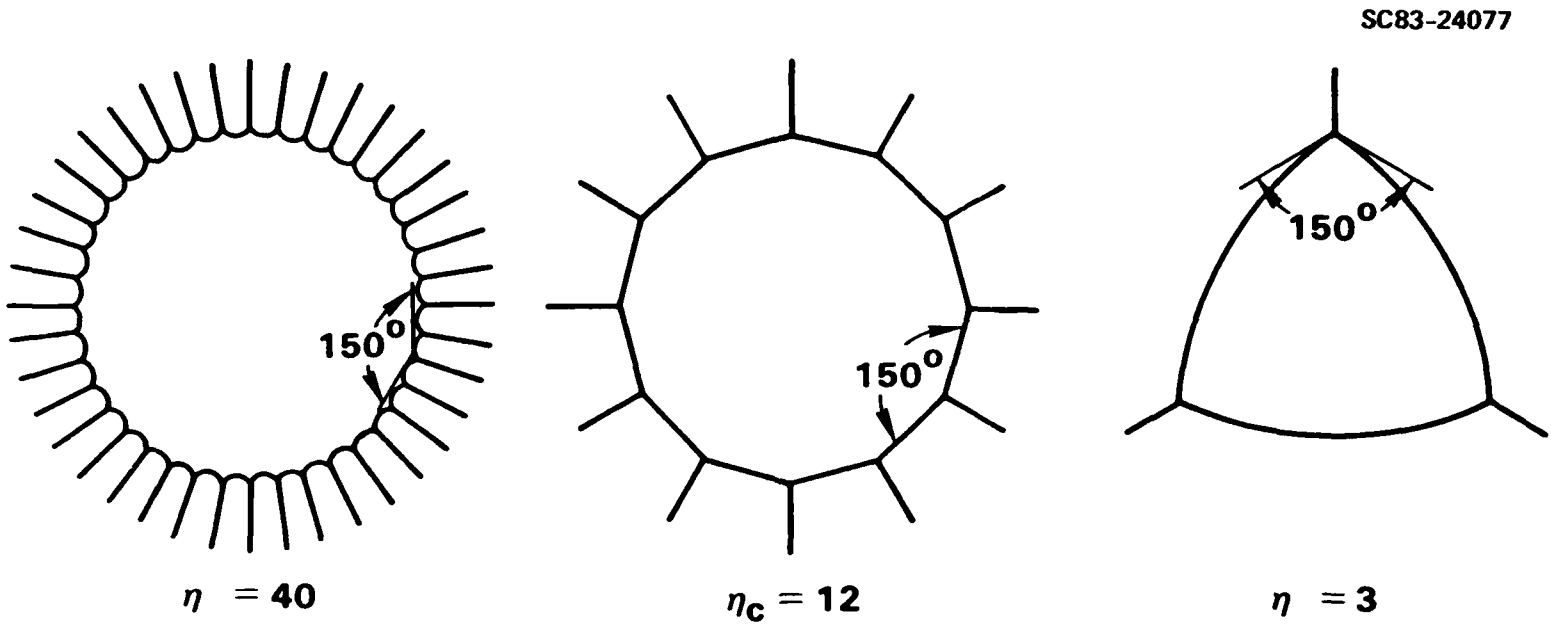

Fig. 1 Pore curvature as the coordination number of the pore decreases during grain growth, for a dihedral angle of 150°. The dihedral angle is the equilibrium angle that forms at the grain boundary solid-vapor junction.

SC34877

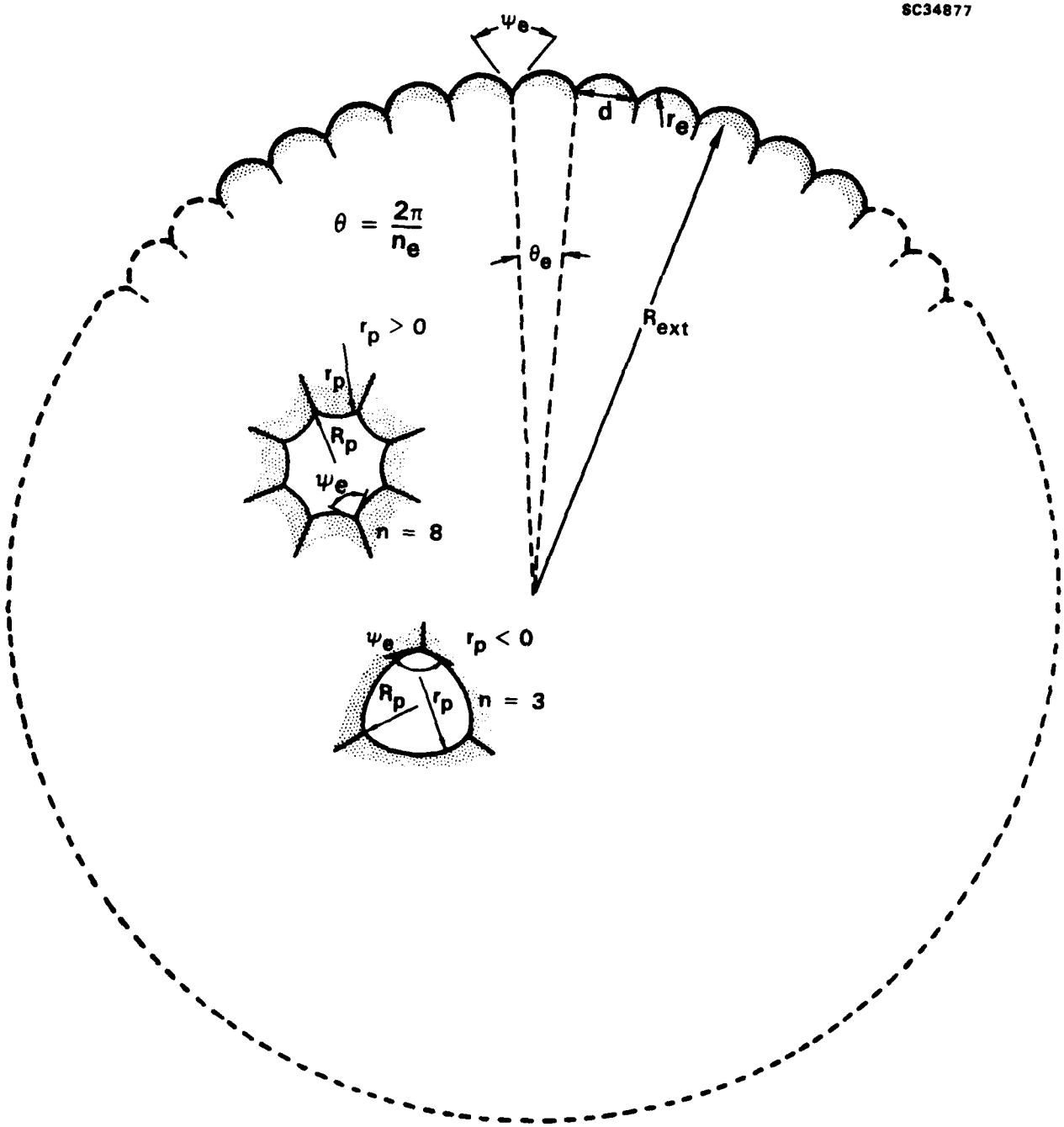

Fig. 2 Surface curvature for two pores of coordination (n) 8 and 3, and a region of the exterior surface.

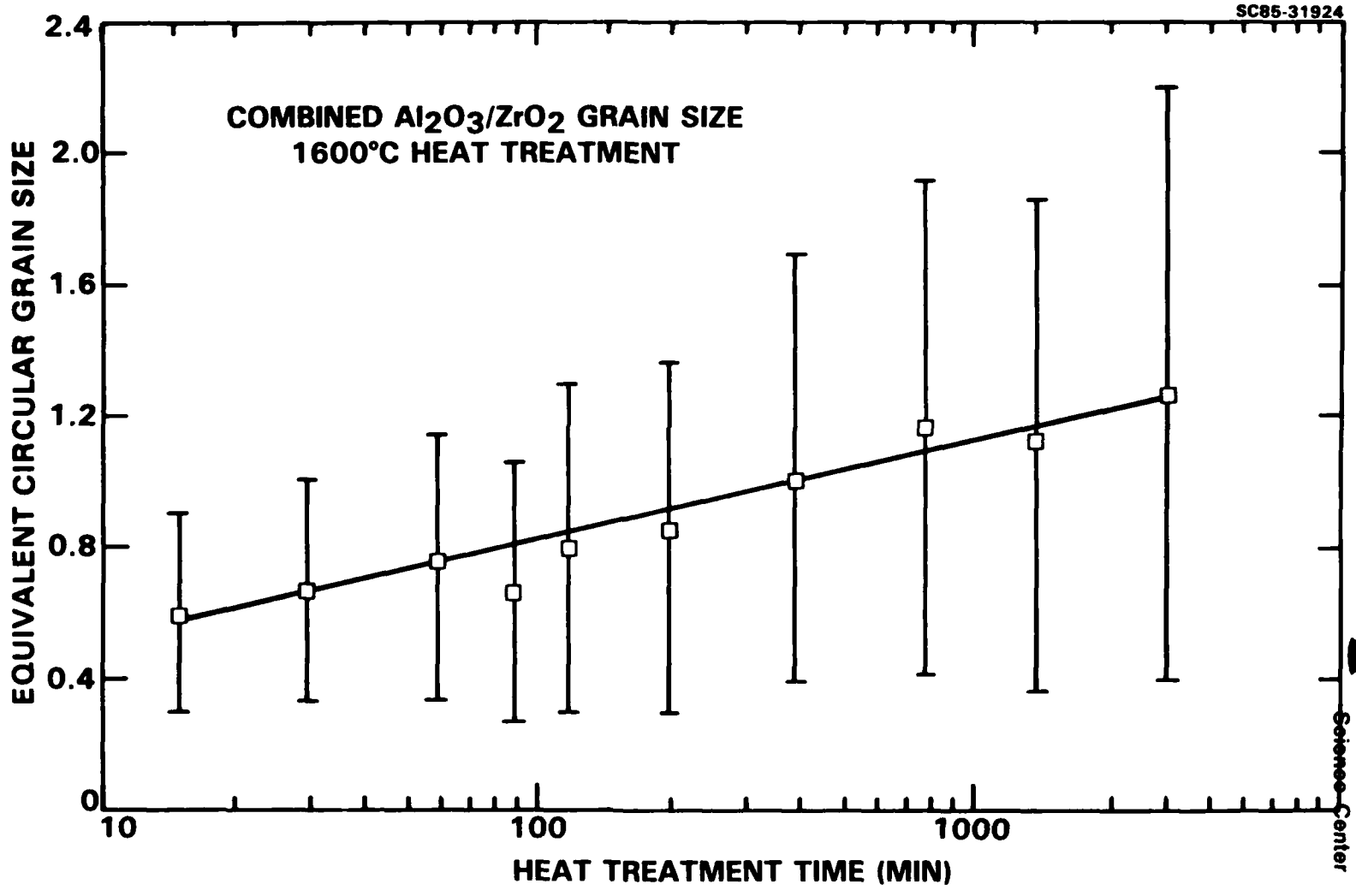

Fig. 3 Combined Al_2O_3/ZrO_2 median grain size, expressed as the equivalent circular diameter as a function of log time. Bars illustrate the standard deviation.

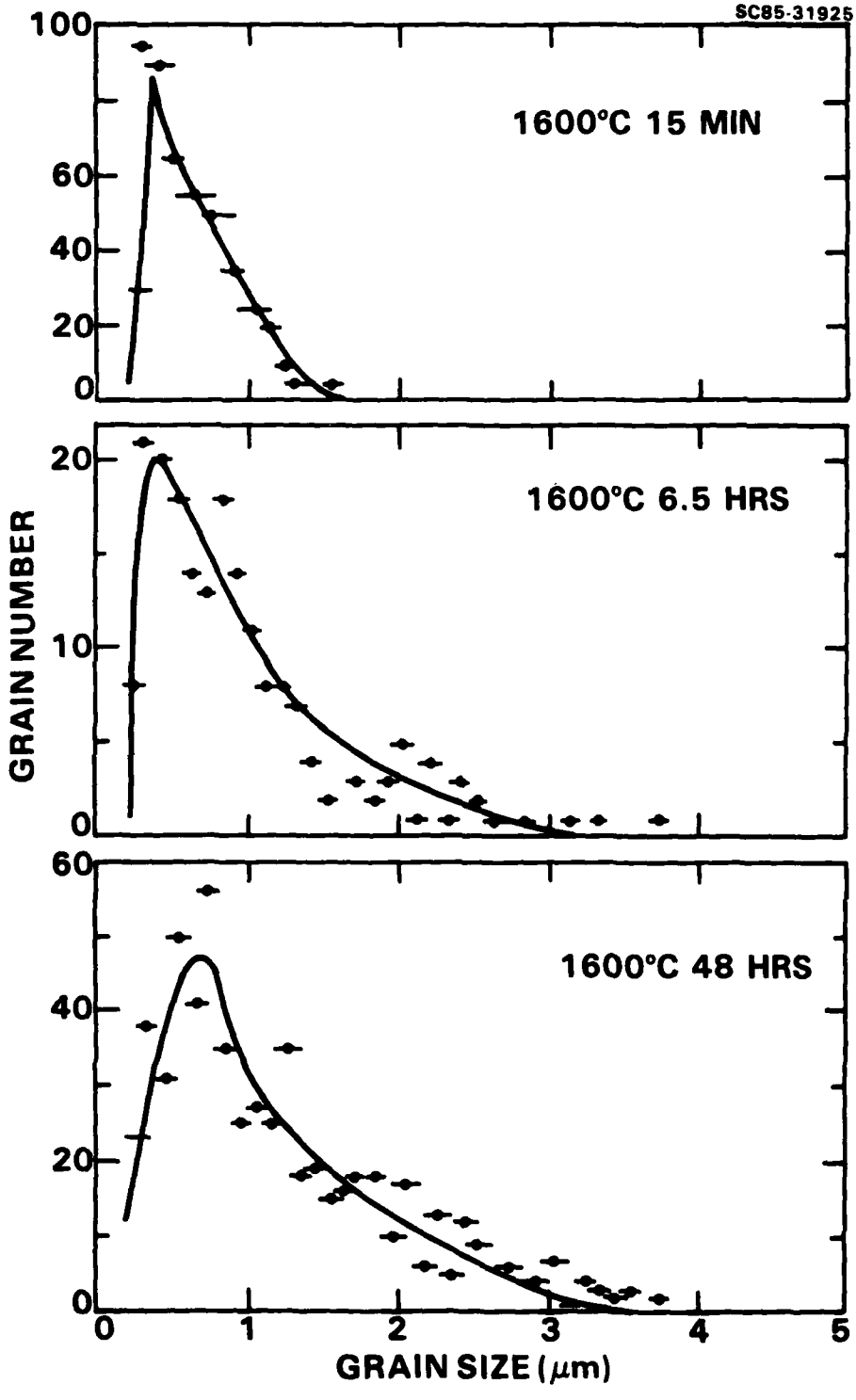

Fig. 4 Grain size distributions of combined Al_2O_3/ZrO_2 grains for three different heat treatments at 1600°C (heating periods of: a) 15 min, b) 390 min, and c) 2880 min).

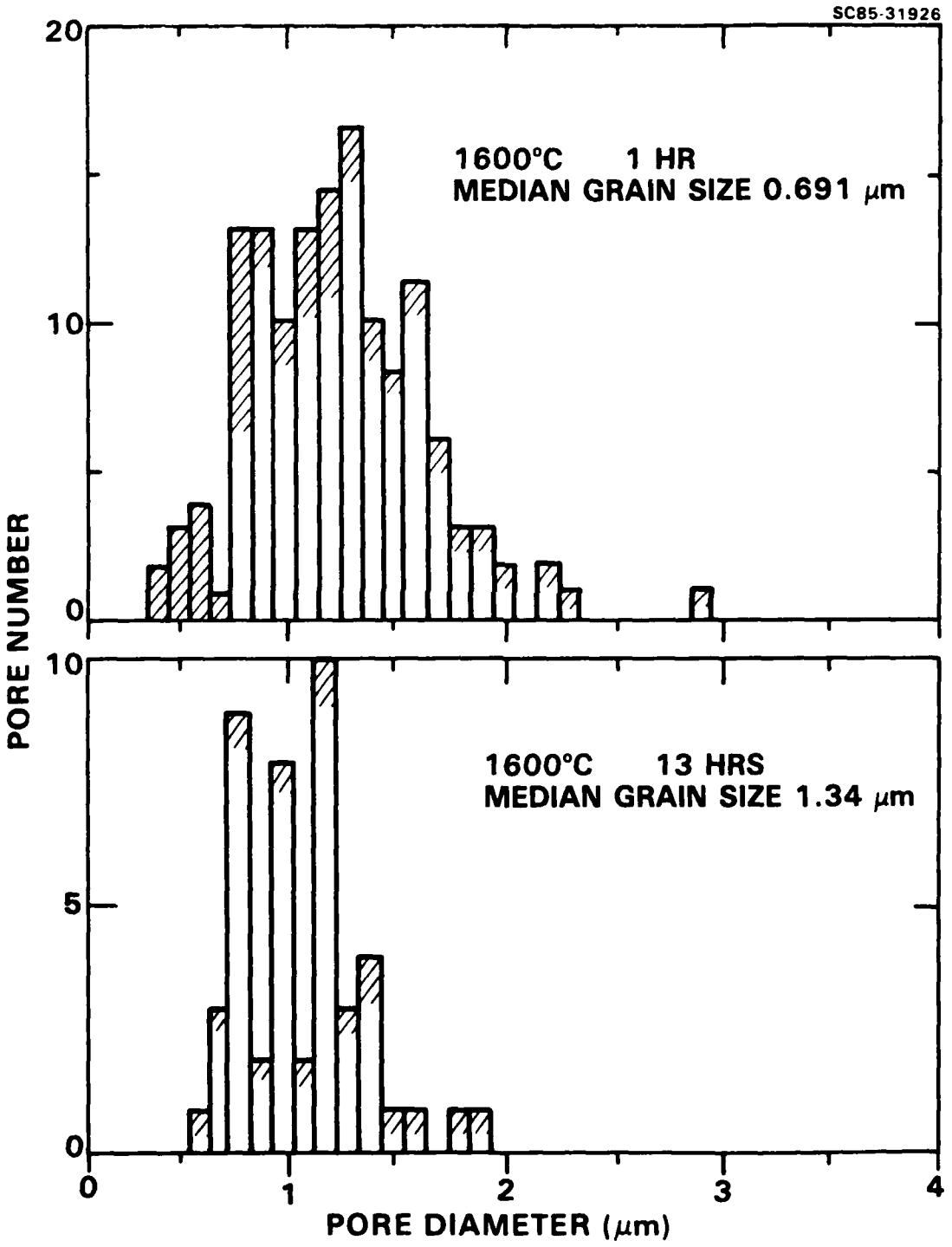

Fig. 5 Pore size histogram of the material fabricated from 2 μm plastic spheres after heat treatments of a) 1 and b) 13 h.

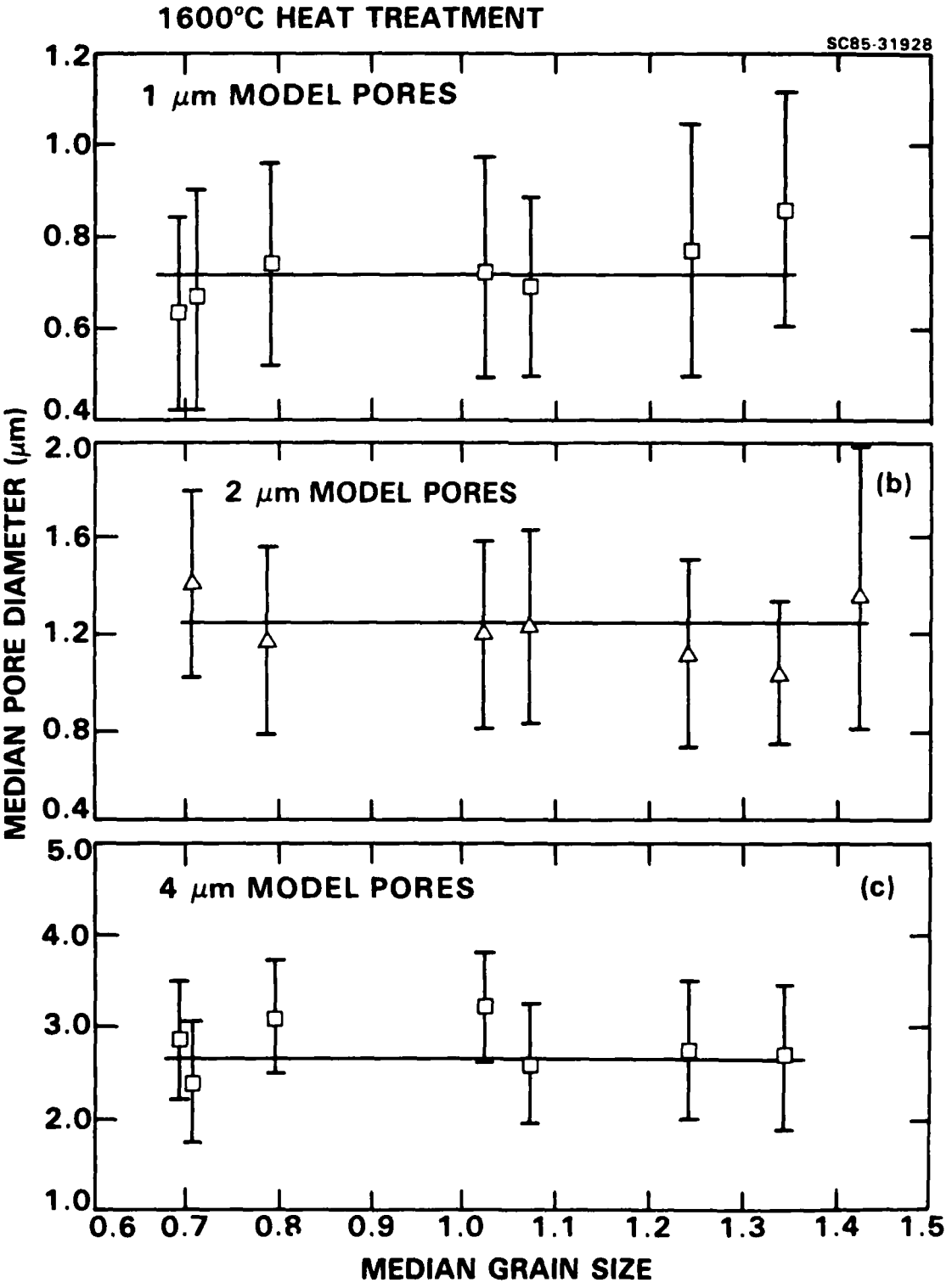

Fig. 6 (a) Median pore size and (b) number pore density of material fabricated from 1, 2, and 4 μm plastic spheres as a function of the combined Al_2O_3/ZrO_2 median grain size, for heat treatments at 1600°C.

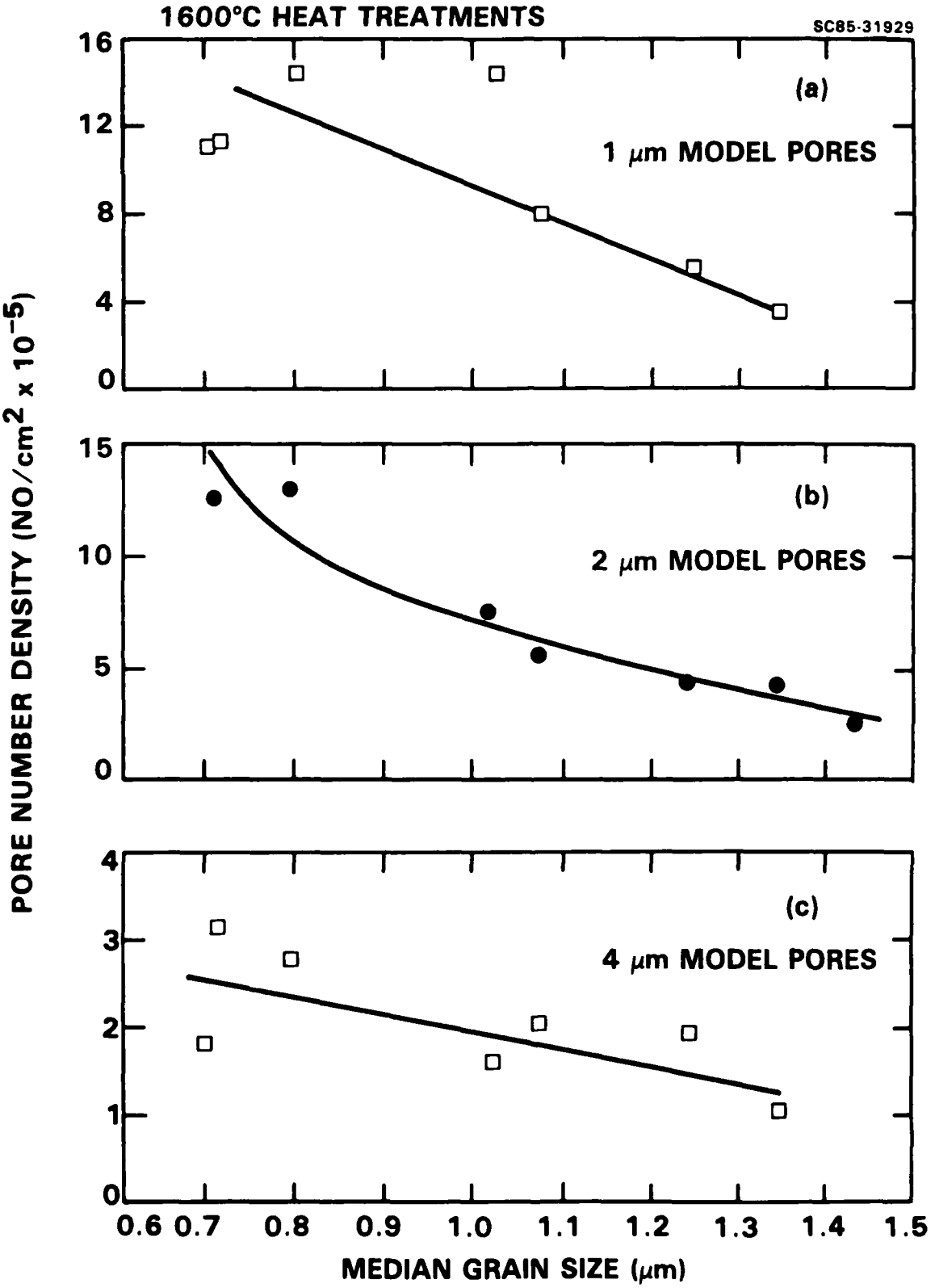
1600°C HEAT TREATMENTS
SC85-31929
(a)
1 μm MODEL PORES
(b)
2 μm MODEL PORES
(c)
4 μm MODEL PORES
PORE NUMBER DENSITY (NO/cm² x 10⁻⁵)
MEDIAN GRAIN SIZE (μm)
0
4
8
12
16
5
10
15
1
2
3
0.6
0.7
0.8
0.9
1.0
1.1
1.2
1.3
1.4
1.5

Fig. 6b

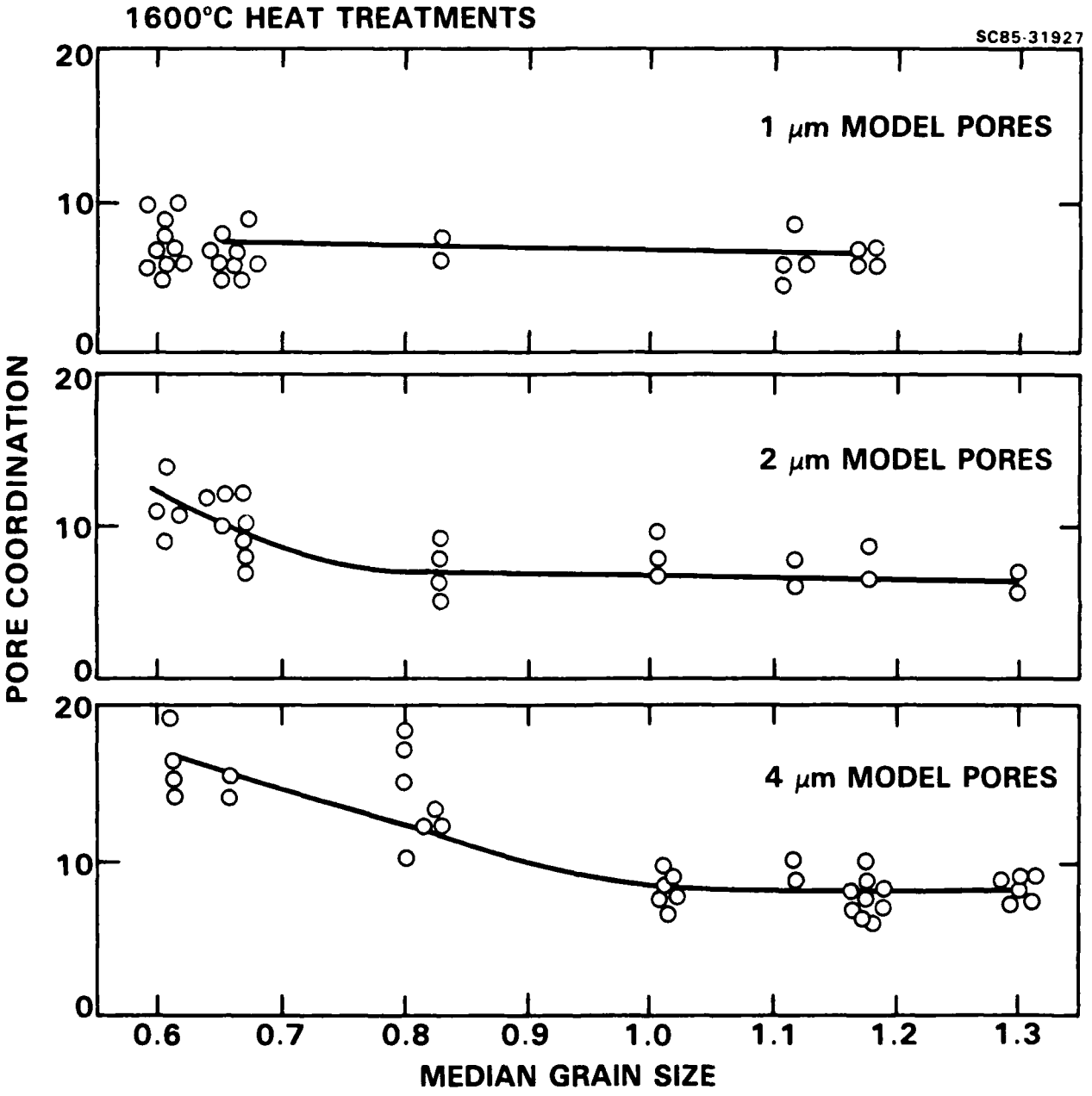

Fig. 7 Pore coordination, in the plane of polish, of the 1, 2, and 4 μm plastic spheres fabricated material, as a function of the combined Al_2O_3/ZrO_2 medium grain size, for heat treatments at 1600°C.

SC5410.FR

EXPERIMENTS ON PORE CLOSURE DURING HIPing AND FORGING

B.J. Kellett and F.F. Lange
Rockwell Science Center
Structural Ceramics Group
1049 Camino Dos Rios
Thousand Oaks, CA 91360

and

University of California, Los Angeles
Department of Materials Engineering
Los Angeles, CA

EXPERIMENTS ON PORE CLOSURE DURING HIPing AND FORGING

B.J. Kellett and F.F. Lange

Rockwell Science Center
Structural Ceramics Group
1049 Camino Dos Rios
Thousand Oaks, CA 91360

and

University of California, Los Angeles
Department of Materials Engineering
Los Angeles, CA

ABSTRACT

The effect of stress on pore closure was studied by HIPing (Hot Isostatic Pressing) and hot forging sintered Al_2O_3, cubic-ZrO_2, and finer grained Al_2O_3/ZrO_2 (cubic) composite materials containing pores remnant of monosized plastic spheres. For the temperature-time conditions explored, plastic deformation was the dominate mechanism for pore shape change and closure. Namely, only pores in the highly deformable two-phase material where observed to either change shape (under uniaxial forging) or uniformly shrink (during HIPing). Large plastic strains (0.3 to 0.6, dependent on location) were required to produce pore closure under forging conditions. At temperatures where the two-phase materials were sufficiently deformable to affect pore closure, pores near the surface would puncture as the thin web of material separating the pore from the surface was deformed into the pore.

These results are discussed in terms of the common practice of HIP finishing sintered materials.

1.0 INTRODUCTION

Even though HIPing and hot forging has long been recognized as a technique for increasing densification kinetics, and end point density, disagreement exists on the mechanism(s) causing pore shrinkage and disappearance. Two different viewpoints have been used to describe the removal of isolated pores, namely stress assisted sintering and creep induced pore collapse.

Coble[1] assumed that isolated pores within a polycrystalline material could be modeled as spherical voids of radius r_p, and reasoned that an applied compressive stress (σ_a) would decrease the concentration of vacancies at grain boundaries and hence increase diffusional transport of mass to the void to aid in pore closure. He concluded that the applied stress would enhance the driving "stress" (σ_d) for pore closure as expressed by

$$\sigma_d = \sigma_a - 2\gamma_s/r_p \quad . \tag{1}$$

where γ_s is the surface energy of the pore per unit area. Since Coble assumed that pores always have a negative surface curvature (i.e., spherical voids) all pores were thermodynamically unstable and would disappear. An applied stress would simply aid in their disappearance.

But, as pointed out by Kingery and Francois,[2] the surface curvature of pores within a polycrystalline material depends on the number of coordinating grains and the ratio of the grain boundary to surface energies as expressed through Young's equation. They showed that when the number of coordinating grains is greater than a critical number ($n > n_c$) the pore's surface is convex ($r_p > 0$), and when $n < n_c$, the surface is concave (looking from within the pore) and $r_p < 0$. When the free energy of a body containing an isolated pore is determined as a function of the pore volume, it can be shown[3] that when $n > n_c$, the isolated pore will either shrink or grow until its curvature is identical to the surface curvature of grains on the external surface. That is, only pores with $n \leq n_c$ ($r_p < 0$) are thermodynamically unstable and disappear, kinetics permitting. With this in mind, it can be shown (see Appendix) that the effect of an applied stress on the driving "stress" for pore closure can be expressed as

$$\sigma_d = 2\gamma_s \left(\frac{1}{r_e} - \frac{1}{r_p}\right) + \sigma_a \qquad (2)$$

where r_e is the radius of curvature of the grains on the external surface. Since r_p changes with pore volume (the absolute magnitude of r_p decrease with pore volume), whereas r_e only depends on grain size, it can be shown (see Appendix) that the equilibrium size R_p of the isolated pore changes with applied pressure as

$$R_p = \frac{\cos\left(\frac{\psi_e}{2} + \frac{\pi}{n}\right)}{\left(\frac{\sigma_a}{\gamma_s} + \frac{2}{D}\cos\frac{\psi_e}{2}\right)\sin\frac{\pi}{n}} \qquad (3)$$

Equation (3) shows that an applied pressure will simply decrease the equilibrium size of the stable pore ($n > n_c$), whereas unstable pores ($n < n_c$) are expected to disappear faster with an applied pressure.

Deformation induced pore collapse is chiefly dependent on the material's ability to deform in a plastic manner and, in particular, on the material's stress-strain rate behavior. Wilkinson and Ashby,[4] assuming power law creep behavior (i.e. $\sigma = A\varepsilon^n$), determined that spherical pores under pure hydrostatic conditions remain spherical and collapse at a constant volume rate. More recent work by Budiansky, et al,[5] determined that under forging conditions pores collapse into penny shaped cracks, as one might expect. It was also found that slight perturbations from hydrostatic stress also cause initially spherical pores to collapse into either a penny (crack) or rod shaped pores. Perturbations from hydrostatic stress might arise during HIPing (e.g., from the interaction of the stress state about neighboring pores), suggesting that pore closure during HIPing might proceed by a pore shape change instability.

To determine the effects of stress and strain on pore closure, sintered specimens, fabricated with mono-sized pores with $n > n_c$, were both HIPed at different temperatures, and hot forged to different strains. Microscopic examination as used to follow pore closure conditions. Results

indicate that conditions that promote bulk deformation are much more effective for pore closure relative to stress enhanced sintering.

2.0 EXPERIMENTAL PROCEDURES

Pores of uniform size were created by mixing a small fraction of plastic spheres, manufactured to a narrow size distribution,* into a ceramic powder slurry which was colloidally processed to remove large agglomerates as described elsewhere.[6] Both single-phase Al_2O_3** and ZrO_2‡ and a two-phase mixture of these Al_2O_3/ZrO_2 powders were used (the ZrO_2 powder was prealloyed with 12 weight% (6.6 mole%) Y_2O_3, which produces the cubic structure after densification). The slurry was ultrasonicated in the dispersed state, to insure good mixing, and then flocced to prevent separation (due to differences in the settling rates between the plastic spheres and the ceramic powder). Slurries were consolidated by pressure filtration, as described elsewhere,[7] dryied overnight in an oven, and sintered in air for one hour at either 1600°C, for the Al_2O_3/ZrO_2 composites and Al_2O_3 material, and 1500°C for the ZrO_2 material. The plastic spheres burn out prior to bulk shrinkage, leaving highly coordinated pores. Different specimens containing different size pores, remnant of the different size plastic spheres (4 to 50 μm) where fabricated. Specimens were diamond cut and polished.

*Duke Scientific, 445 Sherman Ave., Palo Alto, CA 94306.
**Alcoa A 16-SG.
‡Zircar Products Inc., 110 North Main St., Florida, NY 10921.

HIPing was performed in a MiniHIP*. The pressure-temperature schedule consisted of an initial pressurization to 70 MPa, ramping to temperature (either 1400°C, 1450°C, 1475°C, and 1500°C), a temperature hold for 10 min, followed by cooling and depressurization to ambient conditions.

Hot forging was performed with a cantilevered dead-weight creep apparatus, previously described.[8] Uniaxial stresses were applied to the specimen with SiC rams through polished silicon carbide pads. Forging was done at constant temperature (1500°C) and at constant load. The load bearing area of the specimen increases during forging decreasing the actual stress on the specimen. Also, frictional constraint between the specimen and the loading pads create hydrostatic stresses within the specimen which diminishes toward the specimen free surface (*friction hill stress*).[9] The lack of significant specimen barreling suggests that friction hill stresses were relatively minor.

Forged or hiped specimens were diamond cut and polished for microstructural observations.

*Conaway (now manufactured by ASEA, Sweden).

3.0 RESULTS

3.1 Deformation Characteristics

Figure 1 illustrates the deformation behavior of the two single phase materials and one of the two-phase materials for data obtained under hot-forging conditions at 1500°C under a constant load that produced an initial stress of 70 MPa. Both single phase materials, which had a larger average grain size (3 μm, Al_2O_3; 7.5 μm, ZrO2) failed in ternary creep, whereas the fine grained (1 μm) two-phase materials exhibited extensive deformation without developing tears or cracks. The deformation behavior of the two-phase materials is detailed elsewhere.[10]

3.2 HIPing Experiments

Optical micrographs of diamond cut and polished surfaces of HIPed, Al_2O_3/20 vol% ZrO_2 specimens containing pores remnant of the 25 μm plastic spheres are shown in Fig. 2. These micrographs show that the pore number density and pore size decrease with increasing temperature. The pores within the single phase materials showed no measurable change over this same temperature range.

Figure 3 shows a polished surface of a Al_2O_3/20 vol% ZrO_2 specimen (a) before and (b) after HIPing and illustrates that sub-surface pores collapse to form craters. Normarsky phase interference microscopy illustrates that the craters are much larger than the pores. As expected pores previously

open to the surface do not close. SEM micrographs of these craters (Fig. 4) illustrate that while some craters are a local depression in the surface, others have punctured.

The single phase materials did not exhibit cratering.

Occasional pores appreared slightly elliptical in shape suggestive of the perturbation suggested by Budiansky et al.[5]

3.3 Hot Forging Experiments

SEM micrographs of polished and thermally etched surfaces (Fig. 5) show pores remnant of 4 μm plastic spheres located near the edge of a two phase specimen (containing 10 vol% ZrO_2) where triaxial stresses generated by frictional constraint at the loading pads are expected to be insignificant. Pores develop a crack like morphology with increased applied strain, and significantly, these relatively small pores are still present after an applied engineering strain of 0.3. These large strains were not obtainable for the single phase materials.

Larger pores, remnant of 50 μm plastic spheres, show (Fig. 6) similar behavior in more detail. These pores, located near the edge of the specimen, maintain a uniform width normal to the applied load while their height in the direction of the applied load decreases. Contact between the top and bottom of the pore is followed by complete pore disappearance for an applied engineering strain of approximately 0.6.

Pores located toward the center of the forged specimen, show similar morphological changes, but appear to disappear at somewhat lower strains (about 0.3) It is expected that pores close to the center of the specimen might experience a hydrostatic stress (generated by frictional constraint) in addition to the applied uniaxial stress.

Pores in a two-phase, ZrO_2/20 vol% Al_2O_3, material, which also exhibits high ductility at 1500°C , albeit somewhat less than the alumina rich compositions, developed cracks where tensile stresses are expected to develop during forging. Smaller tears and cavities, developed along the top and bottom of the pores (location of tensile stresses) are commonly observed in the more deformable materials (see Fig. 6).

4.0 CONCLUSIONS

Pore disappearance only occurred in the fine grain alumina-zirconia material which exhibited extensive deformation at the hiping and forging temperature. Cratering and puncturing of near surface pores during HIPing and the observed change in pore shape during forging strongly suggests that plastic deformation was responsible for pore closure.

Pore closure during forging appears to occur at an engineering strain of approximately 0.6 near the free surface, and 0.3 near the center of the specimen where hydrostatic stresses generated by frictional constraint are expected to be greater. These results are consistent with those of Budiansky

et al[5] who determined that pore closure should occur at an engineering strain of 0.46 under uniaxial conditions, decreasing to 0 for hydrostatic condition.

The current observations strongly suggest that HIP finishing of sintered materials, commonly used to decrease the flaw populations associated with irregular voids,[11,12] should be carried out in a pressure-temperature regime where the material exhibits extensive plastic deformation. In addition, although it is commonly recognized that pores at the surface will not be closed during HIPing, the current observations show that near surface pores can create extensive surface damage during HIPing.

ACKNOWLEDGMENT

This work was supported by the Office of Naval Research under Contract No. N00014-84-C-0298.

APPENDIX

EFFECT OF AN EXTERNAL PRESSURE ON THE EQUILIBRIUM BETWEEN A PORE AND AN EXTERNAL SURFACE

Previous calculations[3] concerning the free energy of a polycrystalline body of uniform grain size, D, containing an isolated pore showed that the derivative of the total free energy of the system (pore plus external surface) with respect to the volume of the pore (V_p) can be expressed as

$$dE/dV_p = \gamma_s(k_e - k_p) \quad , \tag{A1}$$

where k_e and k_p are the surface curvatures of the external grains and the grains surrounding the pore, respectively and γ_s is the energy per unit area of the surface. k_e is always positive. It can also be shown that the absolute magnitude of k_p decreases with the size of the pore (R_p). It was shown that when the number of grains coordinating the pore is greater than a critical number (e.g., $n > n_c$), k_p is also positive. Thus, when the coordination number of an isolated pore is greater than the critical value, the pore will either shrink or grow until the surface curvature of the surrounding grains is identical to that of the surface grains (viz. $k_p = k_e$). The surface curvature of grains surrounding pores with a coordination number less or equal to the critical number ($n \leq n_c$) is negative. Such pores are always unstable and disappear, kinetics permitting. For symmetric pores, $n_c = 2\pi/(\pi - \psi_e)$, where ψ_e is the dihedral angle which defines the ratio of the grain boundary and surface energies through Young's equation.

The effect of an applied pressure, P_a, on pore stability can be ascertained by noting that $dE/dV_p = P_a$. Combining this term with Eq. (A1) results in

$$dE/dV_p = \gamma_s(k_e - k_p) + P_a \quad . \tag{A2}$$

Using the relation between the radius of curvature for the grains on the external surface and grain size (e.g., $r_e = D[2\cos(\psi_e/2)]^{-1}$ and the relation between pore radius (R_p) and pore volume (see Ref. 3), one can obtain the following expression between equilibrium pore radius (i.e., when $dE/dV_p = 0$) and the applied pressure

$$R_p = \frac{\cos\left(\frac{\psi_e}{2} + \frac{\pi}{2}\right)}{\left(\frac{P_a}{\gamma_s} + \frac{2}{D}\cos\frac{\psi_e}{2}\right)\sin\frac{\pi}{n}} \tag{A3}$$

Equation (A3) shows that when ($n > n_c$), the pore always has a finite size.

REFERENCES

1. R.L. Coble, "Diffusion Models for Hot Pressing with Surface Energy and Pressure Effects as Driving Forces," J. Appl. Phys. 41 [12] 4798 (1970).

2. W.D. Kingery and B. Francois, "Singering of Crystalline Oxides, I. Interaction Between Grain Boundaries and Pores," pp 471-98 in Sintering and Related Phenomena. Ed. by G.C. Kuczynke, N.A. Hooton, and G.F. Gibbon, Gordon Breach, New York (1967).

3. B.J. Kellett and F.F. Lange, "Thermodynamics of Densification, Part III: Experimental Relation Between Grain Growth and Pore Closure," submitted to the J. Am. Ceram. Soc.

4. D.S. Wilkinson and M.F. Ashby, "Pressure Sintering by Power Law Creep," Acta Met. 23, 1277 (1975).

5. B. Budiansky, J.W. Hutchinson, and S. Slutsky, "Void Growth and Collapse in Viscous Solids," in Mechanics of Solids: The Rodney Hill 60th Anniversary Volume, Ed. by H.G. Hopkins and M.J. Sewell, Pergamon Press, Oxford.

6. F.F. Lange, B.I. Davis, and E. Wright, "Processing-Related Fracture Origins: IV. Elimination of Voids Produced by Organic Inclusions," J. Am. Ceram. Soc. 69 [1] 66-9 (1986).

7. F.F. Lange and K.T. Miller, "Kinetics and Mechanics of Pressure Filtration," submitted to the J. Am. Ceram. Soc.

8. F.F. Lange, B.I. Davis and D.R. Clarke, "Compressive Creep of Si_3N_4/MgO Alloys: Part I," J. Mat. Sci. 15, 600-10 (1979).

9. K.R. Vendatachari and R. Raj, "Superplastic Flow in Fine-Grain Alumina," J. Am. Ceram. Soc. 69 [2], 135 (1985).

10. B. J. Kellett and F. F. Lange, "Hot Forging Characteristics of Transformation Toughened Al_2O_3/ZrO_2 Composites," to be published.

11. V. Engle and H. Hubner, "Strength Improvement of Cemented Carbides by Hot Isostatic Pressing," J. Mater. Sci., 13 [9] 2003-13 (1978).

12. F.F. Lange, "Processing Related Fracture Origins: I. Observations in Sintered and Isostactically Hot-Pressed Composites," J. Am. Ceram. Soc. 66 [6], 398-8 (1983).

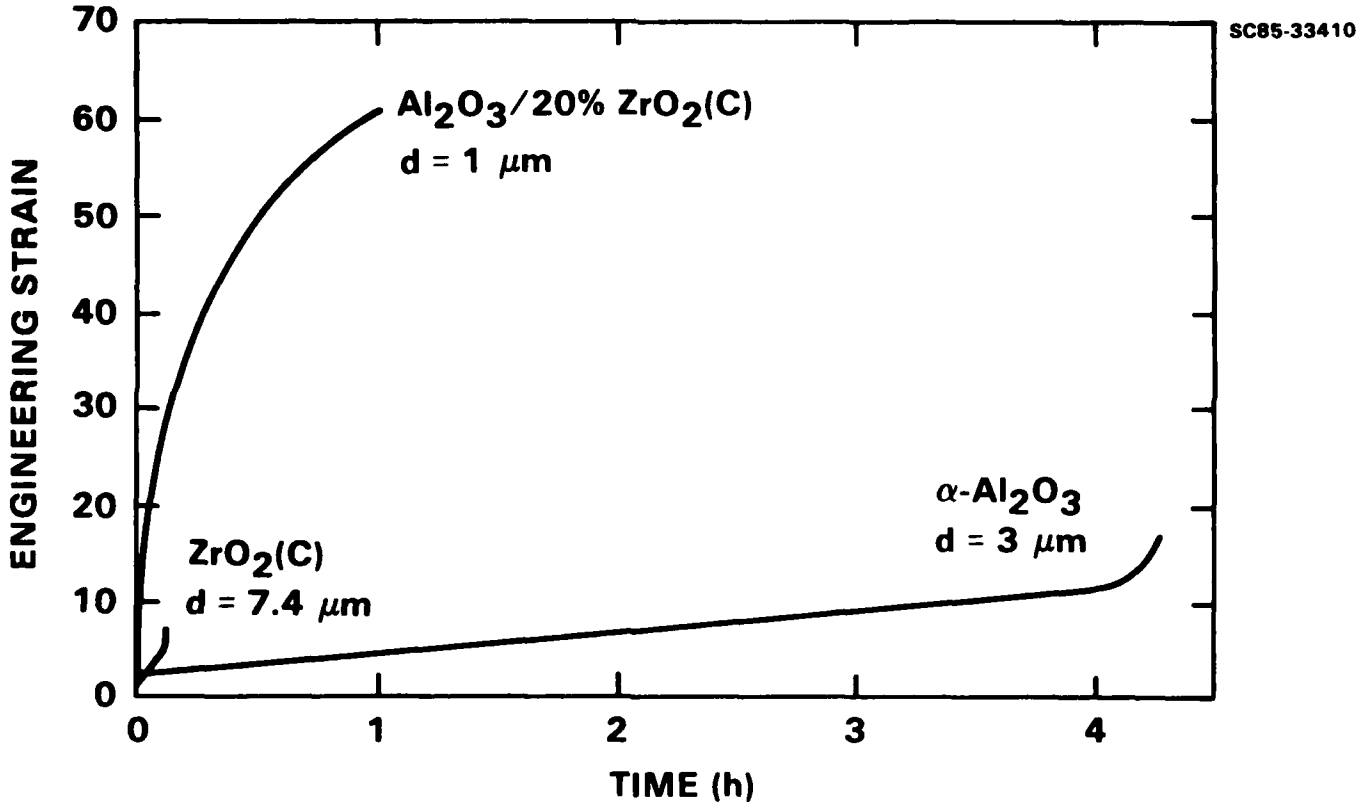

Fig. 1 Deformation strain (engineering) vs time (h) for the three materials. Data obtained during forging experiments at 1500°C at a constant load that produced an initial stress of 70 MPa.

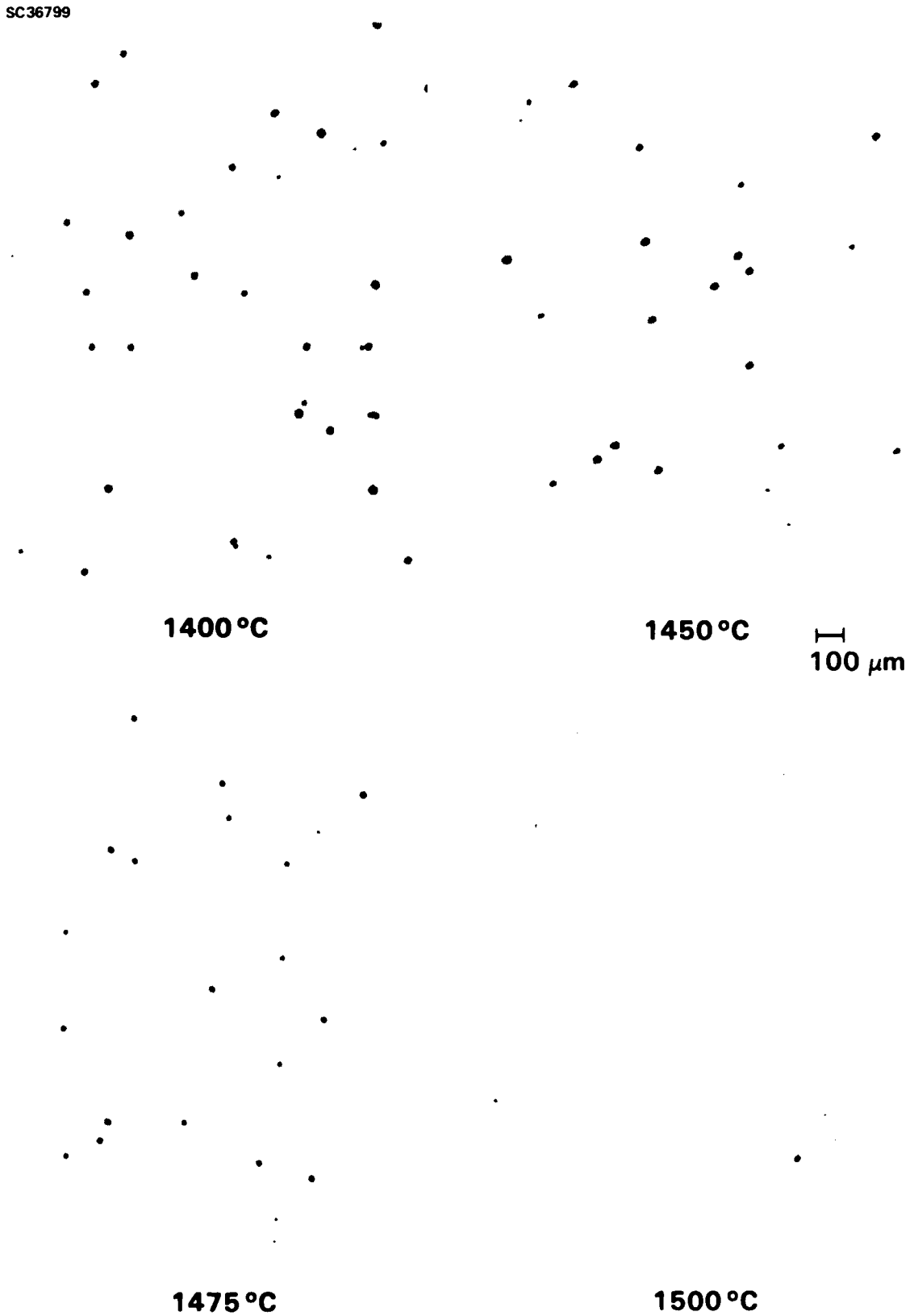

Fig. 2 Optical micrographs of cut and polished surfaces of Al_2O_3/(20 vol%) ZrO_2 materials containing pores remnant of 25 μm plastic spheres sintered at 1600°C and HIPed at either 1400°C, 1450°C, 1475°C, or 1500°C at 70 MPa for 10 min.

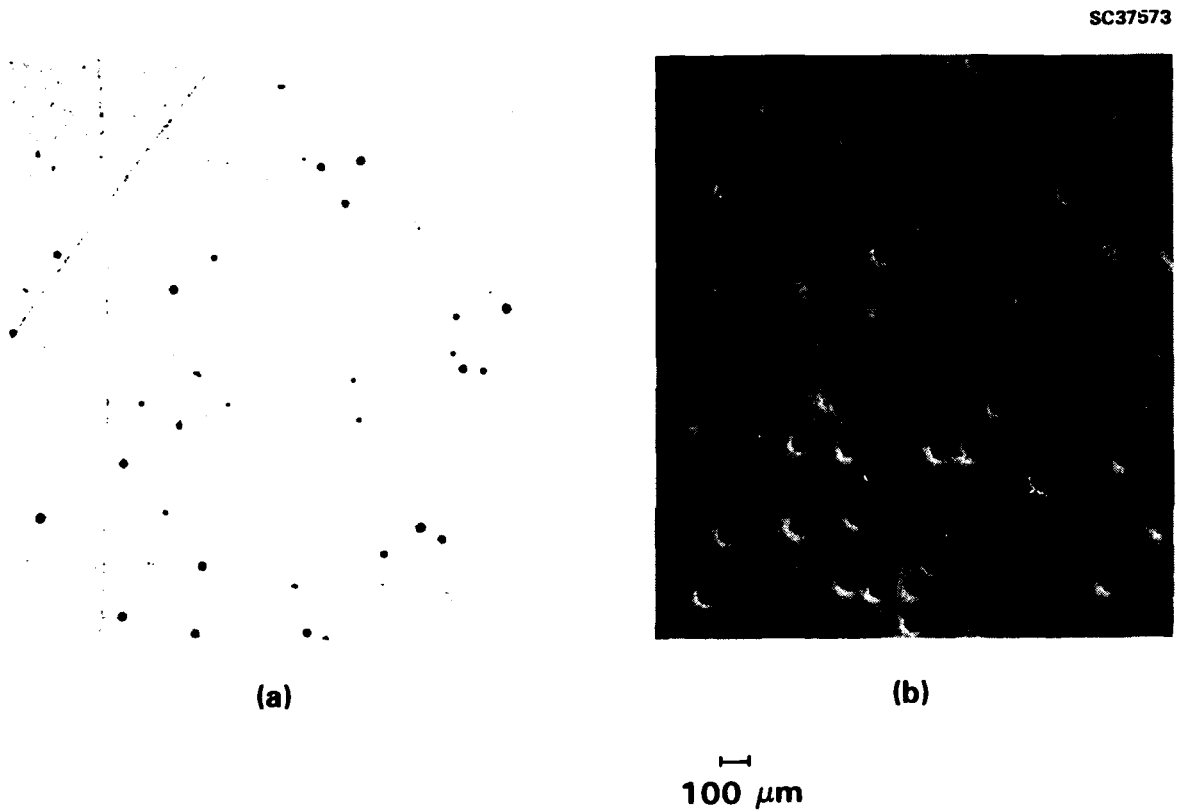

Fig. 3 Normarsky micrographs of a polished surface of Al_2O_3/20 vol% ZrO_2 specimen, containing remnant of 50 μm plastic spheres (a) before, and (b) after HIPing (1500°C, 70 MPa, 10 min). Note that pores open to the surface remain after HIPing, and that surface depressions (dimples and or craters) are much larger than the pores appear after HIPing.

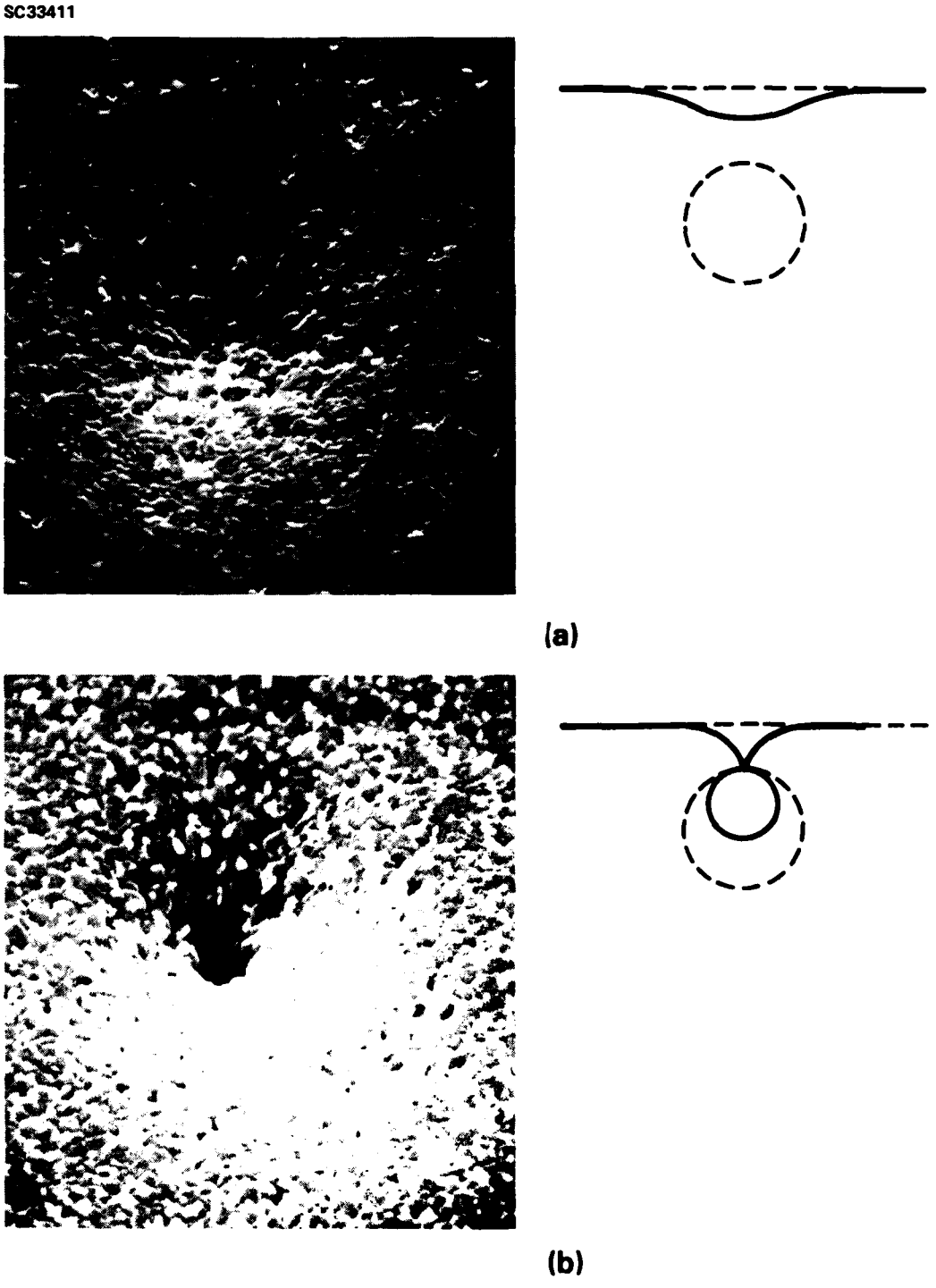

Fig. 4 Scanning electron micrographs of HIPed surface showing surface dimpling and punctures associated with near surface pores.

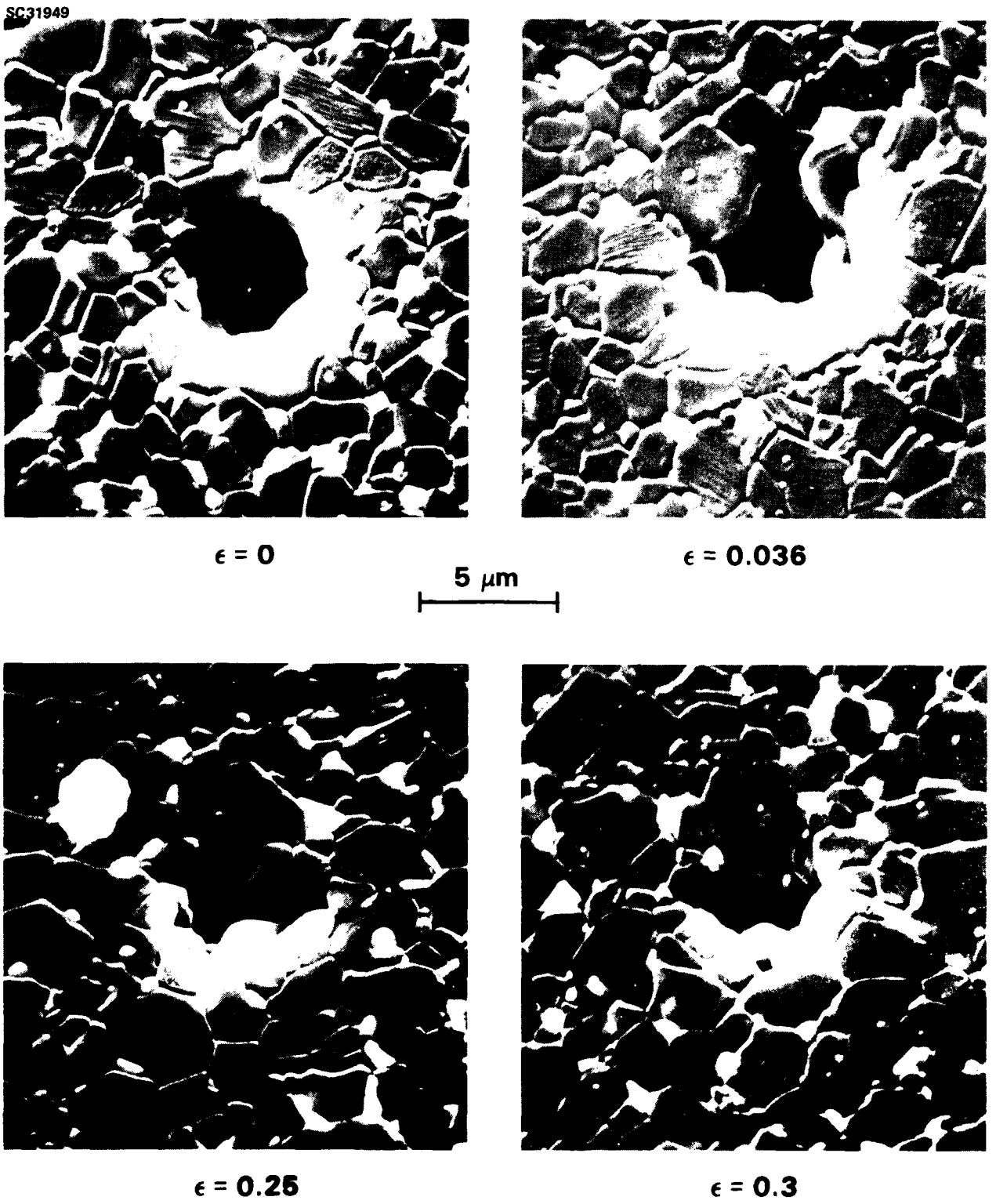

Fig. 5 Subterraneous pores remnant of 4 μm plastic spheres exposed by polishing after different creep strains. Material: Al_2O_3/10 vol% ZrO_2 sintered at 1600°C and forged at 1500°C.

SC37574

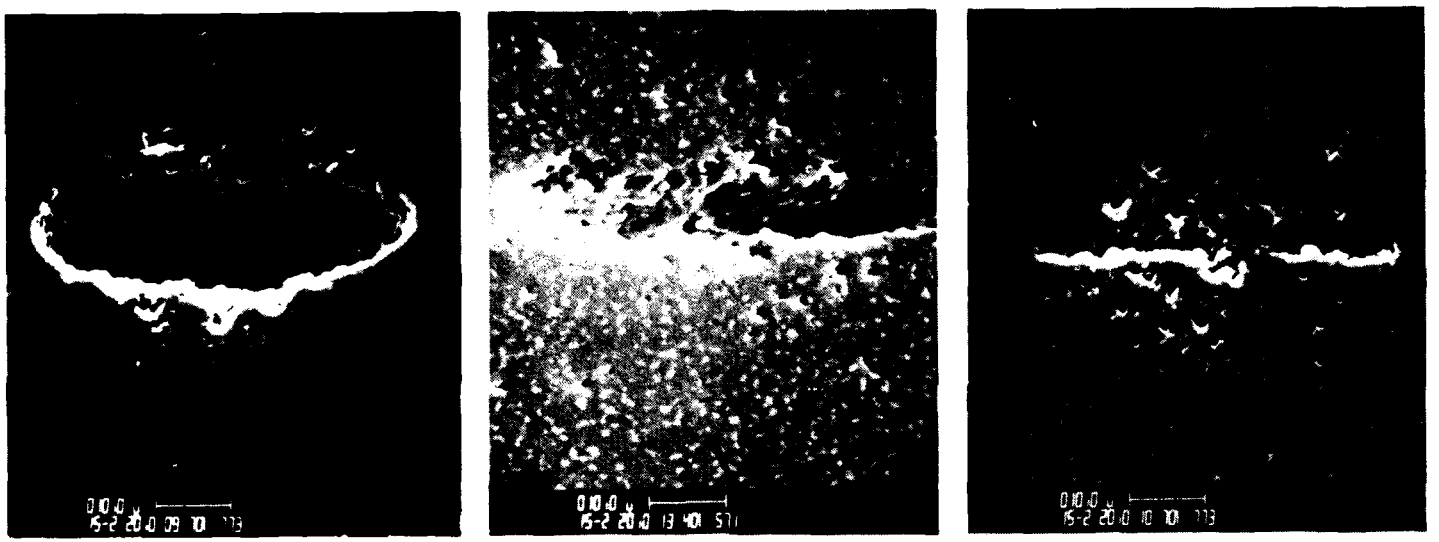

$\epsilon = 0.3$ $\epsilon = 0.5$ $\epsilon = 0.6$

Fig. 6 Subterraneous pores remnant of 50 μm plastic spheres exposed by polishing after different creep strains (eg., 0.3, 0.5, and 0.6). Material: Al_2O_3/20 vol% ZrO_2 sintered at 1600°C and forged at 1500°C.

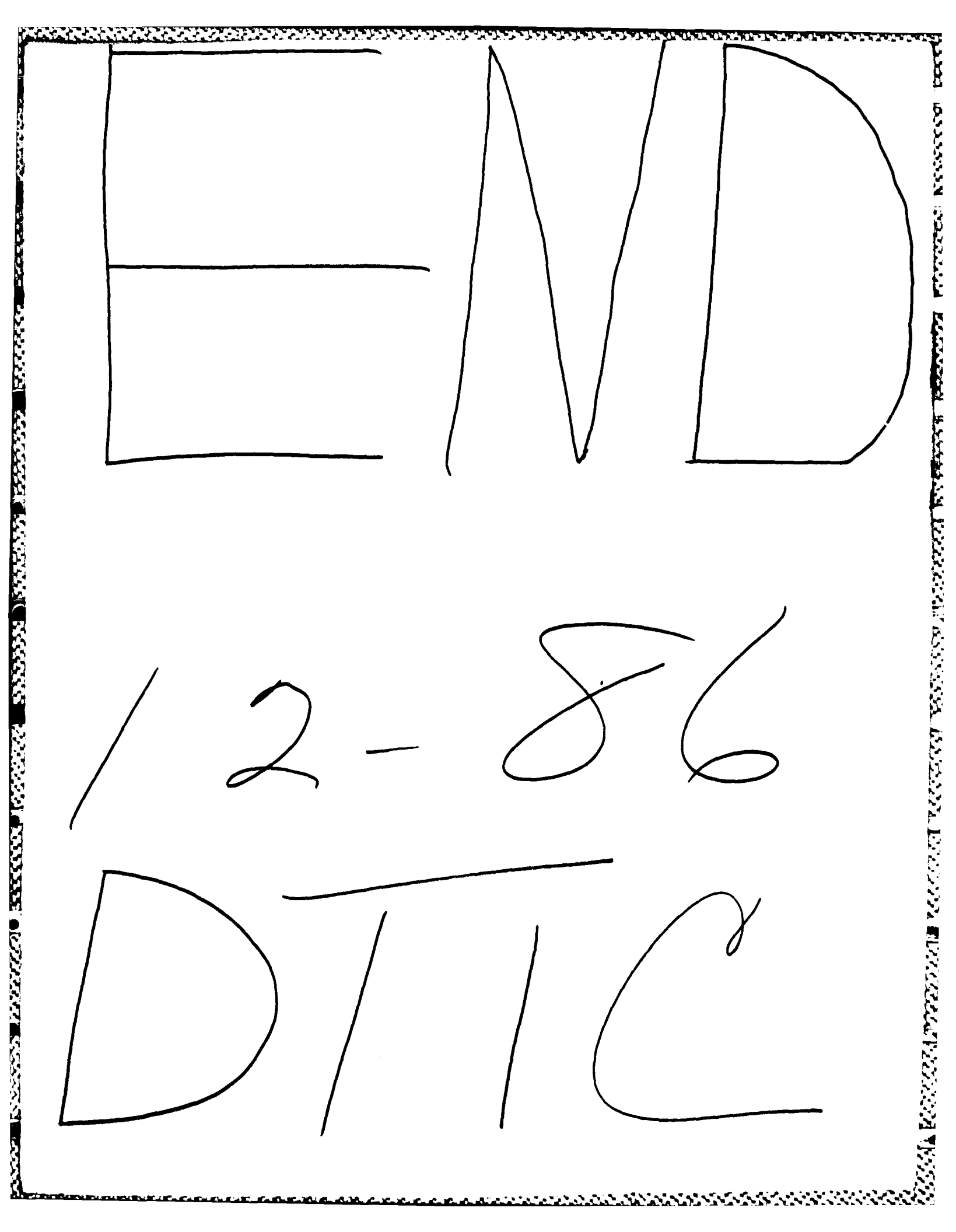
END
12-86
DTIC